9-11-2019

Investigation of Sub 23 Nanometer Particles to Overall Count in Gasoline Engines

Alfredo Tellez-Echavarria
University of Windsor

Investigation of Sub 23 Nanometer Particles to Overall Count in Gasoline Engines

By:

Alfredo Tellez Echavarria

A Thesis
Submitted to the Faculty of Graduate Studies
through the Department of Mechanical, Automotive and Materials Engineering
in Partial Fulfillment of the Requirements for
the Degree of Master of Applied Science
at the University of Windsor

Windsor, Ontario, Canada

2019

Investigation of Sub 23 Nanometer Particles to Overall Count in Gasoline Engines

By

Alfredo Tellez Echavarria

APPROVED BY:

_____

X. (Iris) Xu

Department of Civil and Environmental Engineering

_____

D. Ting

Department of Mechanical, Automotive and Materials Engineering

_____

M. Zheng, Co- Advisor

Department of Mechanical, Automotive and Materials Engineering

_____

A. Sobiesiak, Co- Advisor

Department of Mechanical, Automotive and Materials Engineering

September 11, 2019

Declaration of Originality

I hereby certify that I am the sole author of this thesis and that no part of this thesis has been published or submitted for publication.

I certify that, to the best of my knowledge, my thesis does not infringe upon anyone's copyright nor violate any proprietary rights and that any ideas, techniques, quotations, or any other material from the work of other people included in my thesis, published or otherwise, are fully acknowledged in accordance with the standard referencing practices. Furthermore, to the extent that I have included copyrighted material that surpasses the bounds of fair dealing within the meaning of the Canada Copyright Act, I certify that I have obtained a written permission from the copyright owner(s) to include such material(s) in my thesis and have included copies of such copyright clearances to my appendix.

I declare that this is a true copy of my thesis, including any final revisions, as approved by my thesis committee and the Graduate Studies office, and that this thesis has not been submitted for a higher degree to any other University or Institution.

Abstract

Gasoline direct injection (GDI) engines are becoming the new standard in engine technology; the reduction in fuel consumption, engine size, and an increase in power have made it so within the next year, GDI will replace the current port fuel injection (PFI) method with regards to global market share. The benefits that come with GDI are accompanied with some penalties in particulate number (PN) emissions. The relocation of the fuel injector causes a reduction in fuel and air mixing time, leading to a dramatic increase in PN when compared to the previous technology. As of September 2017, GDI powered vehicles have been limited to 6x 10^{11}Particles/km.

Current legislation also limits the size of these particles. Presently, the only size considered are those of 23nm (Nanometers) and above. As the world moves towards a more health conscious and environmentally friendly society, this range in size is thought to be going down to at least 10nm for the next set of regulations. Existent PN measuring instruments are therefore set with a cutoff of 23nm, and homologation tests are carried out in laboratory settings.

Multiple GDI and one PFI engines were tested in North American and European facilities. It was found that the fuel is a major contributor to particles larger than 23nm during aggressive transients, accounting for as much as 81% of the total count during these periods. Oil consumption also seems to correlate with particles larger than 23nm, as observed by the increase of this size range throughout the performance of two different drive cycles. Lastly, instruments that used particle charging such as the DMS500 by Cambustion or the ICAD (Induced Current Aerosol Detector) were found to have a difference in percentage as low as 30% when compared to their CPC (Condensation Particle Counter) counterparts.

Dedication

A mi madre y padre,

gracias por todo su soporte.

Acknowledgement

As I write this, my stay in Italy is coming to an end and it seems surreal. This work signifies the end of my academic career and I am both excited and scared for the “Real World” that is coming. The work that follows couldn’t have been accomplished without the help of many people, from emotional to literal support; I have many people to be grateful for.

To my CTC advisor, Jordan Easter; thank you immensely for the help you provided me throughout the past two years (now that I type it, it seems crazy it’s been that long since we met). Your commitment to this program as a mentor and most importantly to us, the students, is admirable. I know how crazy it can get at CTC and in your job, so the fact that you were always there when I needed your help will not be forgotten!

Thank you to my academic advisors both at University of Windsor and at Politecnico di Torino. Thank you Dr. Sobiesiak and Dr. Zheng for all the meetings and feedback provided throughout the project and for willing to take part in this special program. Thank you Professor Millo for the excellent Internal Combustion course at Politecnico, and for all the input you provided with regards to my project. It truly is one of the best classes I have taken throughout my academic career and will always remember lessons from it.

To the additional committee members, Dr. Xu and Dr. Ting, thank you for your time and guidance during this process during key milestones such as the proposal and defense.

To my CRF advisor Giovanna Nicol; I can’t believe how lucky I have been to work with you and your colleagues. Not only were you essential in this program with regards to experiment planning, technical advice, feedback etc. you also were so welcoming, and I will be forever grateful for all the insights into Italian culture that you gave me; from language, to history, to food, it was wonderful.

To the coordinators of this program; Dr. Jennifer Johrendt, Prof. Giovanni Belingardi, Mohammed Malik and Marie Mills. Thank you for giving me the opportunity to take part in this program, the initial interview was one of the scariest things I have done to date,

but good things do not come from comfort zones and this was an amazing experience. I hope you continue to lead this program as all of you have been paramount in the execution of its success.

Finally, I want to thank my family and friends. Ma y pa, gracias por todo lo que me han dado en esta vida. Desde pequeno me han facinado los carros, y utedes siempre me enesanaron (y dejaron) que siguiera mis suenos. Este es el fruto de ese soporte y ese sueno. Ahora es mi tiempo de repagarles por todo.

To Maggie O'Connor, thank you for always being there to hear out my frustrations and celebrate my successes. I am lucky to have in my life such a kind and caring person. Thank you for always taking time to look at my work and give me feedback, you definitely made this experience much better even though we were far apart for most of it. I can't wait to see what the future has in store for someone with so much passion, and commitment to her work and life itself. Lastly, to all the people I have met along this program; Caleb, Kyle, the guys from Italy; Carlo, Salvo, and all the others that I crossed paths with, thank you. I take with me memories and stories that will last me a lifetime.

This work has been supported by the department of Mechanical, Automotive and Materials engineering department at the University of Windsor, Politecnico di Torino, and Fiat Chrysler Automobiles.

Table of Contents

List of Figures

List of Tables

List of Acronyms

Chapter 1: Introduction

1.1Background History:

The subject of vehicle emissions has been a growing topic of concern as society realized the health and environmental harm these pose to the communities and the world at large. From respiratory complications and other illnesses, to the degradation of the ozone layer, these two major impacts of fuel exhaust are the key drivers in improving engine technology in automotive companies. As emissions standards become stricter, this improved vehicle and engine technology will help companies deliver a more healthy and eco-friendly product.

Automobile emissions refer to the exhaust gas from engines that contain mainly carbon dioxide, carbon monoxide, lead, nitrogen oxide, and hydrocarbons. As technology evolved, companies found different ways to cope with these elements by targeting them either directly or indirectly. The effects of these harmful pollutants were brought into light with incidents such as the Great Smog of 1952 in London England, as well as the first episode of smog noticed in Los Angeles during 1943 [1]. During the 1940's and 1950's, this phenomenon was thought of being the result of major factories, however, it would later be discovered that automobiles were a major contributor to this escalating issue [1].

Once automobiles were identified as a key contributor in air pollution, the U.S. congress passed the Clean Air Act in 1970 and with it formed the Environmental Protection Agency (EPA). The EPA then possessed the legal authority to regulate pollution from all forms of industry including transportation. In Europe, countries also created Clean Air Acts, however it wasn't until the 1990's where common emissions standard known as the European Union Standards (known as the Euro) and California Air Resources Board (CARB), would take the role of enforcing emission control on different modes of transportation.

Of the pollutants that both of these regulations control, particulate matter (PM) is emitted in solid or liquid states as supposed to a gas form such as Carbon Monoxide (CO) or Nitrogen Oxides (NOx). Since PM can be considered anything from dust on the road to particles resulting from a combustion process, the main focus of this thesis will

be on those emitted by an exhaust system. Over the years, studies in emission control demonstrated the effects these small particles can have on the environment and more specifically, the harm they can cause to human health.

The particles generated from the combustion process are also known as soot. In the automobile sector, soot refers to the formation of material composed mainly of carbon resulting from fuel rich areas in the engine cylinders. Furthermore, they are of major concern to human health due to their ability to penetrate deep into the lungs and in the blood stream [2]. As it can be seen in Figure 1, soot particles vary in size, from nanometers (nm) to microns and can therefore be categorized into three major classes; Nuclei, accumulation and coarse mode [3]

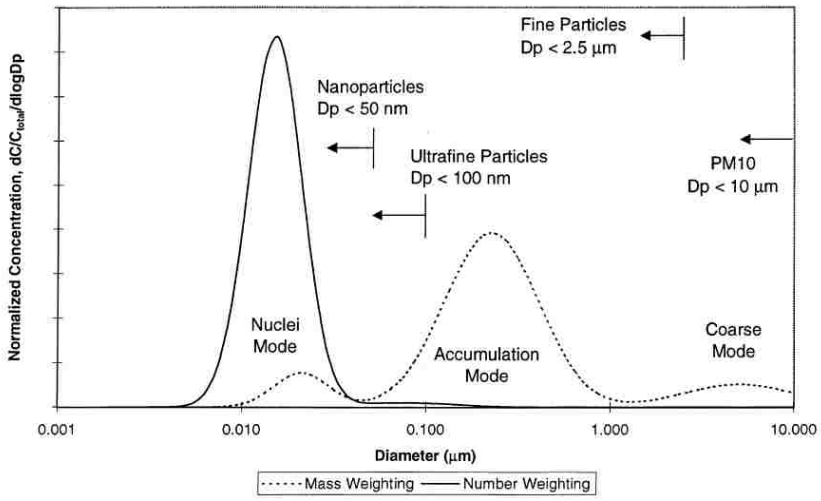

Figure 1: Typical Size Distribution for Exhaust Particles [3]

As technology evolves, emission standards become more stringent, particle sizes that weren't considered in previous year's regulations will then be targeted. Initially, manufacturers of gasoline engines had little concern over PN (Particulate Number) emissions as they did not produce much soot, and it was Diesel engines and their method of combustion that was responsible for most of these emissions. However, changes to gasoline engine technology in recent years have, in part, caused gasoline engines to emit a significant amount of soot particles and raise concern within the industry.

Currently, most gasoline engines on the road use a method of fuel injection called port fuel injection, or PFI. The principle behind PFI relies on the location of the fuel injectors being placed in the intake ports of the engine as well as when the injection is performed (intake stroke). However, this method of injection is being gradually phased out and slowly replaced by gasoline direct injection (GDI) engines. The key difference between the two can be observed in Figure 2.

Figure 2: PFI and GDI Comparison [4]

As it can be seen, the injector placement in the engine has been changed, and with it new advantages and disadvantages have risen. Further explained in section 2.2, this injector location has caused better fuel economy, better power output, and unfortunately, more PN emissions than its PFI counterpart [4]. Because of this issue in new engine technology, the nuclei mode (soot particles <50nm) seen in Figure 1, is being examined extensively in order to determine the composition of these particles and how they can be managed and reduced for future emission regulations.

1.2Hypothesis

The number of particles in the nuclei mode, particularly those of 23nm and below, may vary due to different engine operating conditions (Cold starts vs normal operation) and transient-intensive drive cycles. The major contributor to these types of particles is the unburned fuel left after the combustion process as well as the lubrication oil present during normal engine operation.

1.3 Research Methods

This work sets out to prove this hypothesis through the testing of various GDI engines as well as one PFI equipped vehicle. The change in PN will be examined by submitting the vehicles to different homologation and non-homologation cycles.

In order to measure these particles, multiple instruments will be used and compared against each other for correlation. Two homologation standard condensation particle counters (AVL489 and Horiba MEXA2000SPCS), one fast particulate spectrometer (DMS 500), and one Induced Current Aerosol Detector (prototype in development). The variation in cycle intensity will aid in determining the variation of sub 23nm particles being produced at different stages of the cycles tested (I.e. Cold Start and Normal Vehicle Operations).

In order to determine whether oil entering the combustion process is having an effect in the nuclei range, specific oil consumption cycles were tested on a PFI engine along with a Lubrisence oil consumption system to observe whether there was a correlation in oil consumption and sub 23nm PN emissions.

Chapter 2: Literature Review

2.1 Emission Regulations

Emission regulations are the primary drivers in clean engine technology. These regulations are based on standards such as the EPA (Environmental Protection Agency) in the United States and the European Union standards called the Euro. These standards provide manufacturers with thresholds on the different pollutants vehicles can emit, and are sometimes separated into vehicle classes (cars and trucks), fuel types (diesel and gasoline) and method of injection (GDI and PFI). Figure 3 shows the progression of the Euro standards, representing NOx and PM emissions in mg/km.

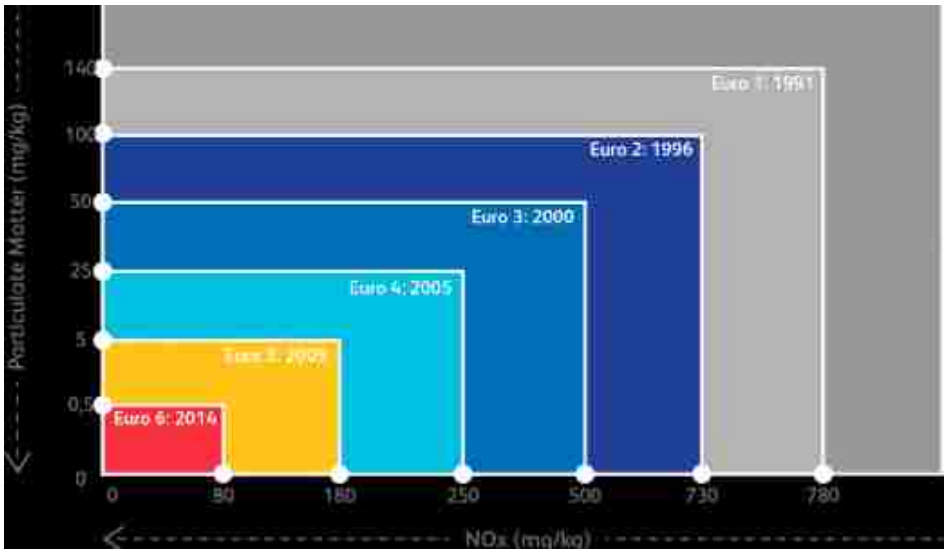

Figure 3: History of Euro Emission Standards [22]

As it can be seen in Figure 3, these standards increase by approximately a single magnitude every few years. When it comes to direct injection engines, as of Euro 6c implemented in September 1, 2017, all new vehicles must meet a particulate emission standard of 6x10^11 particles/km [5] which include only particles 23nm in diameter and above.

With PN standards becoming stricter for GDI engines, these limits will be lowered both in quantity and particle size. Manufacturers will need to further study what these particles are composed of and what can be done in order to combat them. As the

technology currently stands, it will be difficult for GDI engines to keep meeting these standards in the near future; therefore, different technologies will need to be implemented in order to stay compliant with these regulations.

2.2 Gasoline Direct Injection Engines

Gasoline direct injection is a moderately new way of injecting fuel which is changing the landscape of engine technology. From the way ignition occurs, to increase market share of gasoline engines [6], to different emission concerns, GDI engines are expected to overtake the current form of injection (PFI) by 2020 [7].

The increase in popularity of GDI engines over PFI is as a result of fuel economy and power output. Relocation of the fuel injector from the intake port to the combustion chamber has allowed manufacturers to improve fuel economy and engine performance in different ways. Higher injection pressures of 100+ bar in GDI Vs 5 bar in PFI allow for better fuel atomization, which in turn, results in a charge cooling effect [8]. This charge cooling effect at the start of the compression stroke allows for higher compression ratios and increases an engines torque and fuel economy by containing the combustion in a reduced space [9]. Moreover, liquid film formation on the back of the intake valve and wall wetting in the intake port cause metering errors and fuel delivery delay in PFI [10], once again adding to the fuel economy downside and making GDI the more desirable option.

There are different modes and configurations in which direct injection can be arranged, both having their advantages and disadvantages. Defined in Figure 4 are the modes in which direct injection vehicles can be operated, while Figure 5 demonstrates how injectors can be placed and operated according to desired manufacturers' specifications.

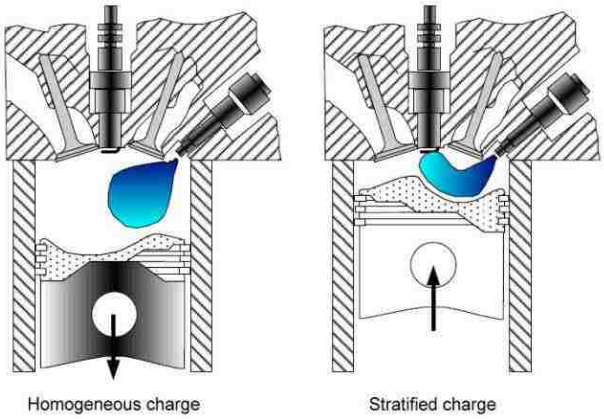

Figure 4: GDI Operating Modes [12]

These modes (Figure 4) represent the timing of the combustion according to engine operation. In the stratified mode, late injection techniques are used during the compression stroke in order to achieve a rich burn close to the sparkplug, and a lean mixture further away [10]. This method also takes into consideration the position of the sparkplug with respect to the injector. Centrally located injectors along with the stratified mode help reduce knock by promoting a shorter path for the explosion from the center of the cylinder. [8]. In the homogeneous charge mode, fuel is injected early in the intake stroke, promoting a more efficient mixture of the air and fuel. The improved mixture promotes charge cooling, resulting in a great number of benefits such as possible increase in spark advance and compression ratio due to lower octane requirement [11]

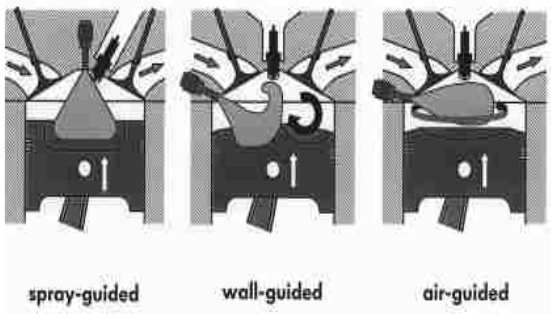

Figure 5: GDI System [12]

The combustion systems shown in Figure 5 can be distinguished by the type of charge stratification obtained. Spray-guided systems obtain this mode based on fuel atomization and fuel droplet distribution. This system is preferred over its wall and air-

guided counter parts due to its efficiency which arrives from the sparkplug and injector proximity placement [10]. Wall-guided systems achieve a stratified charge through the interaction of the fuel spray and the top of a specially designed piston head. This can cause fuel deposits on the piston, leading to unburned fuel and therefore an increase in HC (hydrocarbon) and PM emissions [8]. Air-guided systems achieve stratification through the interaction of fuel spray and charge air. The speed of the air is controlled by air baffles within the manifold, which helps eliminate the wetting of the piston head and cylinder experienced in the wall-guided system [12]. The drawback of this system is the placement of the injector, as it is not as efficient as the spray guided method.

Overall, the switch to direct injection along with turbocharging has allowed manufacturers to downsize their engines and increase both power and fuel economy [13]. However, this method does have its disadvantages. As previously mentioned, the change in injector placement has caused a major topic of concern never faced before by gasoline engines. The increased in power and fuel economy experienced with this method come with a penalty in particle number emissions. Reduced mixing time between air and fuel within the combustion chamber has caused GDI engines in recent years to emit more particles than diesel engines [6].

2.3 PM Formation

As it can be seen from Figure 6, soot particles originate with the formation of nucleation particles often derived from incomplete combustion and fuel rich zones. Under the absence of oxygen and high temperatures, the material goes through a chemical and physical separation into different molecules, a process known as Pyrolysis [14].

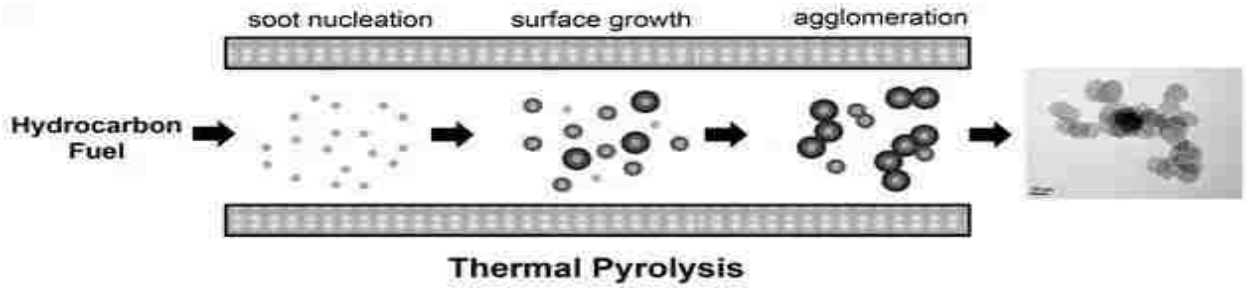

Figure 6: Soot particle Growth [15]

Further collisions of these particles along with Polycyclic Aromatic Hydrocarbons (PAH's) coagulate to form soot particles. (PAH's are a class of chemicals that occur naturally in coal, crude oil, and gasoline. They also are produced when coal, oil, gas, wood, garbage, and tobacco are burned). Large particles develop following these collisions, and as this process continues, metal found in lubrication oils as well as engine wear may adhere to the molecules, forming the branch like structure observed above.

Parameters that can affect the characteristics of soot particles are those of fuel composition, injection timing, combustion temperatures and fuel injection pressure, leading to the complex structure observed.

2.4 GDI Engine After treatment: Three-way Catalytic Converter and EGR

As previously mentioned, automobile emissions include other pollutants besides soot that are created through the combustion process. In order to combat them and be compliant with regulations, a three way catalytic converter was invented. A three way catalytic converter (TWC) is pictured below.

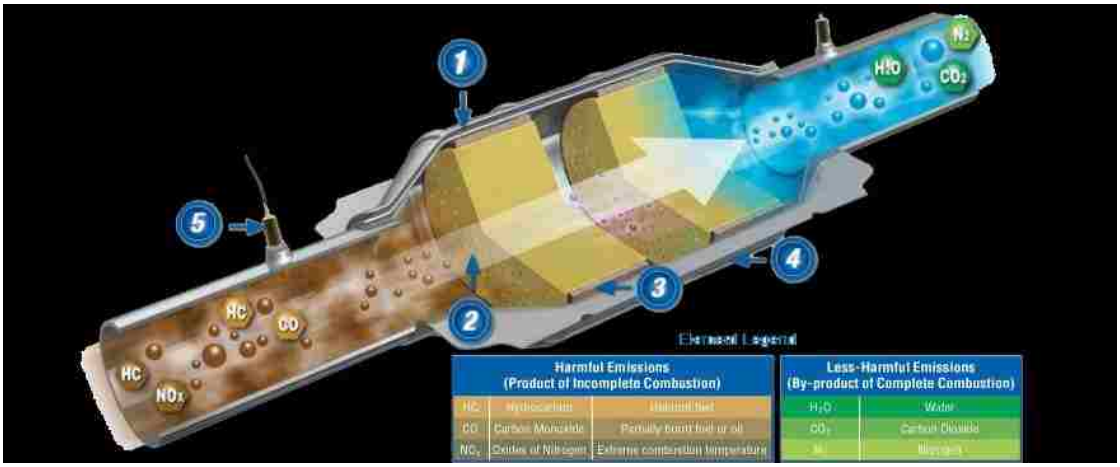

Figure 7: Catalytic Converter Process [15]

The process is simple yet effective. Harmful pollutants such as CO, NOx, and hydrocarbons (HC) enter the TWC, and with use of catalysts such as platinum, rhodium and palladium (the yellow brick-like structures displayed in the figure), these harmful emissions reduce and oxidize into less harmful ones such as carbon dioxide and nitrogen [16]. This method of reducing contaminants resulting from incomplete

combustion has been implemented for years. Combined with improved engine technology such as EGR (Exhaust Gas Recirculation), it has helped automobile manufacturers stay compliant with emission regulations targeting specific pollutants such as, CO, NOx and HC.

EGR consists of rerouting a portion of exhaust gas back into the combustion chamber through a cooler and a valve, as seen in Figure 8.

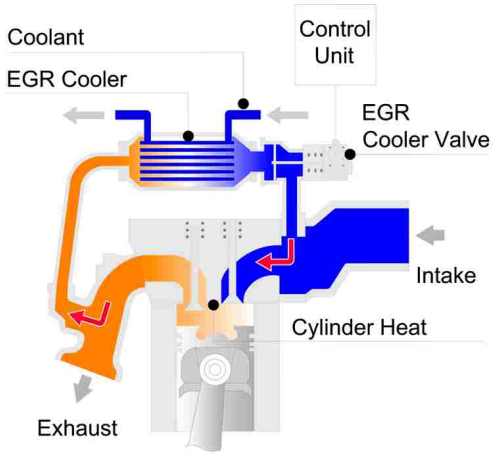

Figure 8: EGR Configuration [17]

This method has allowed manufacturers to reduce NOx emissions by cooling the combustion process. The recycled air from the exhaust that enters the combustion chamber is inert, and takes up some of the volume that would otherwise be filled with fresh air [17]. Since the exhaust gas will not ignite, this makes the combustion process cooler. This cooling allows for lower NOx emissions since this pollutant cannot be formed below 2500°F [17]. Although both of the aforementioned aftertreatment solutions have made great contributions in gaseous emissions reduction, these methods are not able to reduce the solid particle matter (In the nuceli range) emitted during the GDI combustion process.

2.4.1 GDI Engine After treatment: Gasoline Particle Filter (GPF)

One way manufacturers are trying to combat PN emissions in GDI engines is with the implementation of a Gasoline Particle Filter (GPF). This product stemmed from the performance of a Diesel Particle Filter (DPF) in terms of capturing soot which has been in use for many years. A DPF functions by using porous ceramics and catalysts to

collect and burn the soot, and has demonstrated filtration efficiencies in excess of 90% [18]. The most common design of the DPF is the Wall-flow monolith, observed in Figure 9. Although its operation is similar to that of a TWC, plugged alternated channels force the exhaust flow to pass through the porous barriers and act as a filter.

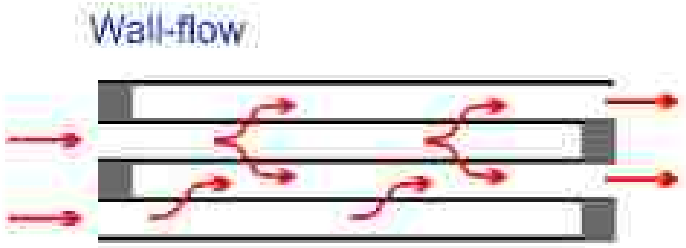

Figure 9: Wall-Flow Monolith [19]

Just like for the Wall-Flow DPF, gasoline particle filters use three mechanisms to trap soot; interception, impaction and diffusion. These three methods all revolve around the size of the particle, and as these particles encounter the filter media, they behave in different ways. Smaller particles do not move uniformly along the gas streamlines, causing them to diffuse from the gas to the collecting body [19]. Bigger particles may follow the streamline and strike the collecting material causing them to be captured. Figure 10 demonstrates a graphical representation of this process.

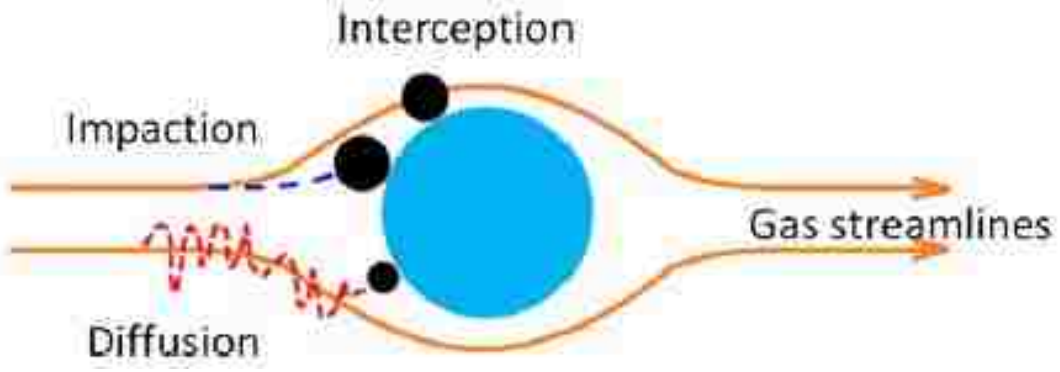

Figure 10: Filtration Mechanism for particles in GPF [20]

There are multiple configurations in which a DPF can be placed and operated. Figure 11 outlines the possible configurations the filter could take when paired with a TWC;

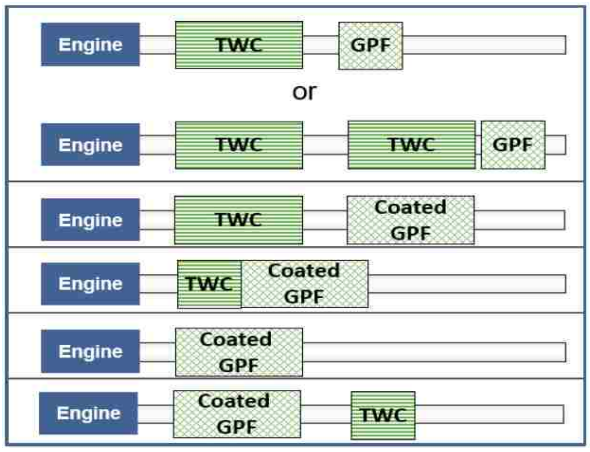

Figure 11: Possible System Architectures [21]

Some of the examples above include a coated GPF, which allows some substitution of the TWC volume. By coating the GPF, its size could be reduced and therefore the implementation cost could also be decreased [20].

Just like DPF's, gasoline particle filters have shown the ability to provide filtration efficiencies in the order of 80-90% [19]. However, these numbers are achieved after a certain amount of soot "cake" has been built up in the filter to help capture the incoming PM. In a relatively clean exhaust system with a new GPF, the filtration efficiency can be expected to be approximately 60% [20]. Although it has been slowly introduced into the market by some manufacturers, this initial efficiency drawback along with added cost to a vehicles exhaust system has permitted the GPF from being fully incorporated into the industry.

2.5 Contributors to Particle Emissions - Fuel

One of the main issues with regards to PM emissions in all types of engines is their material composition. Unlike gasoline PM, soot produced by diesel engines has been an ongoing area of study as compliance with increasing emission regulations has been a major hurtle for engine manufacturers. From these studies, techniques were adapted in order to conduct the similar analysis on GDI soot. The following section outlines some of the studies that have contributed to this subject.

To determine what type of contribution the fuel used in a vehicle truly has on the composition of soot particles, different fuels were used in this experiment conducted by Maier et al (2015). The fuels hydrogen and methane were compared to CEC (Coordinating European Council) fuel and the engine was operated at 4 different mean effective pressures to determine the impact different engine loads had on the soot emitted. The theory behind this experiment revolved around the carbon atoms found in each fuel. Soot emissions from methane and hydrogen were expected to be less (these fuels contain less carbon atoms) than the CEC reference fuel, therefore any remaining particulate emissions tend to include other sources such as metal from engine wear, lubricating oil, intake air, etc. [21].

For the purpose of keeping variables equivalent, the different combustion characteristics of hydrogen and methane were accounted for by diluting the intake air with nitrogen and matching the pressure to those of gasoline operation [21]. This resulted in an experiment which concluded that for particles smaller than 10nm, gaseous fuels produce similar PN (Particle Number) to those of gasoline. Furthermore, particles larger than 30nm were hardly detected when gaseous fuels were used, and the difference between the gaseous fuels and CEC increased as the load of the engine increased. This study suggested that at the ultrafine level of 10nm, for the most part, particles do not originate from the fuel itself [21].

2.5.1 Contributors to Particle Emissions – Metal

Apart from the common gaseous emissions that engines produce, a major concern for the automotive industry and most importantly, society's health is the emission of Nano size metal particles. These particles can be derived from sources such as the abrasion between piston rings and cylinder, bearings, valves and cams, catalysts coatings and lubrication oil additives [22]. As previously mentioned, particles of this size are of particular concern due to their ability to penetrate deep into the body. Soot particles below 200nm have the ability to deposit in the alveoli, with increasing quantities as diameter is reduced [22]. Moreover, the metal oxide particles resulting from IC engines can cross the blood brain barrier as well as the placenta and enter into the fetus [22].

Previous studies by Hannoschock [23] have shown that metal abrasion particles are more stroke reversal dependent (number of revolutions per minute (RPM)) rather than based on the velocity of piston. These findings explain why SI (Spark Ignition) engines that usually operate at higher RPM produce twice as much metal particulate than Diesel engines [22]. These types of particles are more prevalent during periods of low lubrication such as cold start and short trips (urban driving). In a study conducted by Gautam M. (West Virginia University), various HDV (Heavy Duty Vehicle) tests compared Diesel engines both with and without a DPF to those against CNG (Compressed Natural Gas) fueled SI engines. It was found that the Diesel engines without a particulate filter emitted around 0.5mg/km of abraded metals such as Fe (Iron) and Cu (Copper), while those fueled by CNG emitted twice as much [24]. Once again, confirming metal abrasion particles are caused by number of cycles rather than speed of piston. It is important to note that while there is contact between moving metal parts there will always be a form of metal oxide emissions.

While abrasion in an IC engine can only be reduced and not eliminated, it is important to analyze which other components of the overall engine operation can be altered in order to reduce metal oxide emissions. As mentioned above, lubrication oils play a key role in these types of emissions. The metal additives in the lubricant provide several benefits to engine operation such as decreased friction, prevent corrosion, and clean deposits [22].

2.5.1 Contributors to Particle Emissions – Lubrication Oil

Apart from the metal that is abraded from the cylinder walls due to friction, the metallic additives in lubricant role may play a key role in Nano-size particle emissions. Under normal operation of an IC engine, trace metals can be vaporized and absorbed by soot particles. A study by De Petris et al. demonstrated that most often, these metal particles originate from lubrication oil that is spread onto the cylinder walls by the piston rings or that it enters the combustion chamber via reverse blow by of the rings [25].

Extended research has shown that there are five potential oil consumption sources that contribute to the overall oil consumption during normal engine operation of a spark ignition engine. These are outlined in Figure 12.

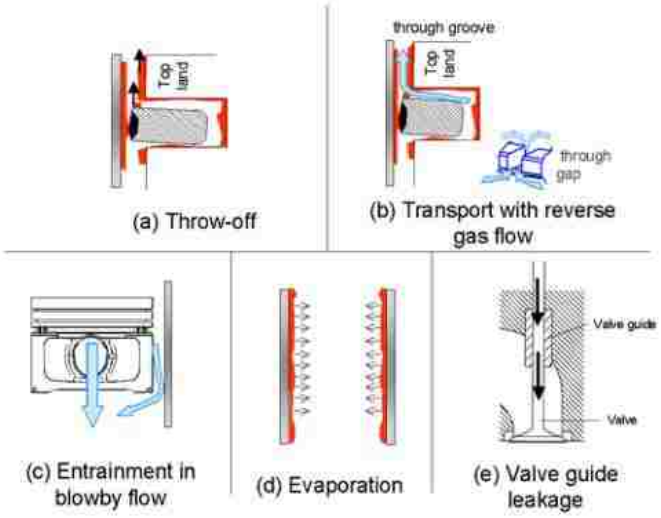

Figure 12: Schematic of Oil Consumption Sources [26]

Acceleration and deceleration of the piston assembly can cause oil throw off (Figure 12a) by mechanically transporting liquid oil film into the combustion chamber via Inertia forces. This type of oil consumption was found to be dependent on the accumulated oil film accumulated on the top land and ring [27].

Another way oil has been found to enter the combustion chamber is via reverse gas flow, observed in Figure 12b. In this mechanism, the pressure in the second land clearance (not pictured) can become greater than that in the combustion chamber. This

Increase in pressure causes a reverse flow (which includes liquid oil particles and mist) back into the combustion chamber.

Figure 12c demonstrates consumption of oil via blow by. In this scenario, small amounts of fuel, air, and oil escape past the piston and enter into the crankcase. These gases then enter once again into the combustion chamber via the intake manifold. PCV (Positive Crank Ventilation) systems have been implemented to serve both as a ventilation system and pollutant control device.

Oil evaporation from the piston ring liner (Figure 12d) has been found to contribute to the oil consumption, more specifically during periods of severe operation of the engine, when the temperature of the engine components is high [27]. Lastly, Figure 12e outlines the oil consumption caused by valve leakage. Although it this source has been greatly reduced in modern engines (better tolerances), below atmospheric pressure in the manifold caused oil to escape through the valves.

A study conducted by Miller et al. set out to examine the impact oil had on a hydrogen powered engine. It was found that Nanoparticles in the range of 5-50nm were usually spherical in nature and composed mainly of Iron or a combination of Iron and Carbon. The Iron rich nanoparticles were said to largely be self-nucleated early in the combustion process while the temperatures were high. The carbonaceous nanoparticles were said to be originating from nucleation of volatile hydrocarbon vapors as they exited the engine [28].

Particles in the range of 30-300nm however, were observed frequently in the tests performed and were composed mainly of elements found in lubricant oil such as Calcium, Phosphorus, Zinc, and Magnesium. Although the researchers concluded the particle formation was unclear, it was thought that they were residue particles created from unburned oil droplets heated enough to evaporate most of the hydrocarbon species [28].

This work sets out to contribute to the understanding of sub 23nm soot particles derived from oil consumption by submitting a PFI engine to specific oil consumption cycles and comparing spikes in emissions to those of oil consumption.

2.6 Particle Measurement Instrumentation Used - North America

Within the purpose of this thesis is the validation of PN measuring instruments, particularly the APC489 by AVL and the DMS 500 by Cambustion. The much stricter standards of Euro 6 and CARB have forced manufacturers to examine the current method of particle measurement and the instruments being used. Although exhaust samples (either for certification or research) can be taken from multiple sources along a vehicles exhaust system and through different dilution procedures, all the instruments used in the industry set out to accomplish a common goal; collect the most accurate number of particle emissions possible. This section will concentrate on two instruments, one used for homologation and one used for calibration. The goal is to examine how well they compare to one another when measuring PN's through different engine cycles.

One of the most popular instruments in the industry used for the certification of a vehicle is AVL's APC 489 particle counter (Figure 13). This Instrument is referred to as a CPC (Condensation particle counter) due to the way it collects and counts particles. Sampling can be done both through a "raw" or diluted exhaust sample. The sample first flows through a volatile particle remover (VPR) and then through the condensation particle counter where butanol is condensed onto the particles (in order to enlarge them). After particles are detected, they are counted using the light scattering method. [29].

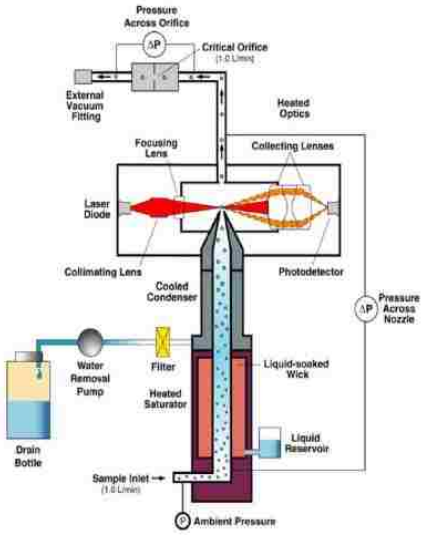

Figure 13: AVL Particle Counter (Product Guide)

Cavina et al. (2013) investigated the performance of both the instruments previously mentioned along with other popular apparatuses to determine how comparable they were to one another. Figure 14 illustrates the set-up of this experiment;

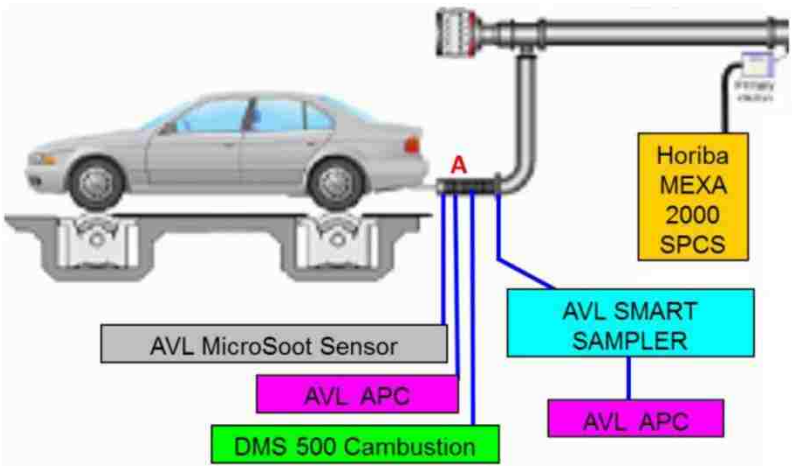

Figure 14: Experimental Set-Up [27]

As it can be observed, the APC was used both in a raw exhaust configuration and in a 2nd diluted arrangement. It is important to note that for these test, the benchmark results were those of the Horiba MEXA 2000 SPCS instrument, another apparatus commonly used in the industry for certifying vehicles. Test variations included different dilution ratios (DR), as well as stationary and transient cycles with the goal being to examine how the instruments results variated from one another.

The various tests that were performed in the stationary mode for all the instruments can be observed in Figure 15. All of the instruments tested were compared to the reference measurement instrument as well as one another. When compared to the reference instrument, the APC had a high correlation factor as can it can be seen in Figure 16. Two linear regressions were calculated for each analysis, one of them obtained by imposing null intercept on the y-axis. The R- squared value can be interpreted as the proportion of the variance in y attributable to the change in x. It is defined as the square of the correlation coefficient. [30]

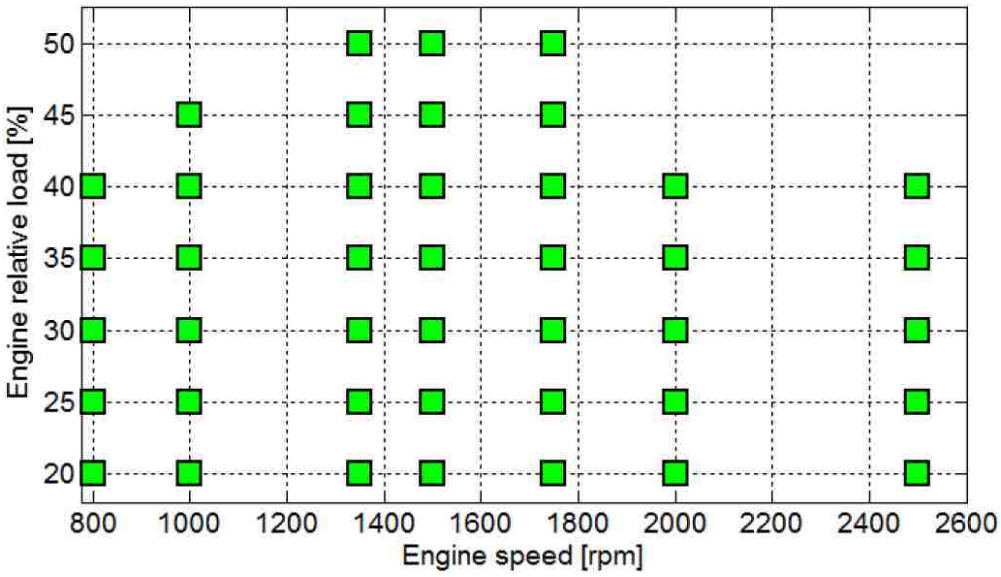

Figure 15: Steady State Engine Operating Conditions (Cavina et al. 2013)

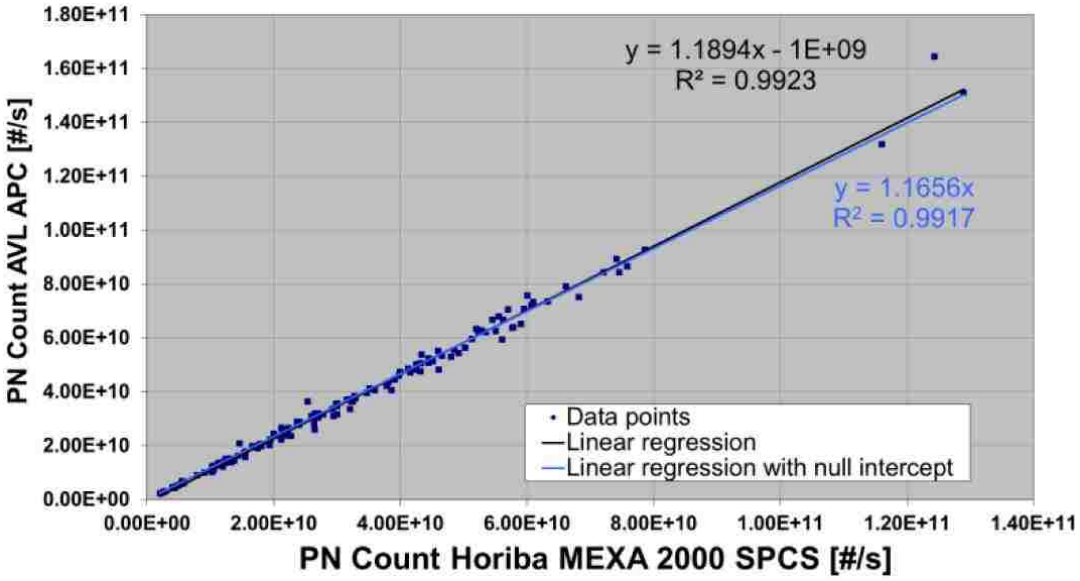

Figure 16: Correlation under Steady State Conditions (Cavina et al. 2013)

As it can be observed by the correlation factor, the APC demonstrated very similar results to those of the benchmark instrument. This experiment also included transient tests in order to examine the instruments accuracy to engine load, speed, and dilution factor variations. The results for the APC can be seen in Figure 17 and Figure 18.

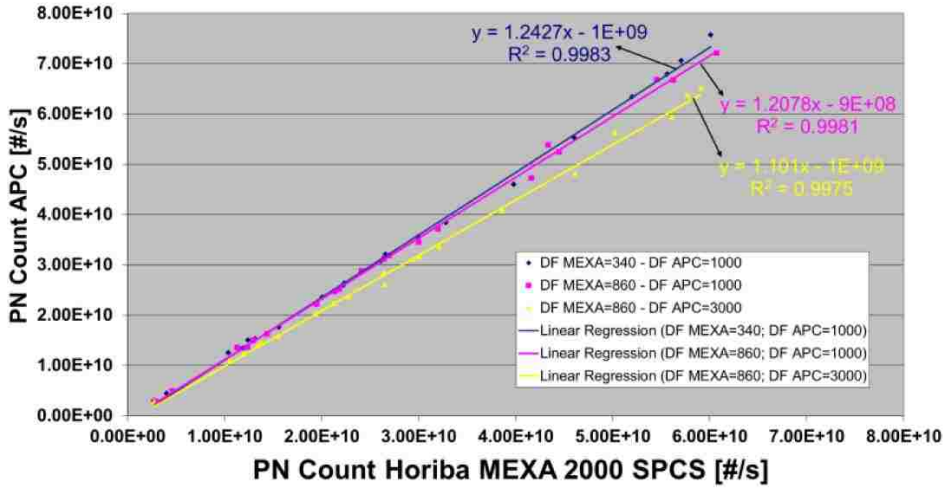

Figure 17: Correlation Analysis for Different Dilution Factors. (Cavina et al. 2103)

Figure 17 represents the APC's capability to measure particles when dilution ratios are changed under steady state conditions. As it can be observed by the yellow line, the sensitivity of this instrument is greatly affected when dilution factors are changed. The researchers concluded this behavior was due to the uncompensated pressure levels found in the CPC of the instrument. [30]

Figure 18 and Figure 19 illustrate an overall comparison of the instruments involved in the experiment, and their capability to measure particle matter emissions under transient conditions, more specifically, a NEDC (New European Driving Cycle) test.

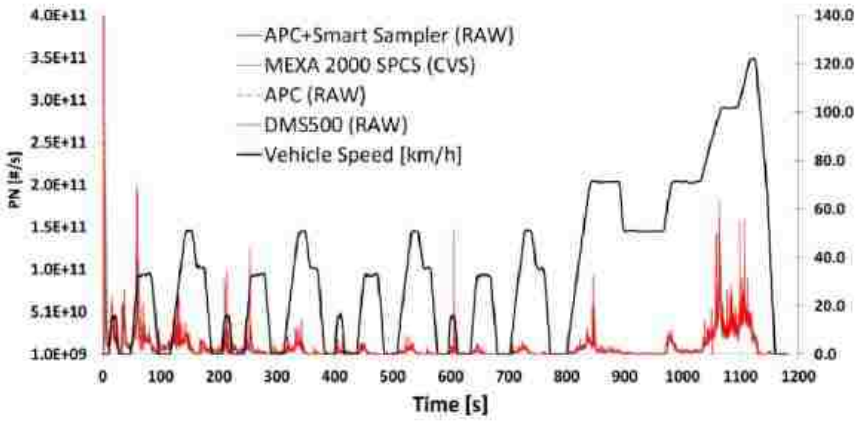

Figure 18: NEDC Results. (Cavina et al. 2013)

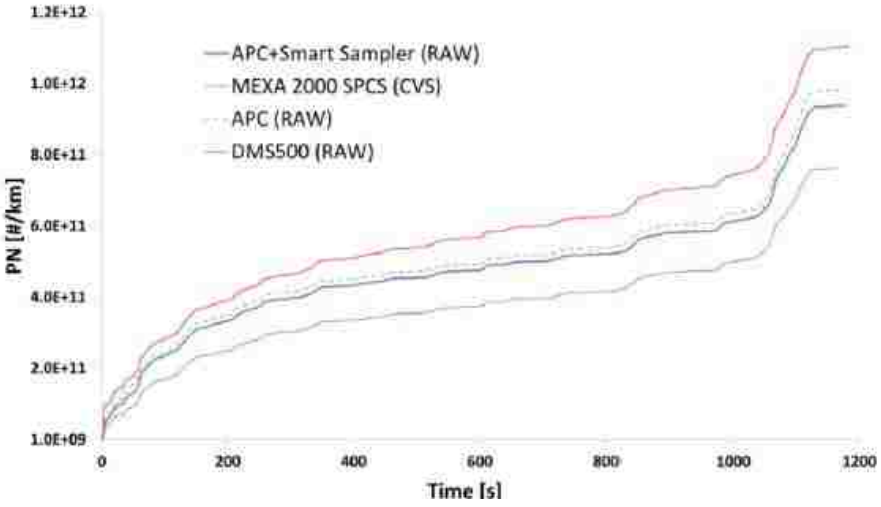

Figure 19: NEDC Results: Cumulated Particle Measurement

As the two previous figures demonstrate, the APC behaved much like the benchmark instrument when examined in a transient mode, while the DMS 500 tended to overestimate the particles present. The following section will outline the inner workings of the DMS 500 and why these overestimations might be occurring.

The DMS500 made by Cambustion is referred to as a fast particulate spectrometer as supposed to a condensation particle counter such as AVL's APC. As particles flow into the machine, a unipolar corona charge is placed on the particles which closely match their geometry. Particles then travel along a high voltage rod (Figure 20) and are repelled towards the grounded electrometer rings. The electrometers then measure the current given by Equation 1 where I_D is the deposited current and I_I is the Induced current.

$$I = I_D + I_I \quad [1]$$

The Induced currents in the equation are problematic since they lead to measuring errors in the instrument due to the fact the algorithms used rely solely on the deposited currents [31]. To combat this, Cambustion has developed different strategies, the most notable being the one physically used in the instrument, which is a grounded screening electrode placed in front of the electrometer rings to reduce the induced currents.

Finally, when the particles yield their charge to the electrometer amplifiers, the resulting currents are translated by the user-interface into particle number and size data.

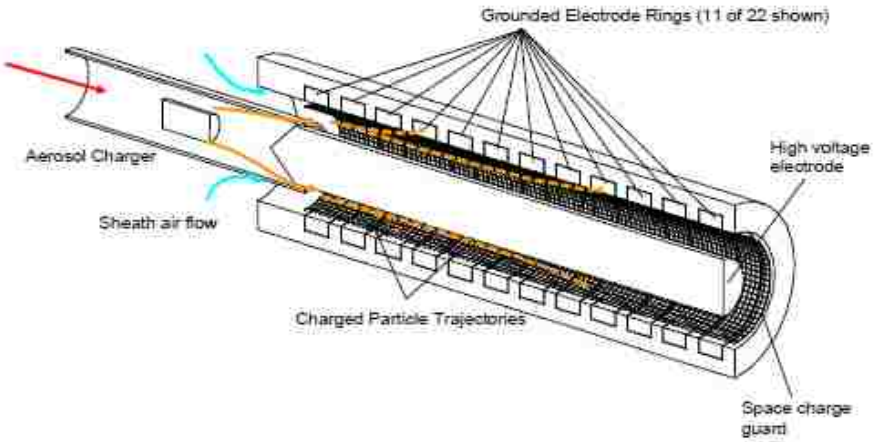

Figure 20: DMS 500 Classifier (DMS 500 User Manual)

As previously mentioned, Cavina et al. 2013, also included this instrument in its experiment. Figure 21 illustrates the DMS 500 correlation analysis results under steady state conditions when compared to the MEXA 2000 SPCS.

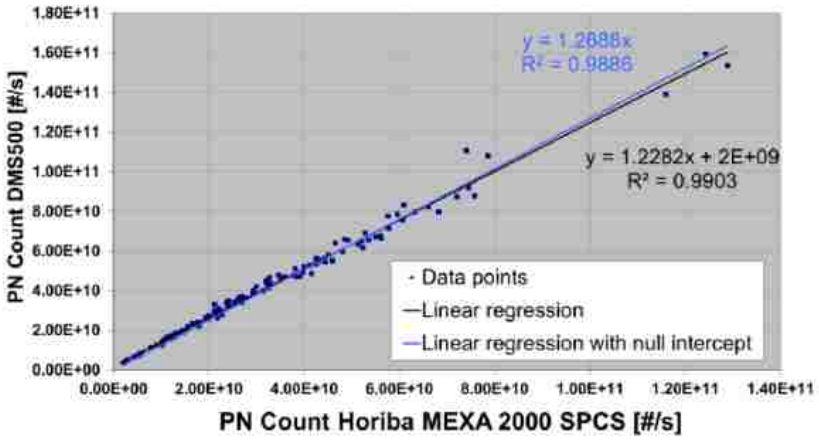

Figure 21: Correlation Results, DMS 500 Vs. MEXA S2000 (Cavina et al. 2013)

Once again, the high correlation factor demonstrates the DMS 500's Accuracy when counting precise number of particles in a steady state environment. However, when this instrument was submitted to transient test conditions (Figure 18), it tended to overestimate the number of particles present compared to its counterparts. The

researchers concluded this could be to the faster dynamics of the DMS which would lead to more particle detection.

The experiment conducted by Cavina et al. provided worthy insight into the accuracy of some of the most standard instruments used in the industry for certification and calibration of vehicles. It is important to note that Cambustion's DMS 500 is not a certification instrument, but simply used for its fast response time when calibrating vehicles as well as its ability to distribute this particle into different size ranges. Furthermore, there have been multiple sources ([30], [32]) outlining the overestimation of the DMS 500 when compared to other instruments which prompts a valuable research point for this thesis. If this instrument can be further validated through experiments involving soot composition and size, it would aid immensely in the confidence automobile manufactures have when certifying vehicles and the time spent calibrating them.

2.6.1 Particle Measurement Instrumentation Used- Europe

A new type of particle spectrometer has been developed by multiple partners in the European Union. The main goal of this new apparatus is to achieve comparable results to the standard homologation instruments, as well as serve as a frontrunner in the area of PEMS (Portable Emissions Measurement System) Instrumentation.

The new instrument, named the ICAD, stands for Induced Current Aerosol Detector. Much like the DMS500 preciously described, it relies on chargers to detect the number of particles being emitted. Figure 22 is a schematic drawing of the new instrument.

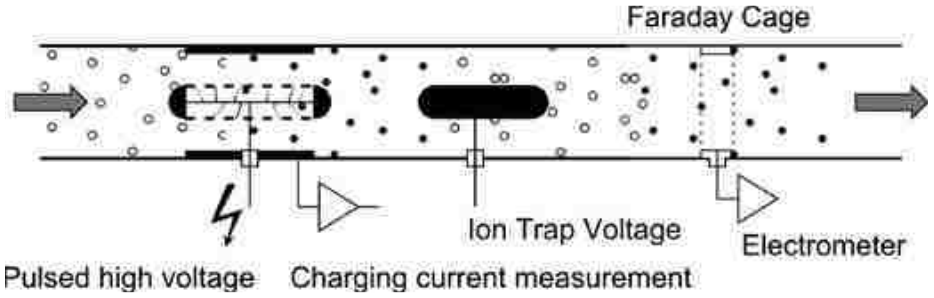

Figure 22: Inner Workings of the ICAD [31]

This instrument relies on Gauss' law and point charges. Gauss' law states that the volume integral of space charge (Q) divided by the permittivity of vacuum (ε_0) is equal to the surface integral of the electric field (E) for any surfaces surrounding this charge:

$$\oint_V \frac{Q}{\varepsilon_0} = \oint_{dV} \vec{E} * \overrightarrow{dA} \qquad [2]$$

Much like the DMS500, the particles are charged as they pass through the instrument. Once a space charge (Q) is placed in the Faraday cage, the electric field outside the cage is shielded by it (E=0 outside the cage). By constructing a surface that surrounds the cage, the right side of Equation 2 is equal to zero, and therefore an opposite and equal charge ($\acute{Q}$) must exist on the cage($\acute{Q} = -Q$) [31]. This negative charge is referred to as the image charge.

Since the faraday cage is grounded, a current flows between ground and cage, which is induced by the space charge inside the cage. This induced current can be measured with an electrometer, and once again, it is proportional to the rate of change of the space charge inside the cage. The key difference between fast particulate spectrometers like the DMS500 and the ICAD is that the DMS500 uses the deposited currents produced by these particles whereas the ICAD uses induced currents.

Due to the novelty of this instrument, there is little research on its performance and accuracy with regards to vehicle emissions. However, the Aerosol & Particle Technology Laboratory (APTL) in Thessaloniki Greece, conducted an experiment where the ICAD was compared to a CPC instrument using CAST (Combustion Aerosol Standard) generated particles. Figure 23 is a schematic diagram of the experimental setup.

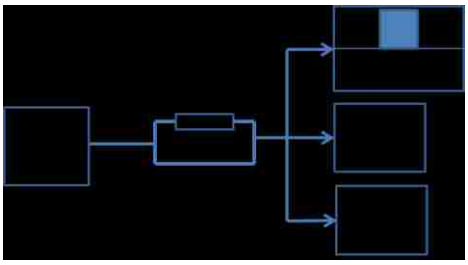

Figure 23: Counting Efficiency Setup

The CAST had a set particle diameter of 71±4nm and when necessary, the generated particles were catalytically pretreated (OxiCat setup) in order to remove volatile material. Moreover, the ICADS were fitted with a neutralizer in order to reduce electrostatic losses of particles within the tubing or other surfaces and to gather reliable data since the instrument is based on electrical mobility.

The experiments showed good linearity when compared to the CPC as Figure 24 shows. It was also determined the neutralizer improves the slope of the graphs, however, the researchers concluded that counting efficiency and linearity campaigns showed differences, and repeatability tests are required.

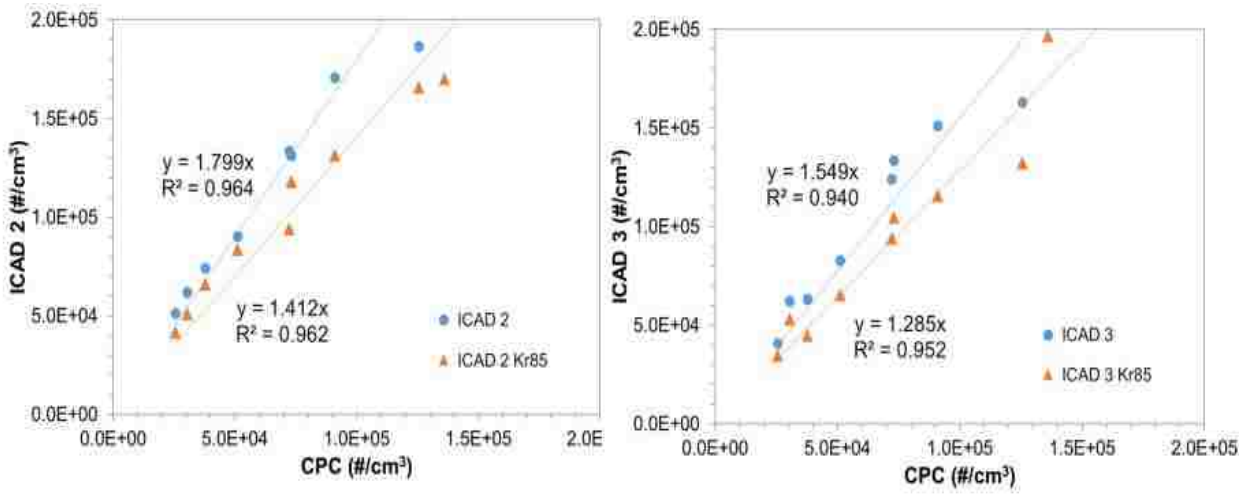

Figure 24: ICADS vs CPC

This work sets out to build on previous experiments like the one previously mentioned, by testing the ICAD both in a rolling chassis dynamometer as well as an RDE cycle in a PEMS configuration. The results (from the chassis dynamometer) obtained from the ICAD will be compared to those obtained from homologation instrument such as the Horiba MEXA-2000SPCS. During the PEMS testing phase of this thesis, the instrument will also be compared with the current PEMS system by Horiba (OBS one). Other instruments that were included in these experiments (but not analyzed in this work) include those of TSI's Engine Exhaust Particle Sizer (EEPS), and a differential mobility analyzer (DMA).

Chapter 3: Experimental Set-Up

3.1 Test Cell Set-Up- 2.0L GDI Engine

For this work, a 2.0L, 4 cylinder, GDI turbocharged engine was used. A listing of the engine specifications are given in Table 1.

Bore	**84mm**
Stroke	**90mm**
Compression Ratio	**10**
Valve Train	**DOHC, 16 Valve**
Turbo Charger	**Borg Warner**
Fuel Injector Position	**Wall Guided**

Table 1: GDI Engine Specifications

Tests were performed on a rolling chassis dynamometer. Figure 25 is a schematic diagram of the set up with the collection instruments located in the tailpipe of the vehicle.

Figure 25: Schematic of Experimental Set-Up

3.1.2 Instrument Set up – 2.0L GDI

A catalytic stripper (CS) was used with the DMS to remove volatile organic carbon (OC) fraction by oxidation to CO_2 and H_2O. The dilution of the DMS was varied in order to avoid over saturation of particles that may lead to early contamination in the start-up phase, and a heated line was used and set at 150°C to avoid condensation. The first dilution ratio was set at 5:1 as per recommendation of the manufacturer for raw sampling, while the second dilution was changed from 12:1 to 1:1 after PN levels declined in each cycle (usually after 90 seconds when the cold startup phase ended). The same procedure was conducted for all the tests with regards to the DMS. The AVL489 was connected after a flow meter and the dilution, which includes particle losses as an average of 30 nm,50 nm and 100 nm, the so called Particle number Concentration Reduction Factor (PCRFave), was 1000 (100 × 10).

3.1.3 Engine Operation- 2.0L GDI

The engine was operated in a homogeneous combustion mode for all cycles and at different loads according to the transients encountered. For the North America experiments, this engine was tested on WLTP (Worldwide Harmonized Light Vehicle Test Procedure) and RDE (Real Driving Emissions) cycles. Table 2 outlines the characteristics of the WLTP (The RDE cycle conducted for this campaign is considered confidential by the company involved therefore no specific data is included.)

	WLTP
Duration (s)	1800
Stop Duration (s)	242
Distance (m)	23194
Max Velocity (km/h)	131.3
Average Velocity w/o Stops (km/h)	56.25
Average Velocity with Stops (km/h)	51.76
Max Acceleration (m/s^2)	1.58
Average RPM Throughout Cycle	1417

Table 2: WLTP & RDE Cycle Characteristics

These cycles were chosen in order to examine different aspects in this project. These include the performance of the measurement instruments previously mentioned, which will be further discussed in Chapter 4, as well as the distribution in particle size and quantity when comparing the two cycles.

3.1.4 Particle Collection and Analysis – 2.0L GDI

For the 2.0L GDI tests described above, the test parameters were the same (aside from a variation in soak duration and the driver performing the test) and are outlined in Table 3 and Table 4.

	Successful RDE Tests Completed				
Test #	0501	0521	1022	1024	1026
Driver	Driver 1	Driver 1	Driver 2	Driver 2	Driver 1
Start Odometer	22551	22604	22785	22802	22820
Fuel Type	MS12899	MS12899	MS12899	MS12899	MS12899
Test Cell Temp (F)	75	75	75	75	75
Altitude set (ft)	930	930	930	930	930
Soak Duration (Hrs)	23	405	403	20	24
Dilution 1(DMS)	5	5	5	5	5
Dilution 2(DMS)	12 (after to 1)	12 (after to 1)	12(after to 1)	12(after to1)	12(after to 1)
Pre-Test Vehicle Temp	Cold	Cold	Cold	Cold	Cold

Table 3: RDE Test Parameters

	Successful WLTP Tests Completed		
Test #	0430	0502	0504
Driver	Driver 1	Driver 1	Driver 1
Start Odometer	22537	22559	22586
Fuel Type	MS12899	MS12899	MS12899
Test Cell Temp (F)	75	75	75
Altitude set (ft)	930	930	930
Soak Duration (Hrs)	350	22	23
Dilution 1(DMS)	5	5	5
Dilution 2(DMS)	12 (after to 1)	12 (after to 1)	12 (after to 1)
Pre-Test Vehicle Temp	Cold	Cold	Cold

Table 4: WLTP Test Parameters

As it was previously mentioned in Section 2.6, the DMS outputs a file containing different parameters pertaining to the test performed. In order to analyze the data, the outputs had to be converted into different units and then uploaded into proprietary software to allow further investigation of the results.

The DMS classifies the particles into 38 different “bins”, ranging from 5-1000nm and gathers data points every second. The concentration is expressed as a concentration

size spectral density in dN/dlogDp (/cc), with units of N (/cc). This allows easy integration over any size range to give a total particle concentration. dN/dlogDp is chosen as the quantity so the area under a graph gives N [33].

$$N = \int_{Dp_1}^{D_{p2}} \frac{dN}{dlog(D_p)} dlog(D_p) \quad [3]$$

In order to convert dN/dlogDp (/cc) to N/cc, the bins with the data of interest need to be added and divided by 16. This is because the data is separated by 16 bins every decade starting from 10nm to 1000nm. Since the size classes are logarithmically spaced, dividing by 16 (Equation 4) will result in the data being presented in terms of n/cc.

$$N = \frac{1}{16} \sum_{D_{p1}}^{D_{p2}} \frac{dN}{dlog(D_p)} \quad [4]$$

For these experiments, the data was separated into three size categories in order to examine how the different particles were affected throughout multiple cycles. These categories were 0-10nm, 10-23nm and 23-1000nm. After the data was separated into these categories, it had to be changed into N/sec, as this would allow a better representation of particulate emission, especially when comparing it to the results obtain from the CPC. Equation 5 was used to accomplish this.

$$\dot{X}\left(\frac{1}{s}\right) = \bar{X}\left(\frac{1}{cm^3}\right) \cdot \left(\frac{ft^3}{min}\right) \cdot \left(\frac{1min}{60sec}\right) \cdot \left(\frac{28316.84cm^3}{ft^3}\right) \cdot Temp\ C.F.(0.93) \quad [5]$$

Once the data was transformed into N/sec it was ready to be uploaded into the data plotting software and analyzed. This discussion of these results can be found in Chapter 4.

3.1.5 Measurement Uncertainties – 2.0L GDI

The uncertainty for the tests performed with the AVL489, CSV, tunnel and the DMS can be approximated using the error propagation rule:

$$\sigma^2(\mathrm{PN_{AVL}}) = \sigma^2(\mathrm{V_{cvs}}) + \sigma^2(\mathrm{C}) + \sigma^2(\mathrm{D})$$

The results yield an in uncertainty of 9-18%, which is mostly dominated by the uncertainty of the AVL counter (9-18%). The volume flow (2%) and distance uncertainty (<0.5%) were taken as the maximum error permitted in the Euro regulations of 2017. For the data acquired for the DMS, the manual claims a sample flow uncertainty of 10%, using the same value for distance as for the previous; this would yield an uncertainty of a little over 10%. It is important to mention that these values here are approximate, as there does not seem to be studies conducted on the uncertainty of experiments with regards to PN emissions. [34]

3.2 Test Cell Set-Up- 2.4L PFI

For this part of the experiment, a 2.4L Port Fuel Injection engine was used in an engine dyno cell. A DMS500 and an oil emission measurement system by Lubrisense were connected after the TWC in order to measure particle emission as well as oil consumption in g/hr. Table 5 below outlines the engine characteristics;

Bore	**88mm**
Stroke	**97mm**
Compression Ratio	**10.5**
Valve Train	**DOHC, 16 Valve**
Fuel Injector Position	**Intake**

Table 5: PFI Engine Specifications

Figure 26 demonstrates a schematic of the PFI and Lubrisesne experimental set up on the engine dyno cell. It is important to note that in this scenario, the DMS was not connected to a catalytic stripper. The reasoning for this is explained in the following chapter.

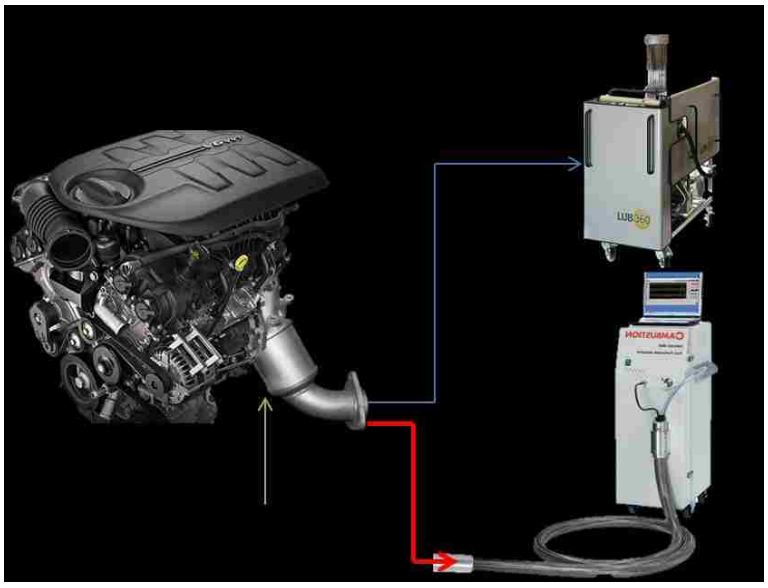

Figure 26: Schematic of PFI Experimental Setup

3.2.1 Particle Collection and Analysis – 2.4L PFI

For the collection and analysis of these experiments, the same procedure was followed for the DMS500 as previously described. In order to assess the oil emitted particles however, an oil emissions instrument produced by Lubrisense was used. This instrument provides a reading of the oil particles in g/h that occur throughout a given cycle by a method commonly known as TOF (Time of flight) mass spectrometry.

3.2.2 Engine Operation- 2.4L PFI

Oil consumption tests also contribute to the understanding of particle emissions as regulations become more stringent. As it was mentioned in the previous chapter, oil derived particles source from trapped oil in different areas of the cylinder caused by in cylinder combustion pressure; therefore, the location of the fuel injector can be neglected when purely analyzing oil emitted particles.

For these tests, two cycles were analyzed in order to compare the oil consumption, an FTP75 (EPA approved) cycle and a specific oil consumption cycle designed to tests for these particles (PT7BRK). Table 6 summarizes the cycle specifications.

	FTP75	PT7BRK
Duration (s)	1950	570
Distance (m)	17767	9414
Max Velocity (km/h)	91.25	129
Average Velocity with Stops (km/h)	34.12	74
Max Acceleration (m/s^2)	1.77	1.33
Average RPM (2.4L PFI Engine) Throughout Cycle	1303	2035

Table 6: FTP75 & PT7BRK Cycle Characteristics

As it can be observed, the PT7BRK is a much shorter and aggressive cycle. It is composed of ten WOT (Wide Open Throttle) transients from 50mph to 80mph and back to 50mph (Braking) in order to fully encourage oil consumption by the engine, and compare it to spikes in particle emission. The hypothesis here is that spikes in oil consumption will correlate with spikes in sub 23nm particle emissions.

3.3 Test setup-EMEA

In this section of the tests, a 1.8L, 4 cylinder direct injection turbo charged engine vehicle was used, along with an underfloor passive GPF (prototype) in order to gain insight on PN emissions for future vehicle models. A list of the engine specifications are given in Table 7.

Bore	**83mm**
Stroke	**80.5mm**
Compression Ratio	**9.8**
Valve Train	**DOHC**
Turbo Charger	**Borg Warner**
Fuel Injector Position	**Wall guided**

Table 7: EMEA Tests Engine Specifications

As previously mentioned in chapter 2, an Induced Current Aerosol Detector (ICAD) was used in a chassis dyno set up and compared to a standard CPC system, the Horiba MEXA-2000SPCS. The ICAD was also tested in its PEMS mode in a dyno cell to determine its capability to count particles against the Horiba PEMS equivalent (OBS one). Finally, the ICAD was tested once again in its PEMS mode on a RDE cycle created by CRF (Centro Ricerche Fiat) around the city of Turin, Italy.

The ICAD was first operated in it PEMS configuration mode, on a chassis dyno. This set up (Labeled Setup 1) can be observed in Figure 27. This was done to determine the amount of particles experienced by the 23nm CPC and compare the ICAD results against these. As it was mentioned in the previous chapter, these set of tests included other instruments (EEPS and DMA), that although not analyzed in this work, served as a base for comparison in the overall Sureal23 project.

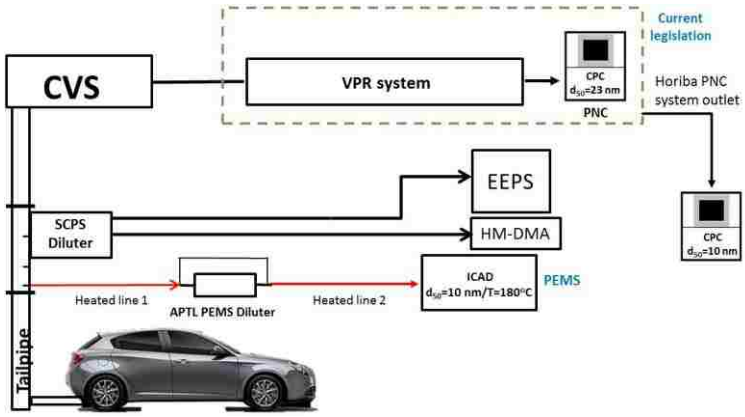

Figure 27: Setup 1- ICAD in PEMS Configuration

For Setup 1, the ICAD was paired with a small, portable diluter developed by APTL (Aerosol and Particle Technology Laboratory). This diluter was set up with a dilution ratio of 8.5:1. It is important to note that in order to compare particulate number measurements of different CPC cutoffs, the Horiba instrument had to be operated in parallel with an external CPC with a cutoff of 10nm. To accomplish this, the external CPC's pump had to be switched off and following the guidelines provided by Horiba, the vacuum required for the critical flow was provided by the instruments SPCS.

Setup 2 observed in Figure 28, sees the ICAD and the extra CPC connected to an SPCS diluter, with a dilution ratio of 35:1. It is composed of one hot dilution stage at 150°C and a cold dilution stage set at 20°C. In between the stages there is a VPR in the form of a catalytic stripper, with an operating range of 280-450°C. This was done in order to compare the particle numbers from Setup 1 for both instruments. In theory, a lot more particles should be observed in the CPC for this configuration, due to the fact the CVS (Constant Volume Sampling) tunnel of the Horiba instrument has a very high dilution ratio of 1:10PND (Particle number diluter) in the first dilution and 1:15 PND in the second stage. The ICAD was arranged in this way to examine the results against those gathered in setup1.

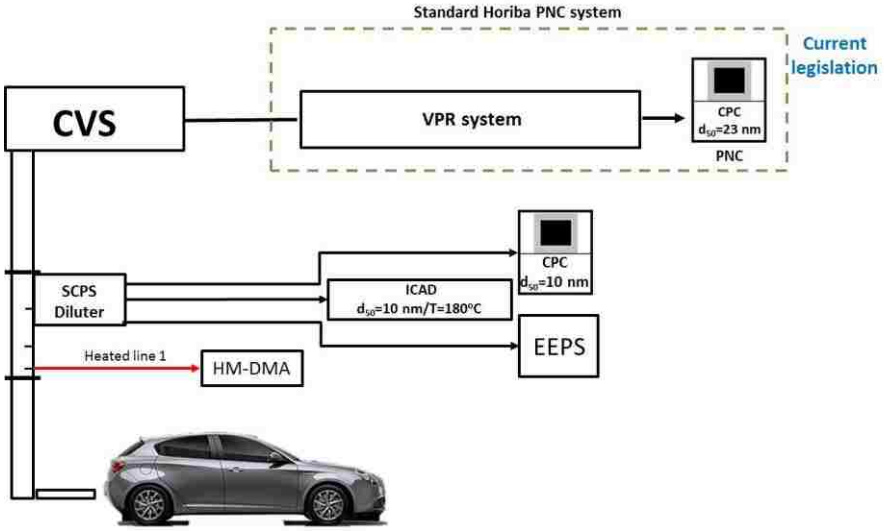

Figure 28: Setup 2- ICAD in Rolling Chassis Configuration

Lastly, the ICAD was put in a raw exhaust configuration, observed in Figure 29. This was done to determine whether the instrument could be operated without any type of dilution. Obtaining reliable data in this configuration would facilitate the RDE tests performed later in the campaign, as it would mean less space needed, and less apparatus' while driving around the city.

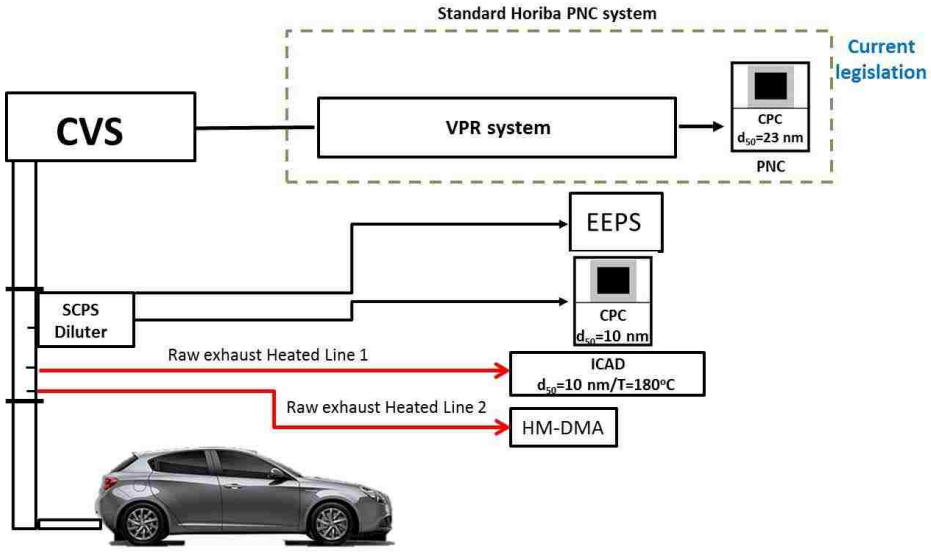

Figure 29: Setup3- ICAD in Raw Exhaust Configuration

For the PEMS configuration tests (both lab and RDE), the ICAD was used in a setup 1 configuration and placed inside the vehicle while Horiba's PEMS system was also attached on the back. Horiba's OBS one PEMS, utilizes a condensation particle counter like its dyno cell counterpart as well as its separate battery pack. The ICAD was paired with a DC/AC 24V/230V converter as well as two batteries providing 24 Volts. Both systems can be seen in Figure 30.

Figure 30: ICAD and Horiba in PEMS Configuration

3.3.1 Engine Operation- 1.8L GDI

The cycle in which the chassis dynamometer tests were performed was the WLTP. The specifics for this cycle can be found in the previous section of the North America tests. Table 8 demonstrates the number of tests performed for the different set ups previously described.

1.8L GDI+GPF WLTP Cycles Performed		
Configuration	Number of Cold Tests	Number of Hot Tests
Setup 1	2	2
Setup 2	2	3
Setup 3	3	2

Table 8: WLTP Tests performed for 1.8L GDI

The cold engine tests were performed after the vehicle had been soaking for at least 10 hours (as per homologation rules) at 20°C while the hot tests were performed when the vehicle's engine had reached an acceptable engine temperature (determined by temperature gauge of the vehicle).

As previously mentioned, for the RDE tests, the ICAD was operated in its PEMs configuration (setup1) with a DC/AC inverter and its separate battery pack. The specifics of the RDE cycle can be found in Table 9 and Figure 31.

	RDE
Duration (s)	6300
Distance (m)	80000
Max Velocity (km/h)	135
Average Velocity with Stops (km/h)	50
Max Acceleration (m/s²)	1.2
City Distance Share	29% ≤ x ≤ 44%
Rural Distance Share	23% ≤ x ≤ 43%
Highway Distance Share	23% ≤ x ≤ 43%

Table 9: RDE Test Specifications

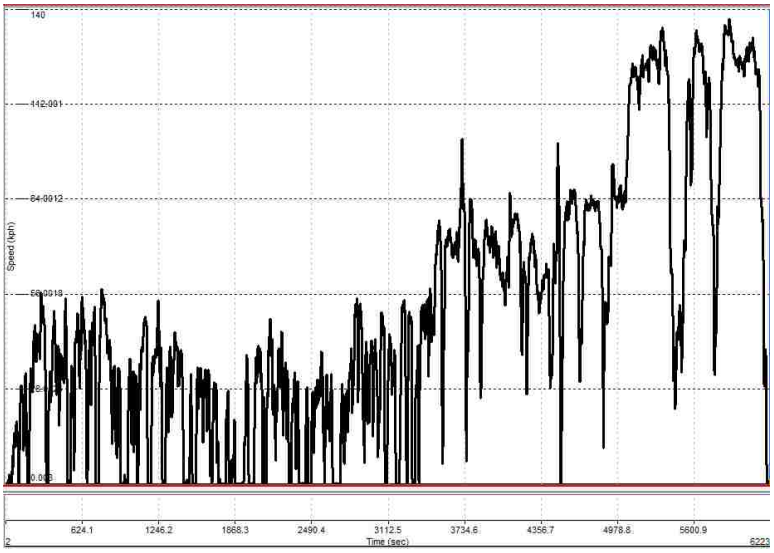

Figure 31: Speed Trace of RDE Test

3.3.2 Measurement Uncertainties- 1.8L GDI

For the ICAD, once again the uncertainty of the tests can be approximated using error propagation;

$$\sigma^2(\mathrm{PN_{ICAD}}) = \sigma^2(\mathrm{V_{cvs}}) + \sigma^2(\mathrm{C}) + \sigma^2(\mathrm{D}) + \sigma^2(\mathrm{SCPS})$$

The uncertainty of the final result (10%) is once again dominated by the Instrument (10%). The volume and distance values were kept the same as with previous tests while the SCPS uncertainty in the flow although small (1.8%), was also added.

Chapter 4: Experimental Results- North America

4.1 Experimental Results- GDI

As it was previously stated, the GDI engine was submitted to WLTP and RDE cycles. The motivation behind these tests was the performance analysis of the instruments currently used for calibration and homologation. Furthermore, the data gathered was used to further understand the particle number size distribution throughout different transients and section of the cycles, with emphasis on the sub 23nm range. The following section outlines the results collected from these tests.

4.1.1 Experimental Results- GDI in RDE Cycle

It is well documented that particle emissions during cold engine start are the main contributors to overall particle number during a test cycle [30]. For this reason, it was important to separate both the RDE and WLTP cycles into a “Cold Start” and “Hot Operation” phase. The first 90 seconds of each cycle were chosen as the cold start phase due to “abnormal” spikes in particle emissions when compared to the rest of the cycle. The remaining time was labeled “Hot Operation”. The data was also analyzed starting from the moment the dynamometer started rolling, as supposed to when the collecting instruments were enabled. This was done in order to keep the entire tests equivalent since the instruments were sometimes started long before the vehicle was “moving” and provided uncomplimentary values.

This separation of cycle (cold vs hot) hoped to contribute in the understanding of the distribution of particle size according to engine temperature, cycle transients, and other engine operating parameters like fuel flow. Figure 32 demonstrates the cycle trace along with the spikes in particle emission averaged from all 5 RDE tests.

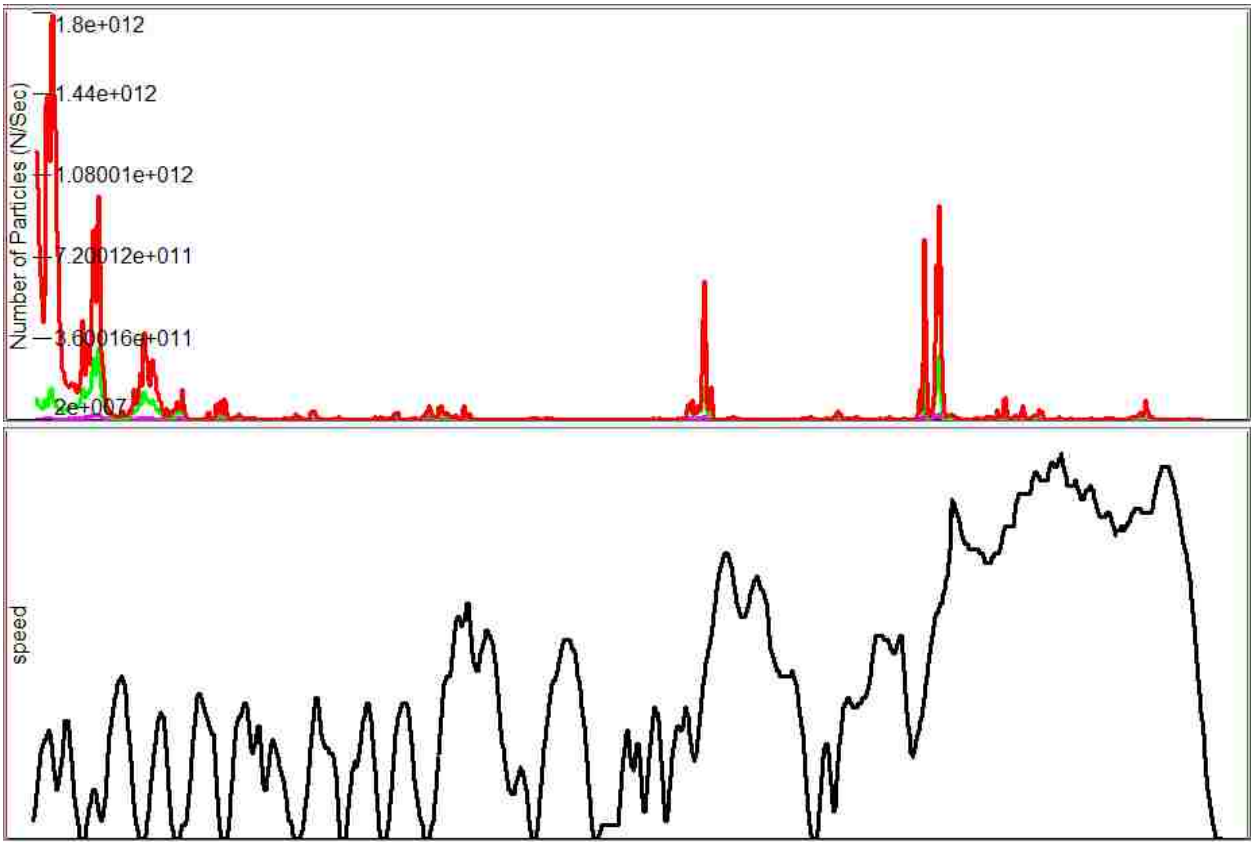

Figure 32: RDE Particle Distribution by DMS500

As expected, most of the particle emissions were found in what was considered in these experiments as the cold start. Figure 33 exhibits the distribution of particles according to their size during the first 90 seconds. Once again, bigger seized particles were expected since they are thought to be sourced from cold combustion chamber surfaces and fuel rich conditions [35].

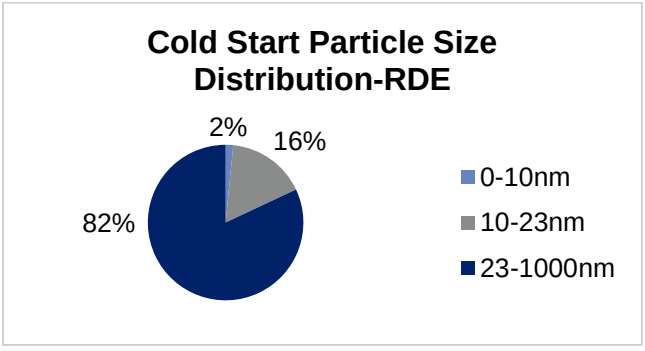

Figure 33: Cold Star Particle Size Distribution

It can be observed (Figure 34) that during some of the more demanding transients of the cycle, emission outputs (outlined by the top graph) seem to significantly increase. Following knowledge of the source of particles during cold engine start, these peaks were further analyzed in order to observe particle size distribution when engine operations change according to aggressive transients.

Figure 34 illustrates how during these aggressive transients, emission spikes correlate to the amount of fuel flow (bottom graph) being injected at the time. As it was mentioned in Chapter 2, fuel derived particles are the most common source of PN emissions in GDI engines due to the direct injection and short mixing time between air and fuel. For these tests, the vehicle consumed an average of 27.3g of fuel during the first peak and 57.6g during the second.

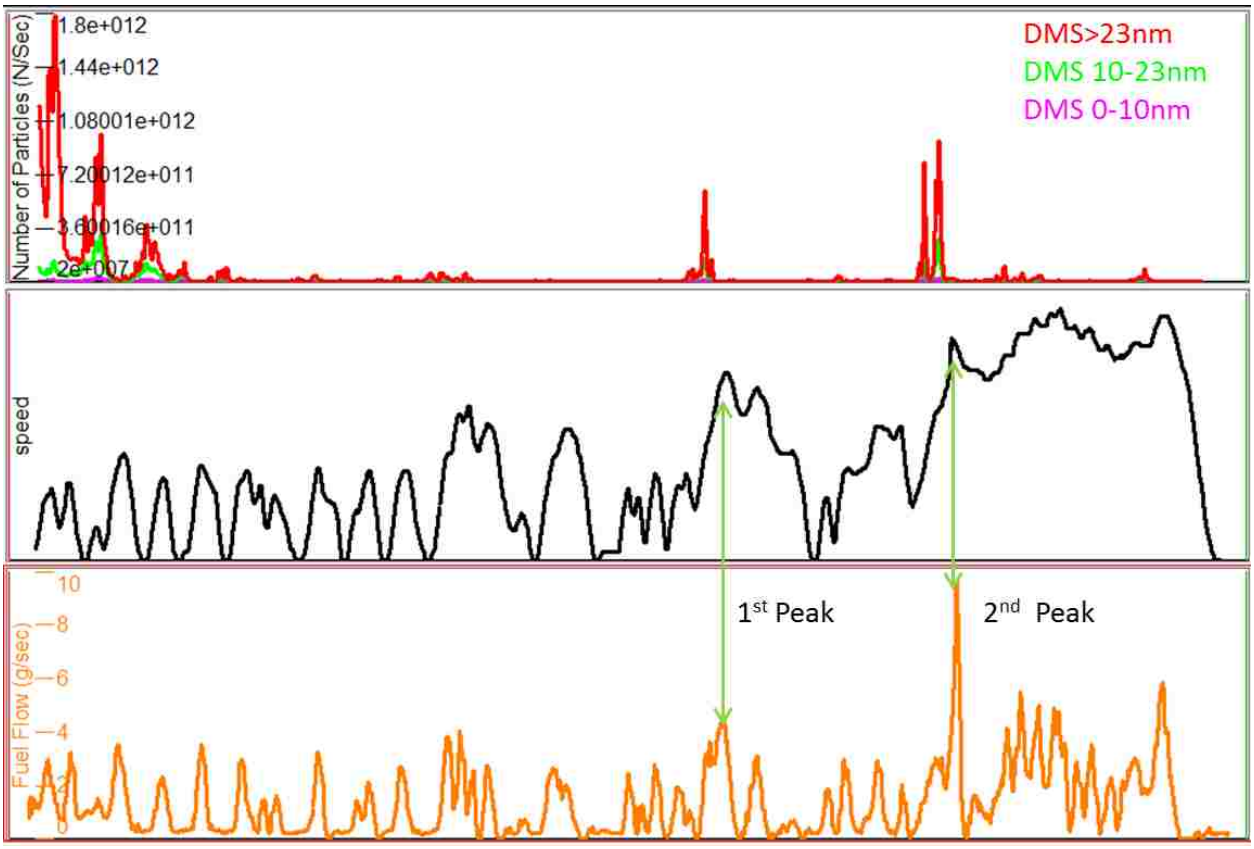

Figure 34: Fuel Flow Effect on Particle Emissions

Moreover, when these particular peaks were deconstructed into the respected size distribution chosen (Figure 35), it was found that the majority of particles belonged to the larger size range (23nm-1000nm) chosen for this project, with respect to the normal distribution observed for the rest of the cycle.

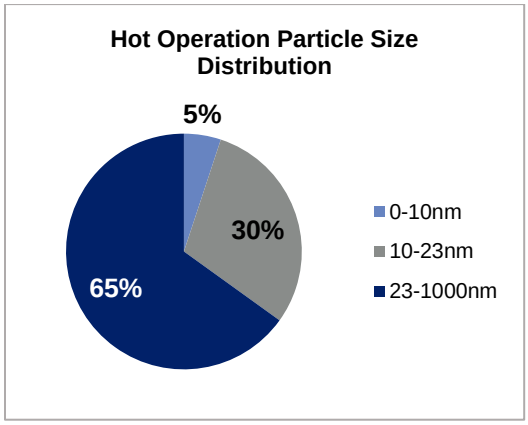

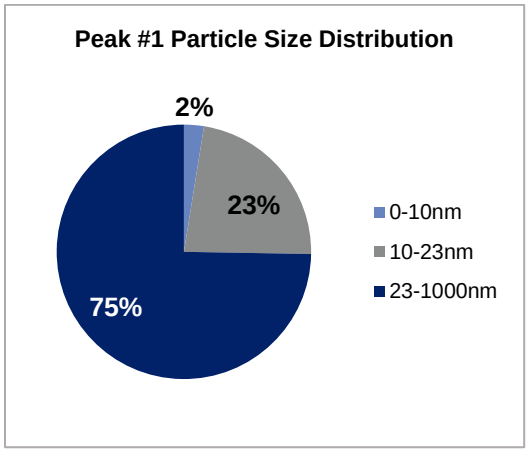

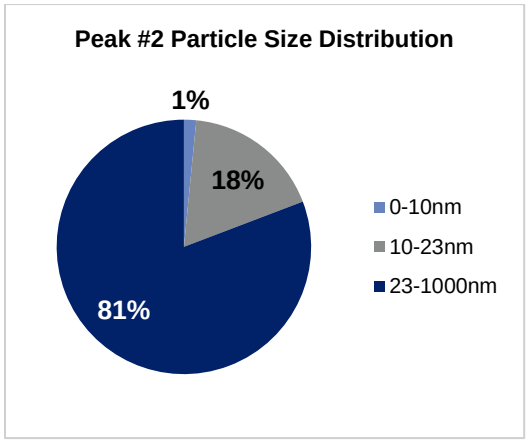

As Figure 35 demonstrates, the more prominent of the two peaks (#2) has a similar spread in particle size to that of the cold start distribution. Therefore, it could be concluded that fuel particles are the primary source of these emission spikes. Additionally, and referring to a copy of Figure 34 below, it can be observed that some of the fuel flow peaks are of similar value (outlined in the shaded area of interest) to those of Peak #1. These however, do not lead to significant spikes in particulate number when compared to those of #1 or #2. This is most likely due to the difference in vehicle speed (engine load) and fuel used. Although they may appear similar in quantities, there is a mean vehicle speed difference of 60% and a mean fuel flow difference of 40% between Peak #1 and the highlighted “Area of Interest” below.

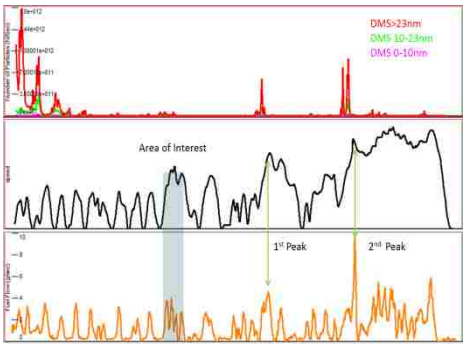

Figure 35: Particle Distribution: Hot operation Vs Emission Peaks

Lastly, it is important to note that the “Hot Operation” particle size distribution observed by the DMS500, matches that of the previous literature [36] with regards to the amount of particles not being counted by current regulations (30% of particles between 10-23nm are being unaccounted for).

4.1.2 Experimental Results- GDI in RDE Cycle (DMS500 Vs AVL489)

The additional outcome expected from these test was the comparison between the calibration instrument (DMS500) and the homologation instrument (AVL489). Previous literature suggests that fast particulate spectrometers like the DMS500 can over-count with respect to condensation particle counters [30]. Therefore, the goal was to determine if the DMS500 could be considered sufficiently reliable for vehicle calibration when compared to an industry standard system like the AVL489. Figure 36 illustrates the particle count in N/sec (top graph) as well as the cumulated count (middle graph) for both of the instruments along with the speed trace of the cycle.

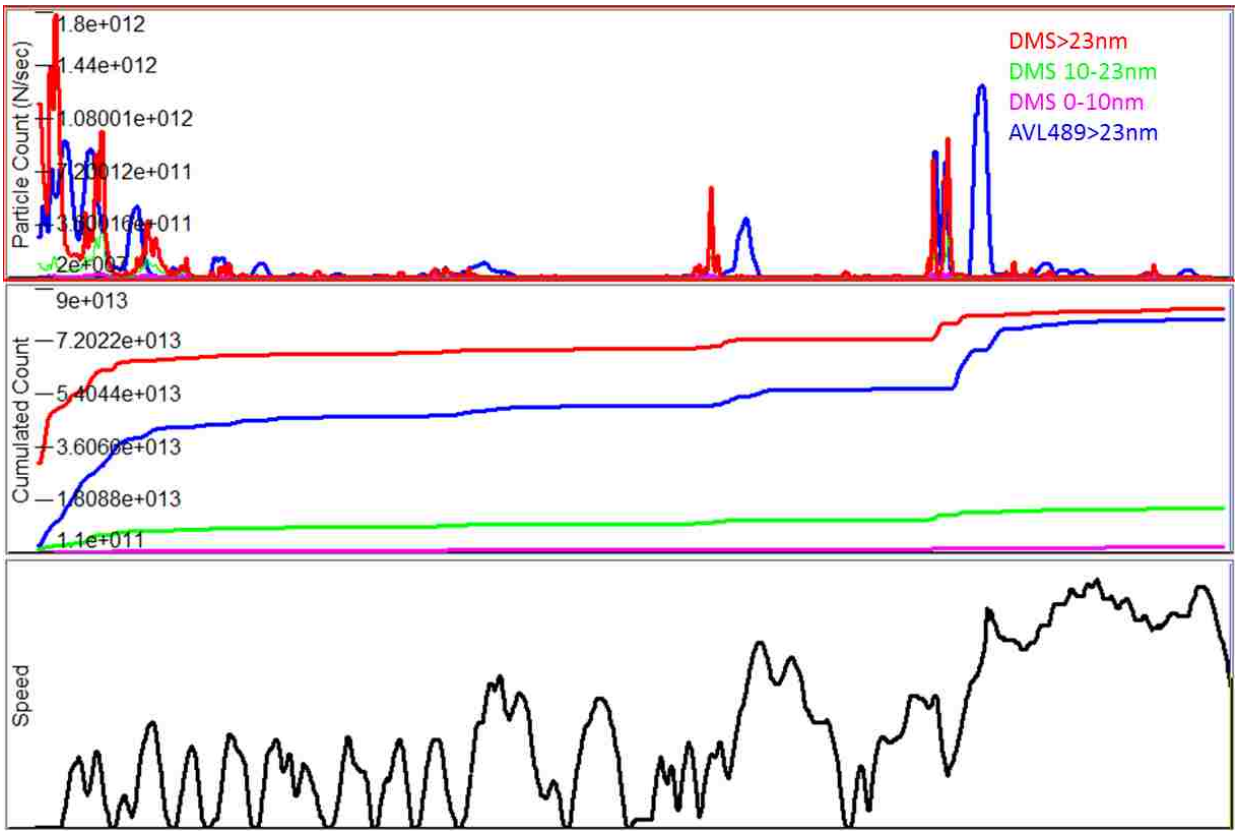

Figure 36: DMS500 Vs AVL489- RDE Cycle

It is important to recall that the AVL is a CPC type of instrument, and in this particular set of experiments, the cut off particle size of the apparatus was set at 23nm. Therefore, the comparisons in this section will be made between the AVL count (blue trace) and the 23nm and above DMS count (red trace).

It was found that during what was designated as the cold start phase, the DMS500 counts more particles than its CPC counterpart. Previous experiments coincide, and conclude that this could be the case due to the faster operating dynamics of the DMS [30], predominantly during the cold start phase. Furthermore, the induced currents (as explained in section 2.6) produced by these particles could also be a source of error in the count [31] particularly during this concentrated particle emission phase.

The DMS also uses a parameter called 'Signal Strength', which analyses the signal to noise ratio the instrument is experiencing during the test. These values range from 0-10, and they help indicate when the sample is too diluted (0-2.4), too concentrated (5.1-10) or in the ideal operating zone (2.5-5). Therefore, variation in this signal strength might also cause the DMS to indicate erroneous particle counts.

However, during the spike in emissions (derived from fuel) that was described in the previous section, the AVL counted more particles than the DMS. This change in particle count could be due to the catalytic stripper used with the DMS in these experiments, which during hot operation could lead to loss of particles <100nm due to diffusion, and particle thermophoresis [37].

Lastly, examining the cumulated count (middle graph) in Figure 36, it can be observed that the difference in count between the two instruments is reduced significantly as the cycle progresses into the more aggressive transients. Table 10 outlines this change as the cycle progress through the transients.

Percentage Increase Between DMS and AVL			
Phase of Cycle	**AVL Cumulated Count**	**DMS Cumulated Count**	**Percent Increase**
Low	2.71E+13	5.76E+13	112.55%
Medium	4.53+E13	6.74E+13	48.79%
High	5.20+E13	7.08E+13	36.15%
Extra High	7.62+E13	8.18E+13	7.35%

Table 10: Percentage increase between DMS and AVL

As it is expected with an increase in load, both instruments count also increase. Peak #2 mentioned previously corresponds to the start of the extra high phase outlined in the previous table, which shows a high surge in count for the AVL and not the DMS. This in turn, produces quite a reduction in instrument discrepancy. It is hypothesized that the DMS might be undercounting at this instant due to the catalytic stripper that was attached to it, causing the aforementioned issues. After conducting various tests with this configuration, it was determined the catalytic stripper is only necessary with the DMS if sampling before or without, a three way catalytic converter in order to avoid particle loss.

4.2 Experimental Results- GDI in WLTP Cycle

As with the RDE cycle, the goal of these experiments was to examine the particle number distribution during this homologation cycle as well as compare the Instruments currently used. Figure 37 demonstrates the combined results of the WLTP cycles performed in terms of particle number emissions and the speed trace.

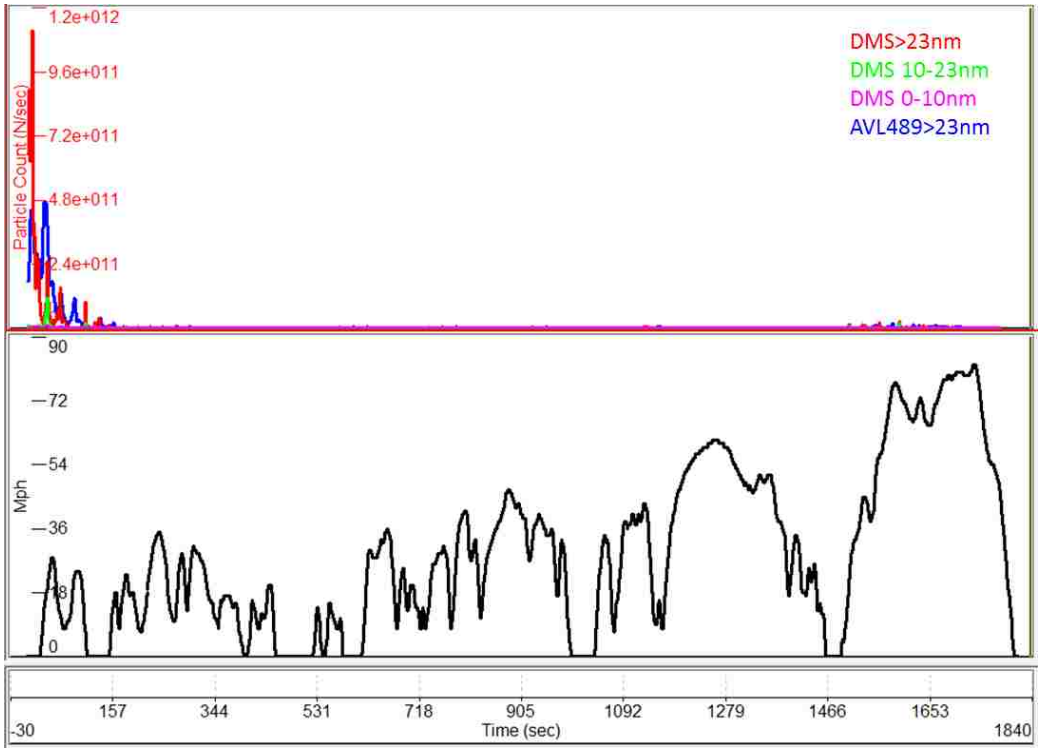

Figure 37: WLTP Particle Distribution Observed by DMS

Due to the less demanding nature of the cycle (Compared to the previous RDE), it can be observed that the most visible emissions occur once again, during the cold start of the engine. Figure 38 outlines the breakdown according to particle size for the first 90 seconds of this cycle:

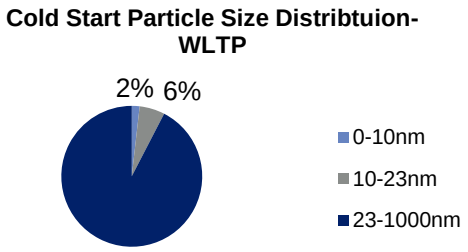

Figure 38: Cold Start Particle Size Distribution-WLTP

It is important to note that although it is difficult to see due to the scale of which the graph had to be set up in the above figure (due to the amount of 23nm-1000nm particles), there is still a significant amount of particles being emitted in the range of 0-23nm. The black y-axis (Allocated to the ranges of 0-10 and 10-23nm) in Figure 39 shows that these ranges are mostly in the magnitude of E+10.

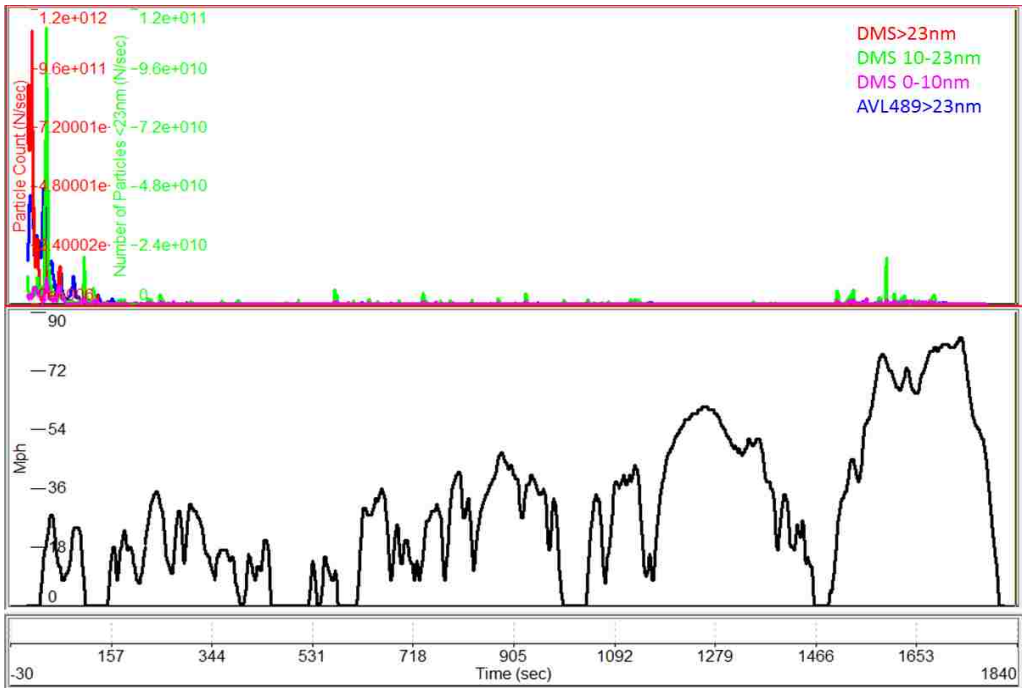

Figure 39: Particle Size Distribution Observed by DMS with Adjusted Axis

4.2.1 Experimental Results- GDI in WLTP Cycle (DMS500 Vs AVL489)

Figure 40 outlines the particles measured by both instrument in terms of N/s, cumulated count, as well as the speed trace of the cycle. As it can be observed, the DMS500 (red trace) constantly counts more particles than the AVL instrument (blue trace).

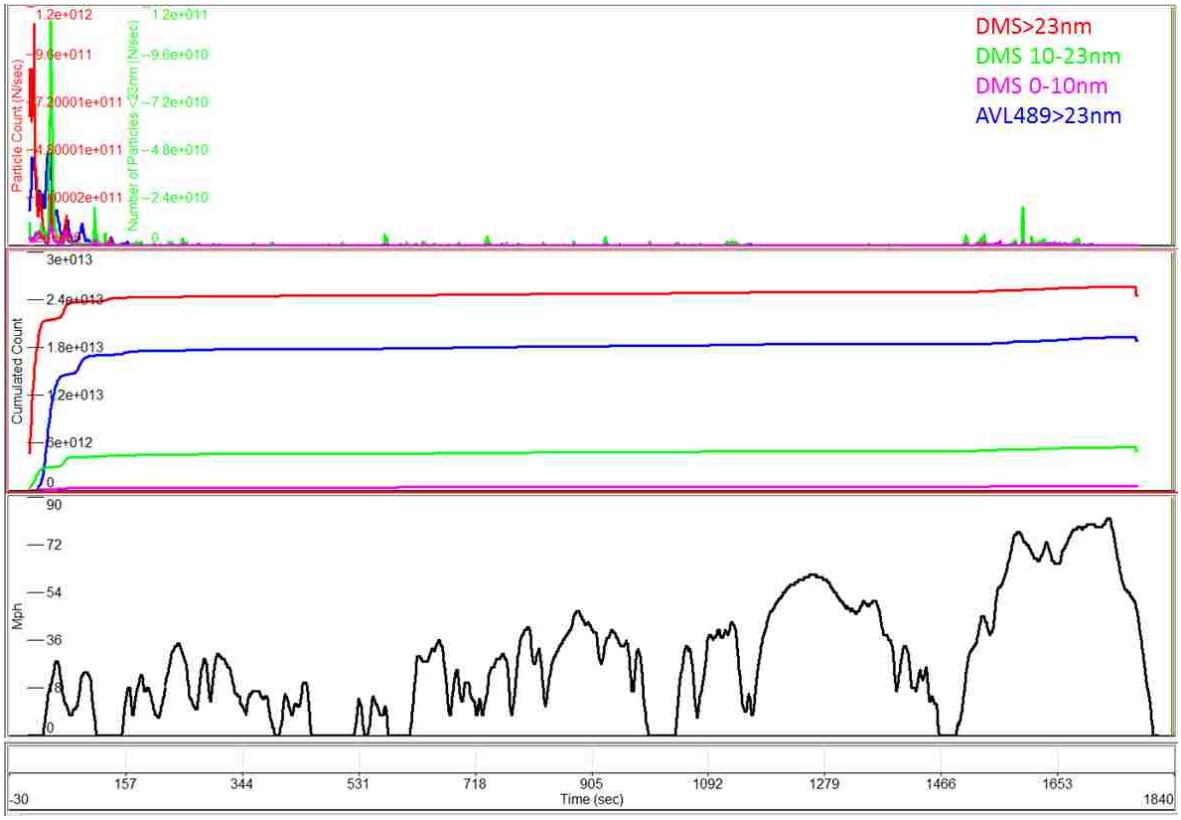

Figure 40: DMS500 Vs AVL489- WLTP Cycle

Unlike in the RDE tests, the instruments do not converge in terms of percentage difference as the cycle goes through the more aggressive transients. Throughout the WLTP, the percentage difference in the readings between DMS>23nm and AVL489 remains constant at 37.6% .This is likely be due to the low signal strength observed by the DMS during the more demanding segment of the cycle. A signal strength lower than 2.4 is considered insufficient for accurate readings, which often occur during deceleration or fuel shut off, both factors are more prominent in the less demanding WLTP cycle [33]. It could be inferred that this is the cause of the much larger differences in the instrument readings when compared to the RDE tests, which have more acceptable signal strength, as observed in Figure 41 (Signal strength in red).

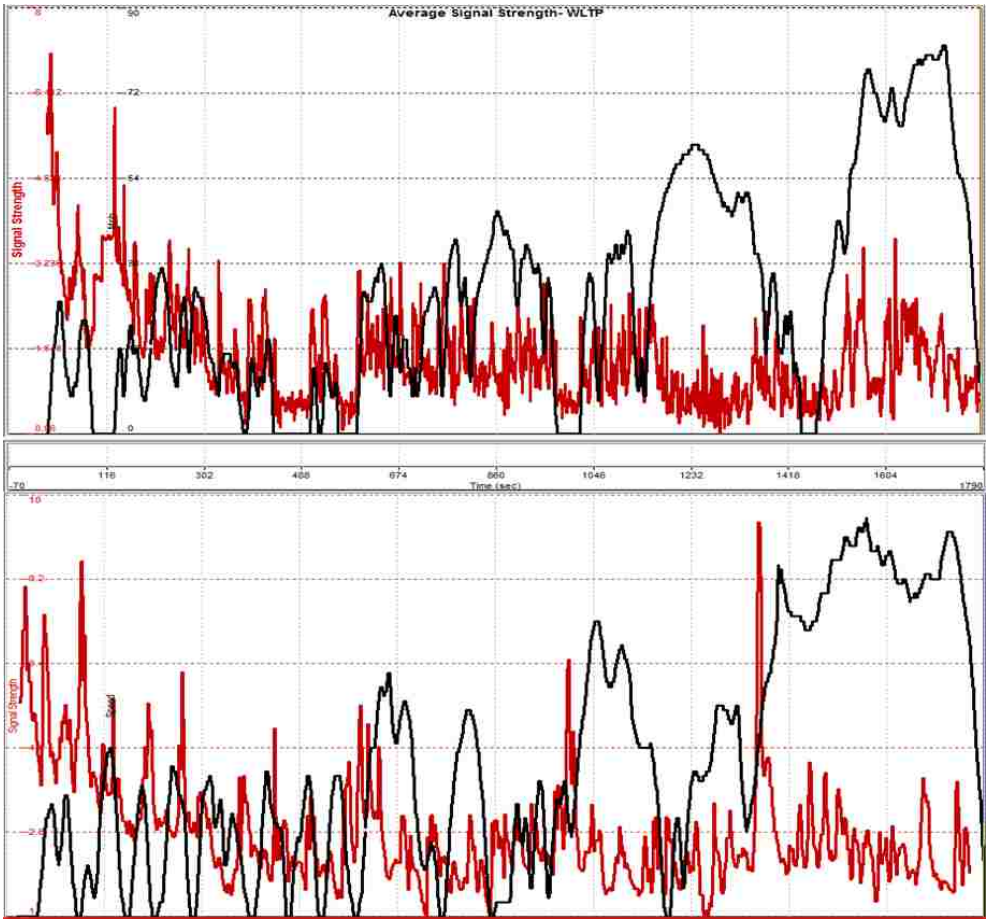

Figure 41: Signal Strength (WLTP vs. RDE)

While the average signal strength throughout the WLTP cycle was 1.52, the RDE cycle had an average of 2.8, which indicates during much of the course of the WLTP, the DMS was experiencing an insufficient signal to noise ratio. The standard solution as per manufacturer instructions is to lower the dilution ratio of the second diluter during these areas of deceleration or fuel shutoff, where a small amount of particles are expected. However, even when this is second diluter is set at 1:1, given the nature of the cycle, some discrepancies in the data may still occur.

4.3 GDI Engine Experimental Results Summary

A 2 liter, 4 cylinder GDI engine was submitted to two different tests cycles (WLTP and RDE) in order to observe particle size distribution and examine the performance of calibration and homologation particulate measurement systems. Each cycle was separated into a Cold start phase, comprised of all the particles in the first 90 seconds as well as a Hot Operation phase, containing the rest of the cycle data.

Figure 42 illustrates the particle distribution for each cycle at each of the phases chosen:

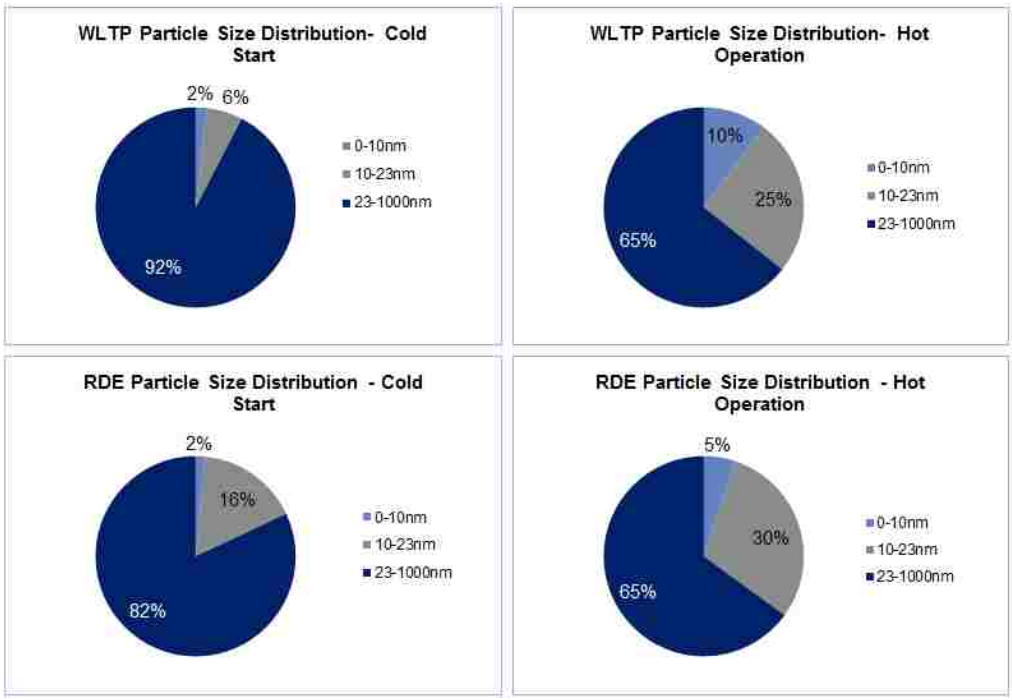

Figure 42: Particle size distribution for both cycles

The cold start phase of each cycle has the expected distribution, with larger particles dominating the total count due to cold combustion temperatures, cold piston and cylinder surfaces, and fuel rich conditions [35]. The hot operation distribution follows previous works with regards to the particles that are not currently considered by PN emission standards [38] . According to the results found in these experiments, if emission regulations were to be lowered to a particle diameter lower than 23nm, such as 10nm, an average of 28% more particles would need to be accounted for.

Furthermore, as discussed in section 4.1.1, spikes in particle emissions during aggressive transients appear to be sourced from fuel born particles as a result of the abundant amount of fuel being injected at the time of acceleration. Deconstruction of these particle emission peaks into the different size categories chosen (0-10nm, 10-23nm-23 and 1000nm) indicated similar distribution to that of the cold start conditions. Without the cold combustion and cold surface elements present in these scenarios, the best explanation is the fuel rich conditions experienced by the engine during these periods of hard acceleration.

Lastly, a fast particulate spectrometer (DMS500) and a condensation particle counter with a cutoff diameter of 23nm (AVL489) were evaluated. Table 11 outlines the comparison of the instruments with regards to the different phases in the two cycles, as well as for the signal strength (S.S) reading from the DMS for each phase.

Percentage Increase & Signal Strength Between DMS and AVL- RDE									
Cold Start (0-90sec)	**S.S**	**Medium**	**S.S**	**High**	**S.S**	**Extra-High**	**S.S**		
112.55%	**4.9**	48.79%	**2.7**	36.15%	**2.4**	7.35%	**2.7**		
Percentage Increase & Signal Strength Between DMS and AVL- WLTP									
Cold Start (0-90sec)	**S.S**	**Low (90-500)**	**S.S**	**Medium (500-1020)**	**S.S**	**High (1020-1470s)**	**S.S**	**Extra-High (1470-1800)**	**S.S**
68.38%	**3.4**	37.85%	**1.9**	36.46%	**1.4**	35.87%	**1.1**	33.68%	**1.4**

Table 11: Percentage Increase and Signal Strength between DMS and AVL

The DMS uses a range of values in the signal strength indicator to indicate if the sample is too concentrated or too diluted. Values between 0 and 2.4 are considered erroneous and indicate the sample is too diluted. Values above 5 are considered too concentrated and long operation under these conditions might damage the apparatus. Therefore, the DMS considers values between 2.5 and 5 as the optimal operating points.

It is interesting to note that after the cold start phase, the difference between the two instruments was reduced as both cycles entered their more transient and aggressive stages. The table above demonstrates that although the RDE is considered a much more aggressive cycle compared to the WLTP in terms of reduced stopping time and

increase loads, the much better signal strengths obtained during these tests result in more accurate readings between the two instruments.

Figure 43 outlines a correlation analysis between the two instruments for both cycles, where the RDE results show a much better correlation (demonstrated by the R^2 value) than the WLTP. This was an unexpected result as previous research [30] showed there was a strong correlation during steady state tests (constant load) and more variation during transient tests. However, the low signal strength previously mentioned for the more passive cycle demonstrates this has a higher impact on instrument relationship than the aggressive nature of a cycle.

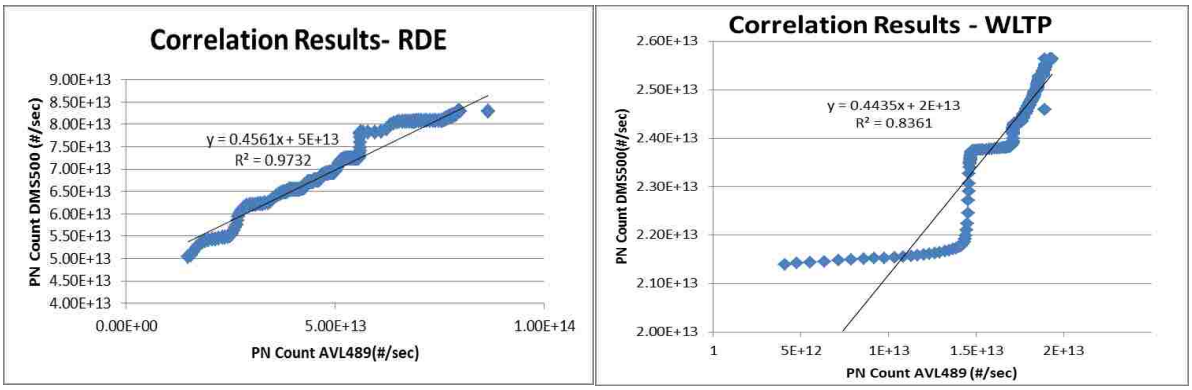

Figure 43: Correlation Analysis for Both Cycles

4.4 PFI Experimental Results – FTP75 Cycle

As it was mentioned in Chapter 3, a 2.4L PFI engine was used to determine the impact oil causes on particulate number and distribution. This engine was subjected to FTP75 and P7BRK cycles. The goal was to analyze an aggressive oil consumption cycle (P7BRK) and a more passive one (FTP75), to determine if the spikes in emissions correlated to those of oil consumption. The following section includes the results for the FTP75 cycle tests.

Figure 44 below outlines the trace of the FTP75 cycle conducted, the particle number detected by the DMS (top graph) and the oil consumption in g/h (middle graph) detected by the Lubrisense system for the tests performed.

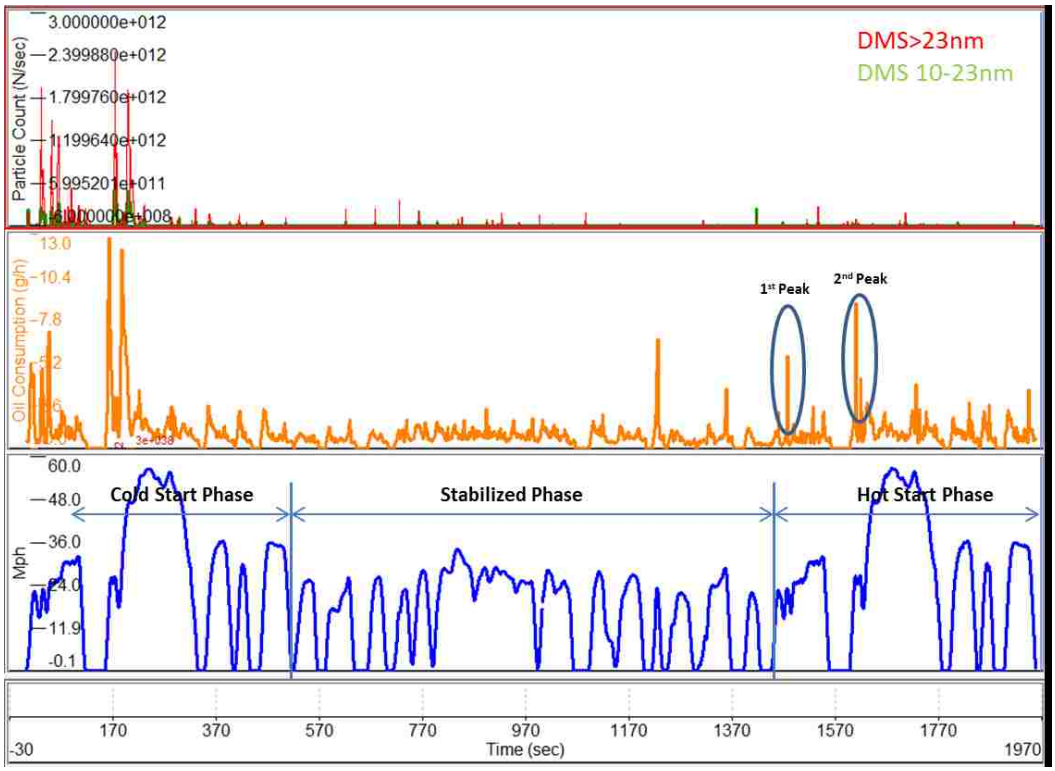

Figure 44:FTP75 Cycle

As it is expected with any cycle, during the cold start phase, a great number of particles are obtained. What is interesting about the FTP75 when compared to other test cycles is that it has a third phase identical to the first, but in a hot start condition (with a hot soak of at least 540 sec). This allows for better understanding of particle sourcing when the factors of a cold engine are eliminated. It can be seen from Figure 44 that when this

last phase begins, the oil consumption increases dramatically in the more aggressive transients, while particle emissions are reduced by a magnitude, from 10^{11} in the cold start phase to10^{10} for the rest of the cycle. Analyzing the corresponding PN peaks to those of oil consumption (highlighted in the figure) in detail reveals their concentrations of 10-23nm particles compared to other cycles. 46% of particles in Peak #1 are composed of particles 10-23nm while Peak #2 is composed of 33% particles in this same range, according to the DMS. In an experiment by Koczak et al [39], it was also found that the last phase of this cycle was composed mostly of accumulation mode particles. However, the unusual amount of 10-23nm particles found in Peak #1 could indicate that the oil is leading to a small increase in particles below 23nm since during harsh transients, these type of PN spikes have been largely dominated (70% of the count and above) by particles 23nm and above (such as in previous GDI, tests).

Lastly, as seen in Figure 45, this cycle has a close particle distribution between the cold start (First 90 seconds) and its “Hot Operation” phase. This was unexpected, as previous experiments showed larger discrepancies between these two phases. It is believed the distribution for the cold start condition shows a reduction in large particles (>23nm) when compared to previous results due to the engine technology used (PFI). An observation more evident in the following test.

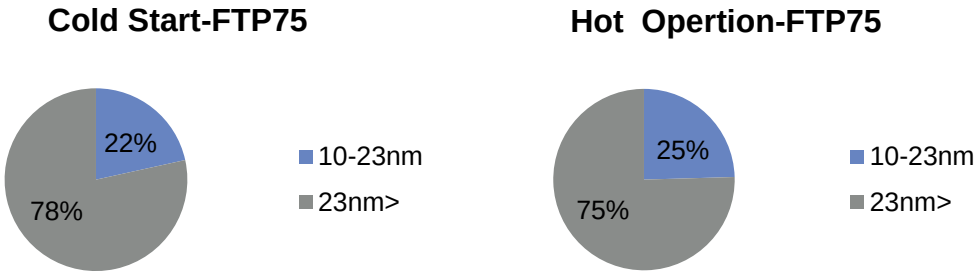

Figure 45: FTP75 Distribution

4.4.1 PFI Experimental Results – PT7BRK Cycle

This cycle was meant to examine oil consumption in an engine by exposing it to WOT (Wide Open Throttle) transients. As it was discussed in section 2.5.1, there are five main sources of oil consumption in an SI engine. In a cycle like the PT7BRK, with its severe transients, the oil consumption is most likely sourced from oil evaporation and oil throw off/reverse blow-by. The high thermal loading of engine components being the cause of evaporation, while the increase pressure gradients during the cycle causing oil throw off and reverse blow-by. Figure 46 below demonstrates the results obtained from the DMS500 (top graph) and the Lubrisesne system (middle).

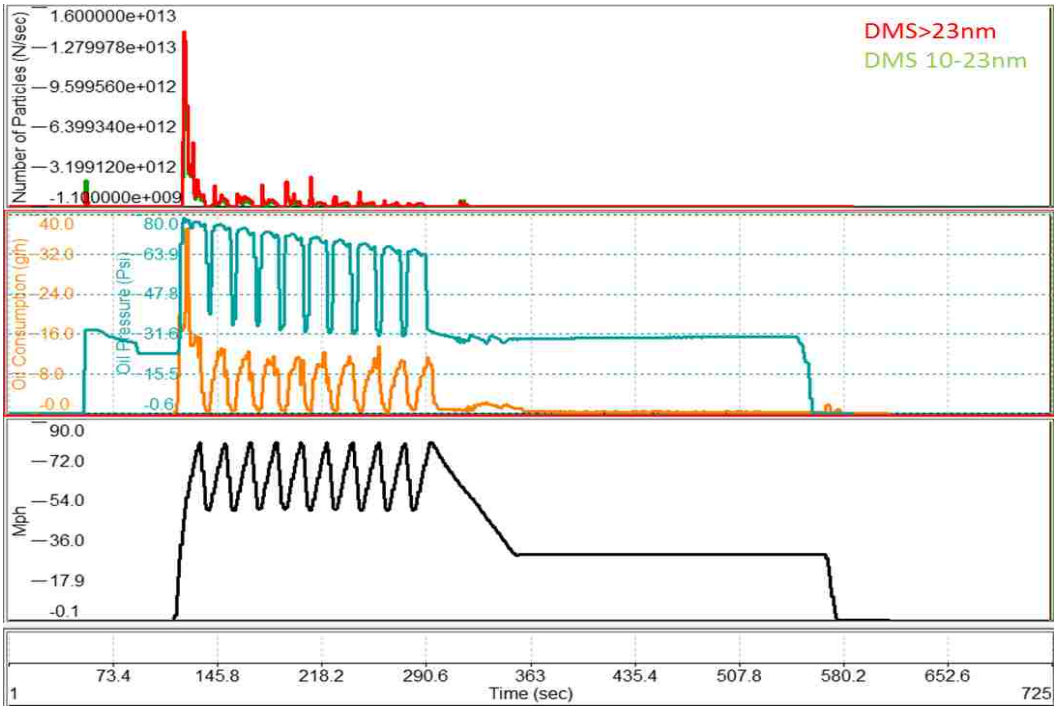

Figure 46: PT7BRK Cycle

As it was mentioned earlier in this work (Chapter 2), PFI engines have notoriously lower PN emissions compared to their GDI counterparts, therefore, some interesting observations can be made from Figure 46. At a glance, it can be observed that the count between the 10-23nm and >23nm particles seems to be more evenly distributed than in other cycles. The actual distribution for this cycle can be observed in Table 12, once again, the cold start phase being the first 90 seconds of the cycle and the “Hot Operation” accounting for the rest.

Particle Distribution	Cold Start (# of Particles)	Hot Operation (# of Particles)
10-23nm	4.97E+13 (43%)	2.52E+13 (35%)
>23nm	6.52E+13 (57%)	4.74E+13 (65%)

Table 12: Distribution of Particles for PT7BRK

This cycle appears to have an abnormal distribution of particle size during the cold start phase due to the fact so many small particles are present. Observing the top graph of Figure 46, a small peak can be noted, mostly dominated by the green trace, and signifying 10-23nm particles. From previous experiments with the GDI Engine, this emission peak upon startup was expected to be dominated by particles larger than 23nm (Induced mostly by fuel enrichment). As outlined in the previous sections of the GDI experiments, particles in the 10-23nm range accounted for 6% and 16% of the total cold start phase for the WLTP and RDE cycles respectively. In this PFI case, (Figure 46), this range (10-23nm) accounted for 43% of the total count for the cold start phase.

An experiment performed by Chen et al. using transmission electron microscopy (TEM) provides some insight as to why this might be the cause. At a 10nm scale, particles emitted from GDI engines are of an ordered nanostructure, with higher crystalline height, length and fringe length when compared to the morphological structure of its PFI counterpart. This morphological structure decreases the feasibility of further oxidation, which could explain the smaller size observed during engine start up [40] [35]. Furthermore, PFI engines have more difficulty following aggressive transients, (due to location of the injector) which favors ultrafine particle generation, while deposits on the intake valve are another factor that produces small particles.

With regards to the oil consumption, Figure 47 demonstrates how this cycle has a larger portion of particles in the 10-23nm range in both phases when compared to previous ones in either a GDI configuration (WLTP, RDE) or PFI (FTP75).

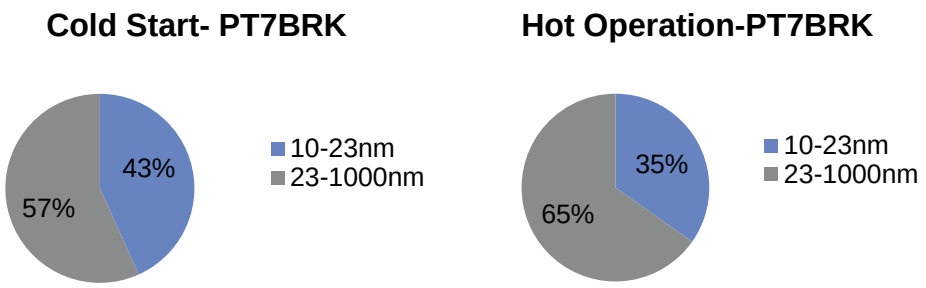

Figure 47: PT7BRK Particle Distribution

The hot operation chart in Figure 47 provides a distribution that is more expected for an SI engine. Therefore, in order to understand if oil might be impacting PN emissions, a more in depth analysis of the cycle was required. Figure 46 also outlines the drop in oil pressure (middle graph, blue trace) as the cycle is conducted, something common in all IC engines. As the temperature of the engine increases, the oil becomes less viscous, reducing the overall oil pressure. What is interesting is what happens to the particle distribution as the oil becomes less viscous and the temperature of the engine/combustion increases. Figure 48 summarizes the average particle distribution for the first and last 5 transients of the cycle.

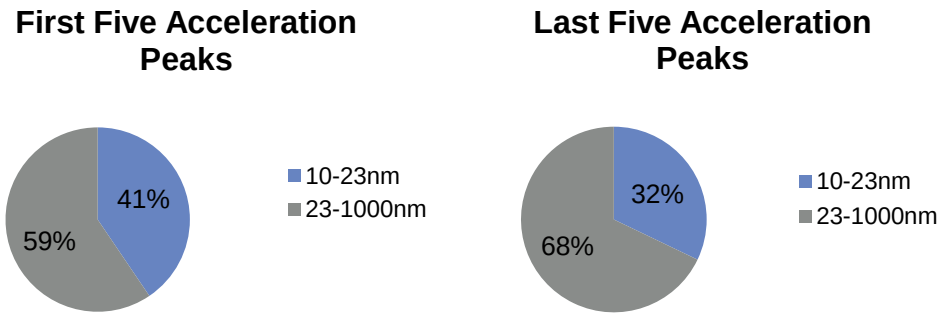

Figure 48: Particle Distribution for first and last five peaks of the PT7BRK

An increase of 9% in the particles larger than 23nm can be observed as the cycle progresses, which could dignify oil impacting the larger size range (>23nm). One of the obstacles of determining the true source of these particles comes as a result of the fuel being used. Because this is a gasoline engine, primary particles of elemental carbon

(EC) form in the flame when carbon based fuels are used, making it difficult to pin point the exact pathway of the particles in this specific test.

However, in an experiment by Miller et al. [28] a hydrogen powered engine was used to analyze the contribution oil has on particle emission. Because hydrogen does not produce any elemental or organic carbon (OC) as a result of combustion, any particulate matter the researchers gathered would be derived from the lubrication oil or abraded engine metal. The experiment concluded that the carbon from the lubrication oil is mostly emitted as OC, more so during periods of high loads and temperatures, which they suggested causes a more complete breakdown of the carbon in the oil.

Moreover, the researchers also conducted a particle size distribution using TEM and EDS (Energy Dispersive spectroscopy) to try and explain the source of these particles. They concluded that particles in the range of 30-300nm could be derived from lubrication oil since they contained high amounts of Ca, P, Zn, and Mg (metals commonly part of the lubricant) and were very dense in nature, but ultimately their pathway was unclear. The particles they classified as Nanoparticles were in the range of 5-50nm. They were composed mainly of C and Fe, where the Fe particles were thought to be self-nucleated in post combustion while temperatures were high, and the carbonaceous particles were thought to be originating from homogeneous nucleation of volatile hydrocarbon vapors.

4.5 PFI Engine Experimental Results Summary

The purpose of this experiment was to compare the same, 2.4l PFI engine in two different cycles (FTP75 and PT7BRK) and determine whether oil consumption correlated with spikes in sub 23nm emissions. The engine was equipped with a DMS500 to measure particle distribution and count, as well as a Lubrisense oil consumption measuring system, both placed after the TWC. The following section is a discussion of the findings for these tests. Table 13 outlines the total particle number and distribution for each phase.

	FTP75		PT7BRK	
Particle Size	Cold Phase (1^{st} 90 Sec)	Hot Operation	Cold Phase (1^{st} 90 Sec)	Hot Operation
10-23nm	4.72E+12 (22%)	1.07E+13 (25%)	4.97E+13 (43%)	2.52E+13 (35%)
>23nm	1.72E+13 (78%)	3.30E+13 (75%)	6.52E+13 (57%)	4.74E+13 (65%)

Table 13: FTP74 and PT7BRK PN Comparison

Although the PT7BRK is around 3 times shorter (570 sec Vs 1950sec) than the FTP75, the cycle produced particle emissions a magnitude higher (1.88E+14 compared to 6.57E+13) than its more passive counterpart. This was expected, as it has been previously discussed, higher transient cycles produce more particles due to the increase engine load experienced. What was interesting about these two tests was the oil consumption experienced by the engine, and how it affected the size of particles emitted.

Over the course of the PT7BRK cycle, the engine experienced an average oil consumption of 2.92g/h. The FTP75, only consumed an average of 0.88g/h. This high oil consumption experienced in the PT7BRK appears to correlate with an increase in Particles larger than 23nm, more specifically during the WOT acceleration transients. Figure 49 displays an exploded view of three of these transients.

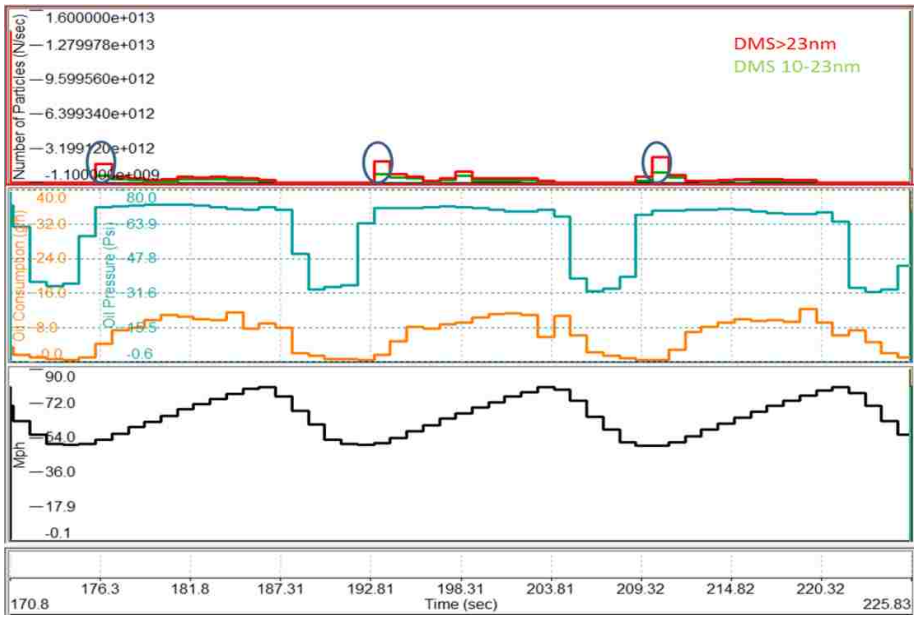

Figure 49: Exploded View of PT7BRK Cycle Transients

Observing the circled sections in the figure above, each time a new transition starts, there is a peak of >23nm particles that forms, followed by a more even distribution between the two ranges (10-23nm & >23nm). This could lead to the conclusion that particles greater than 23nm are influenced by the surge of fuel when these transients start, followed by particles derived from the oil as the cycle continues. At the beginning of each acceleration period, these peaks showed 68% of particles were greater than 23nm while 32% were in the 10-23nm range. The remaining of the 10 second acceleration period (from 50 to 80 mph) showed 62% of particles above 23nm and 38% in the 10-23nm range. As it has been outlined in previous literature [28], during periods of high loads and temperatures, the carbon in the oil breaks down, causing oil derived particles.

However, the overall quantity of particles and oil consumption observed on the top and middle graphs of Figure 46 as well as the values in Table 13 indicate a decrease in particle number (10-23nm) without a decrease in oil consumption. In retrospect, particles larger than 23nm increased (as outlined in Figure 48) as the cycle progressed, suggesting oil might be affecting this size range. Unfortunately, without a method to determine particle material composition (such as TEM) it is difficult to accurately determine the true source of these particles.

Chapter 5: Experimental Results- Europe

5.1 GDI Dyno Bench Tests

As mentioned in Section 3.3, multiple instruments were used to collect data for a European campaign named Sureal23, devoted to the further understanding of sub 23nm particles and the creation of new PEMS. The following section will outline the results found using the standard homologation instruments (Horiba MEXA-2000SPCS and Horiba OBS one) against a new prototype in development labeled the ICAD.

The instrument in question (ICAD) was setup in 3 different configurations to analyze its performance against the current state of art, as well as its ability to operate in a PEMS (Portable Emissions Measurement System) arrangement. These results will aid greatly in the development of new instruments as emissions regulations move towards real emission driving tests.

5.1.1 GDI Dyno Bench Tests – Setup 1

The configuration for the instruments can be observed in Figure 50. As previously mentioned in Section 3.3, the instrument (ICAD) was connected to a small diluter (8.5:1) in order to avoid over saturation while still obtaining reliable data in order to compare it against the Horiba system. Moreover, this was most likely the setup that would be used for the RDE tests, since the road cycle is much longer and the instrument would benefit from having some type of dilution.

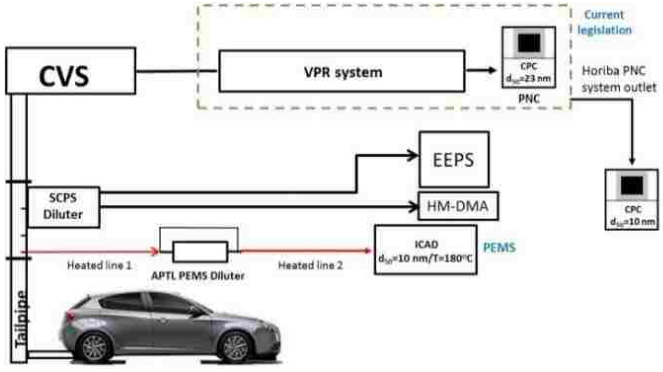

Figure 50: Setup 1

For Setup 1, 2 cold and 2 hot WLTP tests were performed. The cold tests consisted of a vehicle soak of at least 10 at 20°C hours per regulation, while the hot test were performed after the vehicle had reached normal operating engine temperature. Figure 51 demonstrates the results obtained for the cold tests.

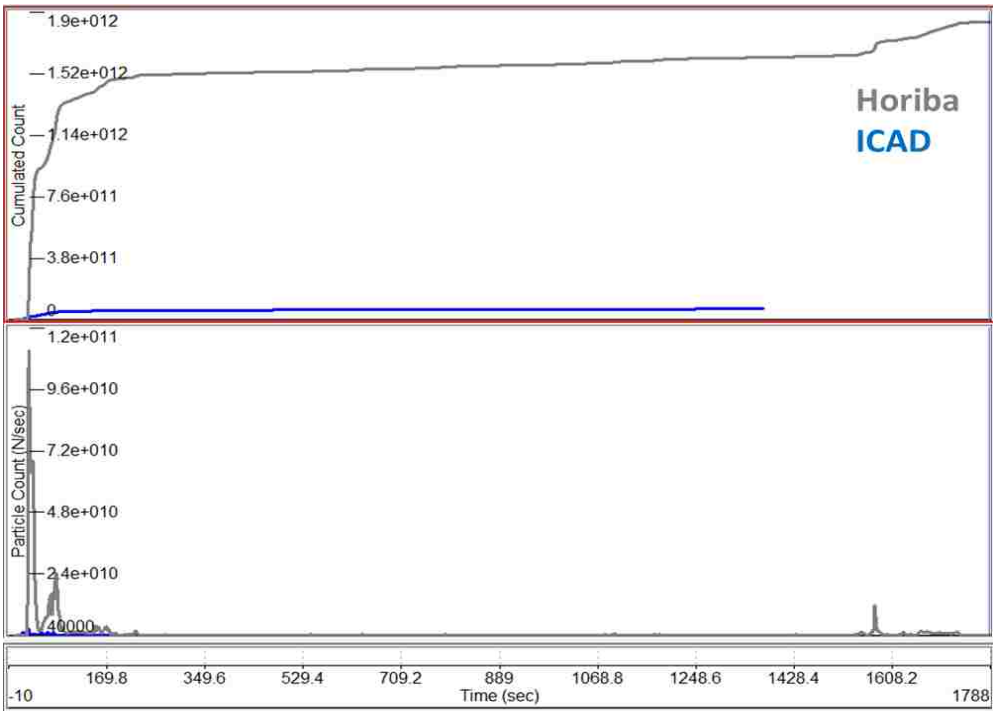

Figure 51: Setup 1 Cold Tests Results

Performing the same type of data analysis that was done for the previous GDI and PFI tests in North America, a large discrepancy can be observed in the figure above. The first graph illustrates the cumulated data for both instruments while the bottom graph illustrates the particles per second. For these test, the Horiba had an overall count of 1.61E+12 while the ICAD counted 6.7E+10.

After analyzing the other tests, it was concluded that the reason for the Horiba counting more than the ICAD was a result of the exhaust flow for the Horiba system being calculated rather than measured. Equation 6 illustrates how this calculation is made in order to determine the exhaust flow;

$$Exhaust\ Volume\ (ft^3) = \frac{Dilute\ Stream\left(\frac{ft^3}{\min}\right) * Sampling\ time(min)}{\frac{CO_2 Tailpipe}{CO_2 Dilute}} \quad [6]$$

It was discovered this measurement was incorrect due to some faults in either the climatic chamber, or the CVS and as the ICAD does not contain a flow meter, this calculated exhaust flow was also used to obtain the particle number per second observed in the bottom graph (Figure 51) for both instruments, and consequently, the top graph outlining the cumulated results.

Therefore, in order to gain a correct comparison, the data for these experiments was analyzed in terms of particles per cubic centimeter, excluding any type of exhaust flow calculation. The number of particles obtained for the ICAD (in a #/cc basis) was corrected for the small diluter (seen in Figure 50). Figure 52 demonstrates the results obtained when the data is analyzed in a particle per cc basis using each of the instruments readings.

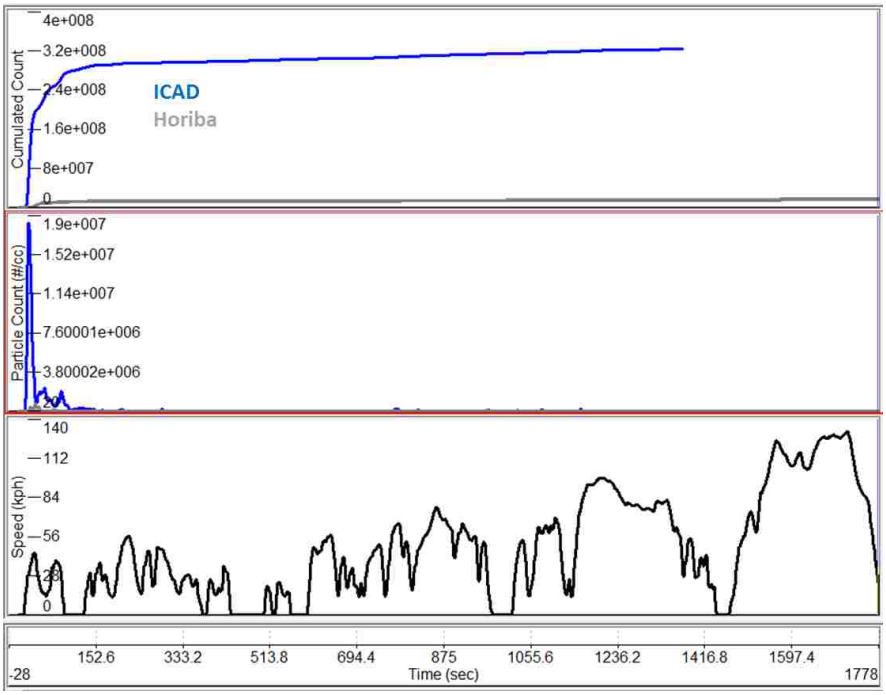

Figure 52: Setup1 Cold Results in #/cc

Although it is less representative of what is occurring at each moment in time (since the exhaust flow is excluded) the data represented in this manner yields better results in terms of which instrument should have the higher count. Due to the lower cutoff of the ICAD a larger amount of particles should be noted. However, these results appear on the extreme side of the theory. For this cycle, the ICAD counted a total of 3.24E+8

particles, while the Horiba Counted 1.68E+7 particles. Both of these results are of a combined average of the two cold tests performed, therefore, in order to gain a better insight of where this discrepancy might be coming from, the two tests were separated.

Figure 53 illustrates the results for the first test of this setup. Although the ICAD stopped recording data 500 seconds before the cycle ended, it can be observed when compared to Figure 52 that the number of cold start particles is much less. The EM (electrometer) signal of the ICAD also displays acceptable values; not exceeding the ±2000mV threshold the instrument has which indicates saturation.

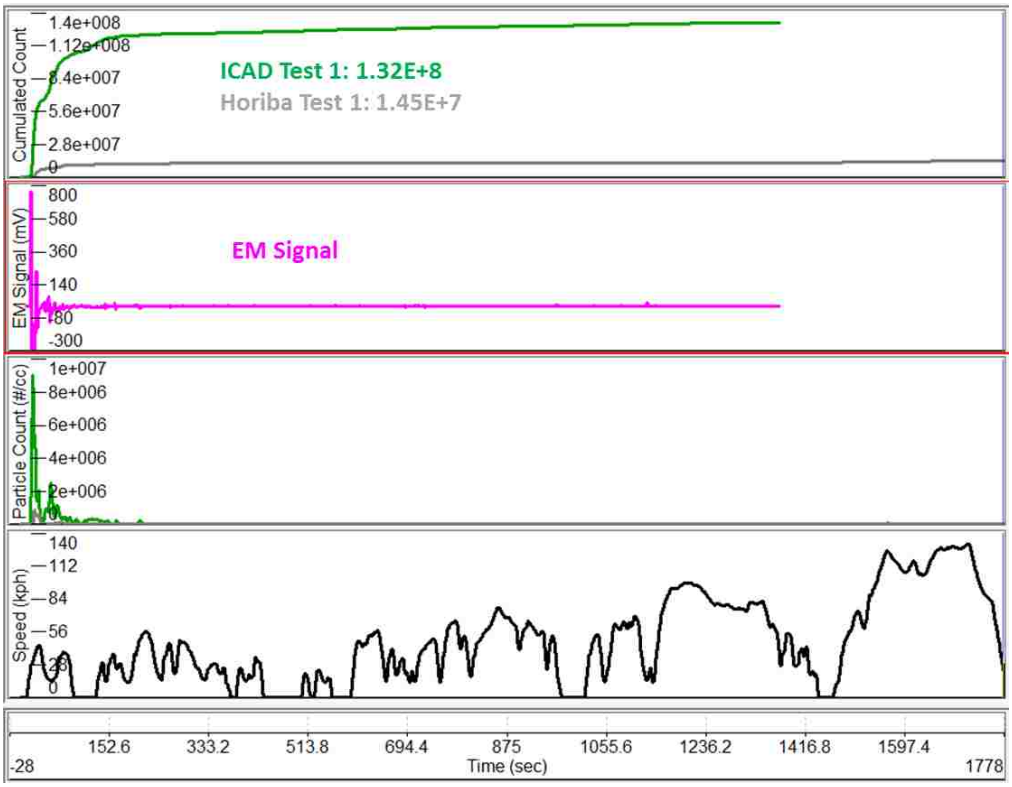

Figure 53: Setup 1- Cold Test 1 Results

For this test the ICAD counted 1.32E+8 compared to 1.45E+7 by the Horiba, a difference in count that is still very high even with the lower cutoff of the ICAD. Test 2 illustrated in Figure 54 demonstrates an even higher difference in count between the two instruments. The ICAD demonstrates a much higher count in the cold start phase, which contributes the most to the overall count. At the end of the cycle the ICAD counted 5.54E+8 particles while the Horiba managed a similar count to the previous test with 1.52E+7 particles. From the EM signal observed in this test, it can be noted the

ICAD was experiencing particle saturation, by reaching the ±2000mv value on multiple occasions during the cold stat phase, which perhaps lead it to an erroneous count value in the end.

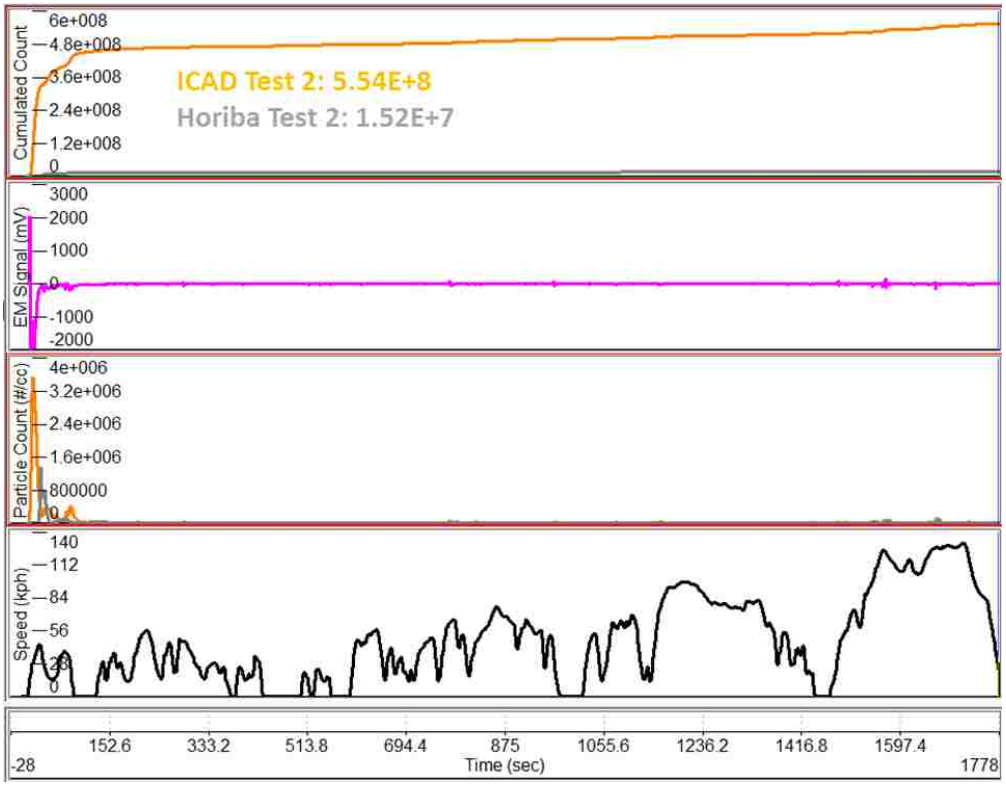

Figure 54: Setup-1 Cold Test2 Results

Observed in Figure 55 are the average results for the hot tests. Although the shape of the cumulated count shows an increasing trend due to the fact cold conditions are absent, similar results with regards to the particle count were obtained.

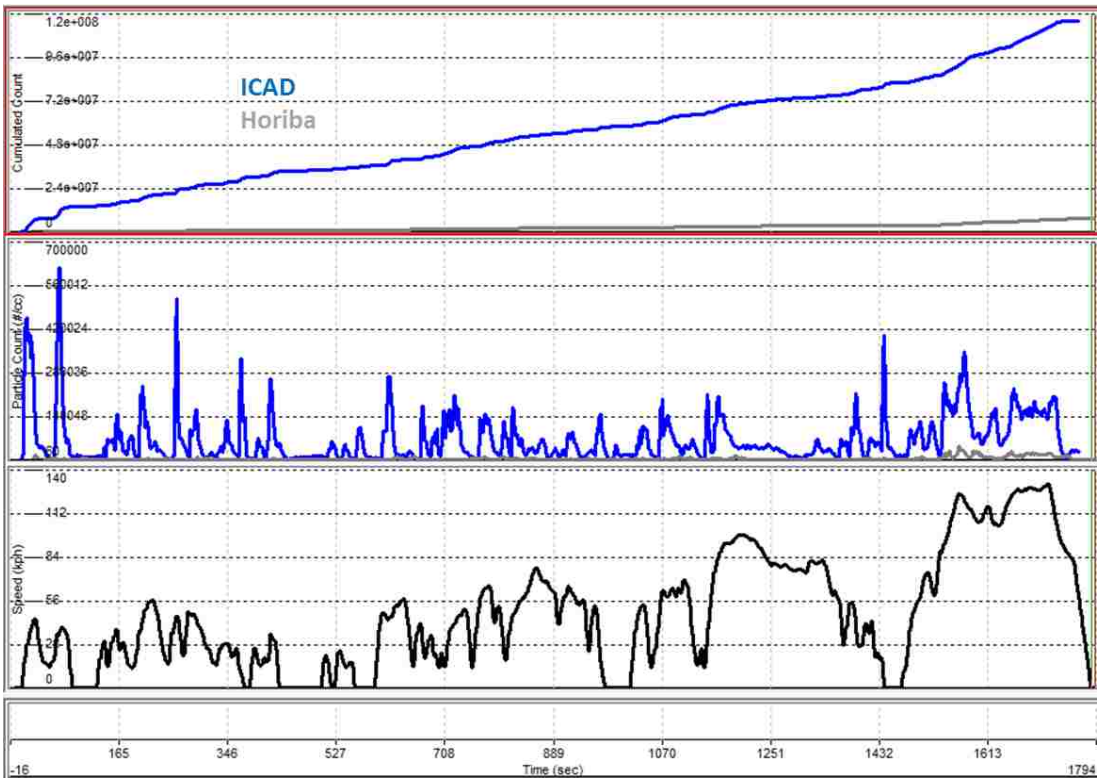

Figure 55: Setup 1- Hot Results

The ICAD measured 1.16E+8 particles while the Horiba counted a max of 7.28E+6 particles. Unfortunately, once again, the average of the ICAD comes as a result of a large difference in measurements from Test 1 and Test 2. Test 1 in Figure 56 below shows a smaller count for the ICAD with a max of 4.63E+7 while the Horiba measures 6.65E+6 particles.

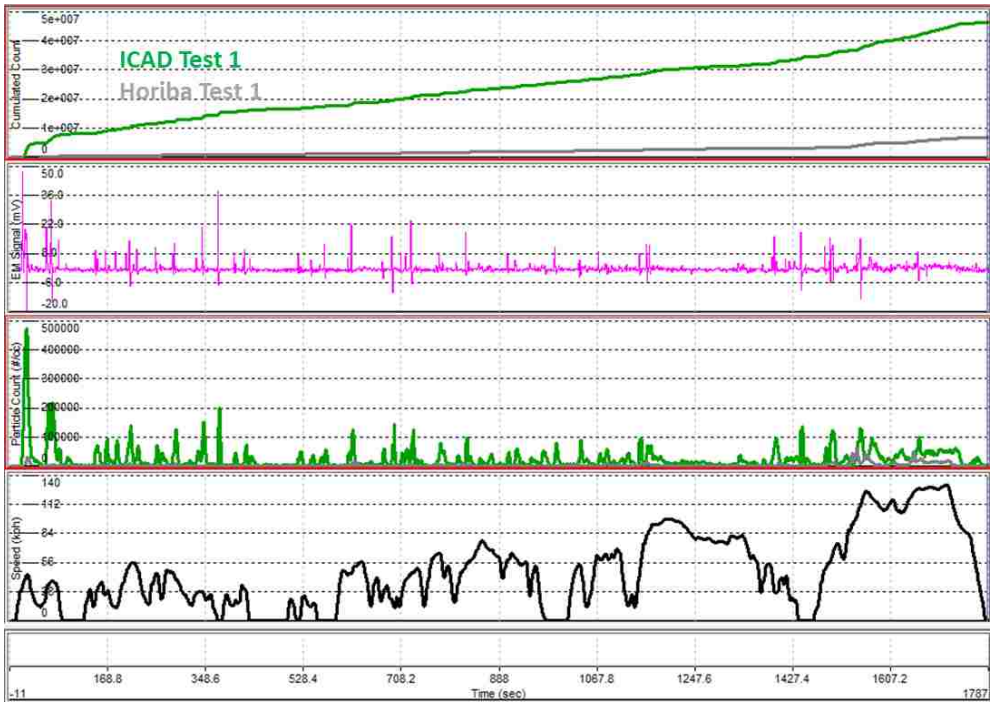

Figure 56: Setup 1- Hot Test 1 Results

Test 2 illustrated in Figure 57 outlines why the average count for the ICAD results (Figure 55) is twice the magnitude of that of the Horiba.

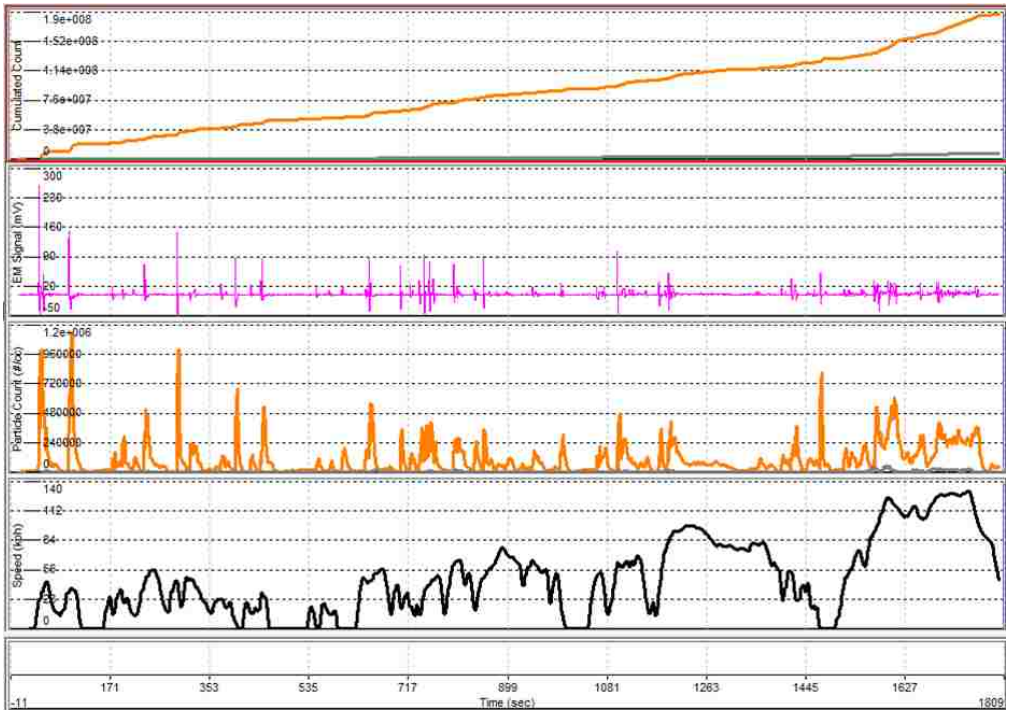

Figure 57: Setup 1- Hot Test 2 Results

For the second experiment, the ICAD measured an overall count of 1.86E+8 while the Horiba instrument measured 7.93E+6. It is important to note that unlike the cold tests, the ICADS EM signal remained well below ±2000mv, avoiding saturation. Moreover, the difference in the total count of the Horiba measurement at the end of each cycle between Test 1 and 2 is only 18%, compared to that of the ICAD at 120%. The possible errors in these measurements will be discussed in the summary section at the end of this chapter.

5.1.2 GDI Dyno Bench Tests – Setup 2

For this setup (pictured in Figure 58) , the ICAD was connected to an SCPS (Sampling and Conditioning Particle System) with a total dilution of 35, consisting of a hot dilution stage at 150°C and one cold dilution set at 20°C. Between these dilutions was a VPR system composed of a catalytic stripper. This was done in order to have an alternate option in the case that particle numbers were too high for the ICAD in setup 1 and caused saturation of the instrument. For this configuration, there were 2 cold and 3 hot WLTP tests performed.

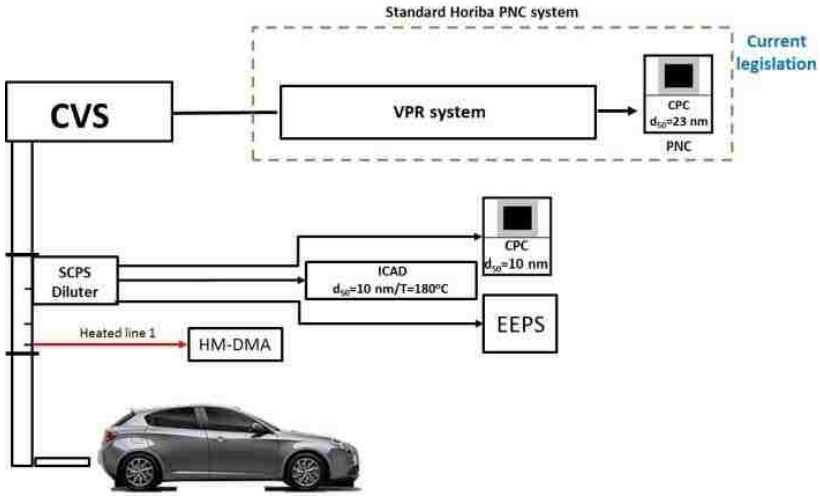

Figure 58: Setup 2

The results illustrated in figure 59 demonstrate a similar outcome to those of setup 1. When the average of the two tests is computed for each parameter, a large discrepancy can be seen in the measurements.

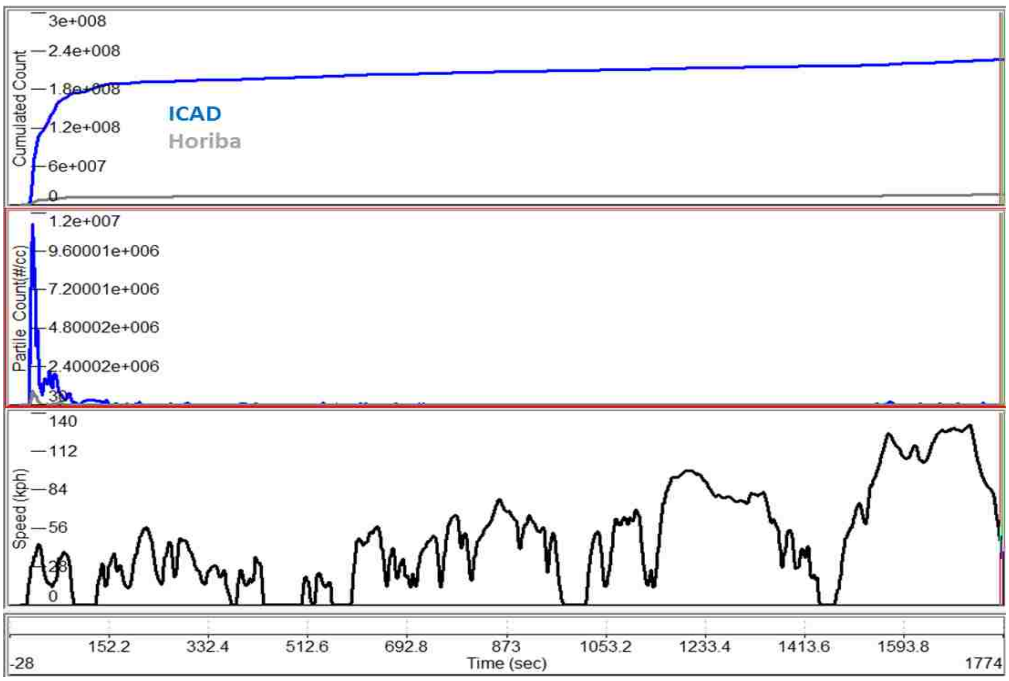

Figure 59: Setup2 -Cold Results

The ICAD measured 2.27E+8 particles, while the Horiba measured 1.6E+7. Comparing these to the average cold results of setup 1, there is a difference of 35% in the ICAD's measurements and 5% in the Horiba's. It is important to note that there was no change in the Horiba's instrument setup; therefore little deviation in the results was expected. For the ICAD however, a catalytic stripper was added. This could indicate that the reduction of particles is a result of this addition, eliminating either volatiles that were making it to the instrument in setup 1 or, eliminating actual particles due to diffusion, and particle thermophoresis (as has been the case in the North America tests).

When examining the tests separately, once again there is one instance where the ICAD counts significantly more particles than the other. Figure 60 illustrates the first test, where the ICAD measured 6.66E+7 and the Horiba 4.14E+6. This was an unexpected result by the Horiba, as the previous cold test both had a total number of particles a magnitude higher. Moreover, the EM signal for both appears to obtain more noise than in the previous setup, but the values remain within the acceptable range.

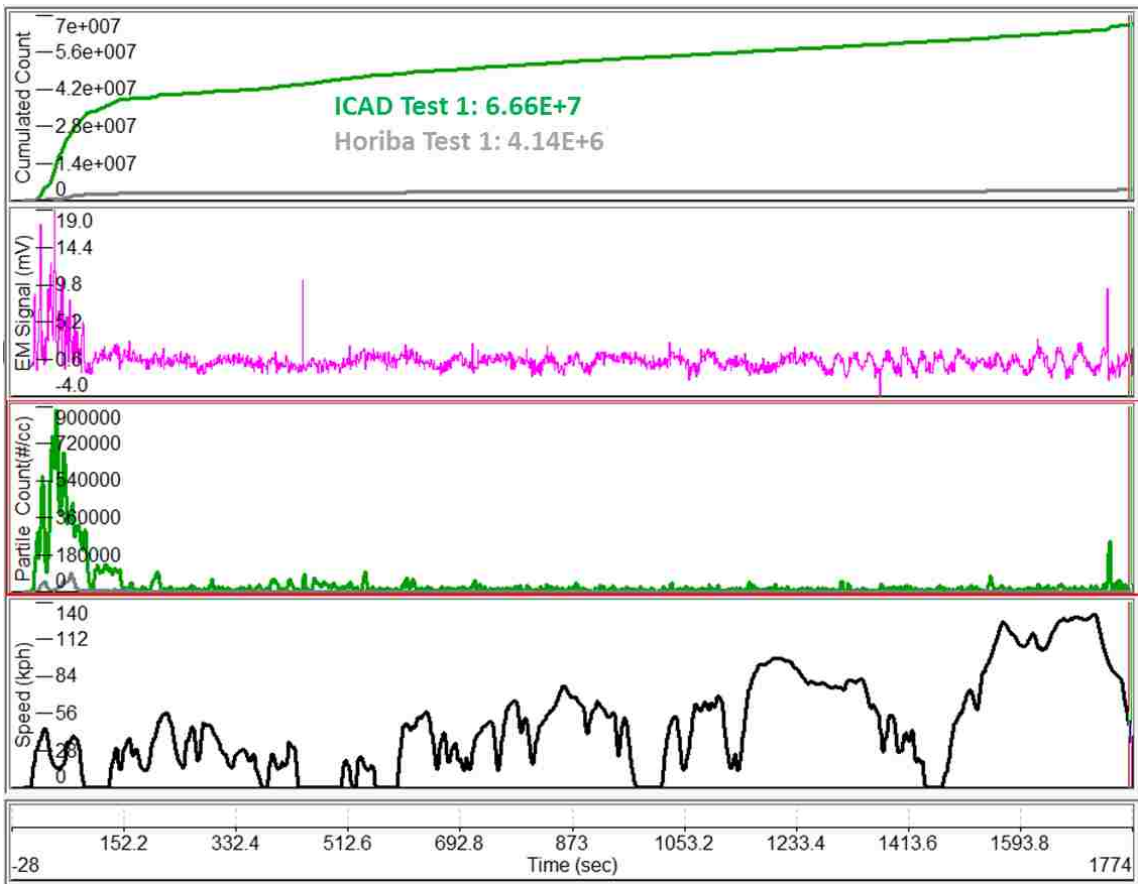

Figure 60: Setup 2 Cold Test 1 Results

Tests 2 illustrated in Figure 61 resulted in higher numbers for both instruments, where the ICAD counted particles one magnitude higher (3.87E+8) than Test 1. The Horiba (2.79E+7) followed a more expected result when comparing it to cold tests in setup 1.

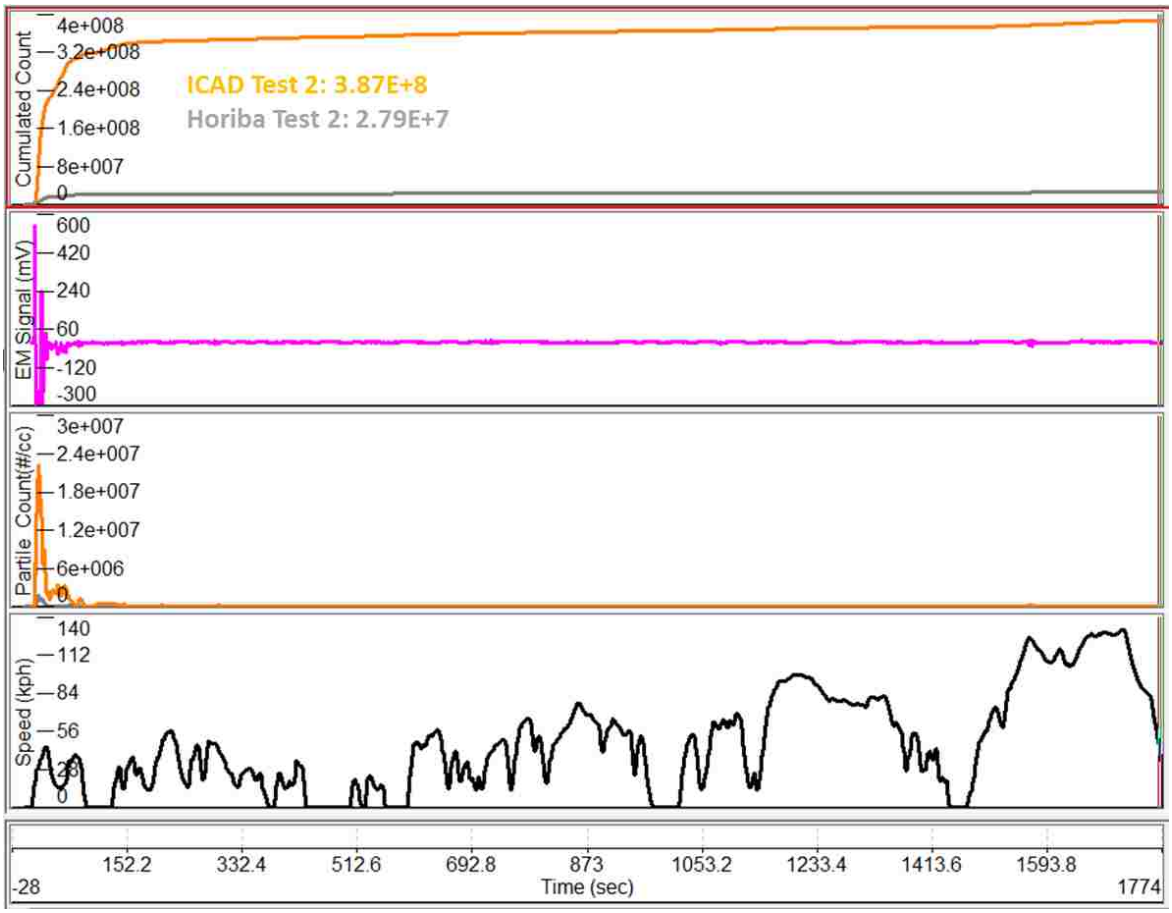

Figure 61: Setup 2 Cold Test 2 Results

The Hot tests results illustrated in Figure 62 demonstrate a trend like that of setup 1, where the overall count is not dominated by the beginning of the cycle since the cold start is absent. The respected final count for each instrument is 1.21E+8 for the ICAD and 1.08E+7 for the Horiba. When comparing it to that of the hot tests for setup 1, both instruments have an increase in count. This was unexpected for the Horiba since its setup does not change throughout the experiments, but also for the ICAD, since fewer particles are expected with the use of a VPR.

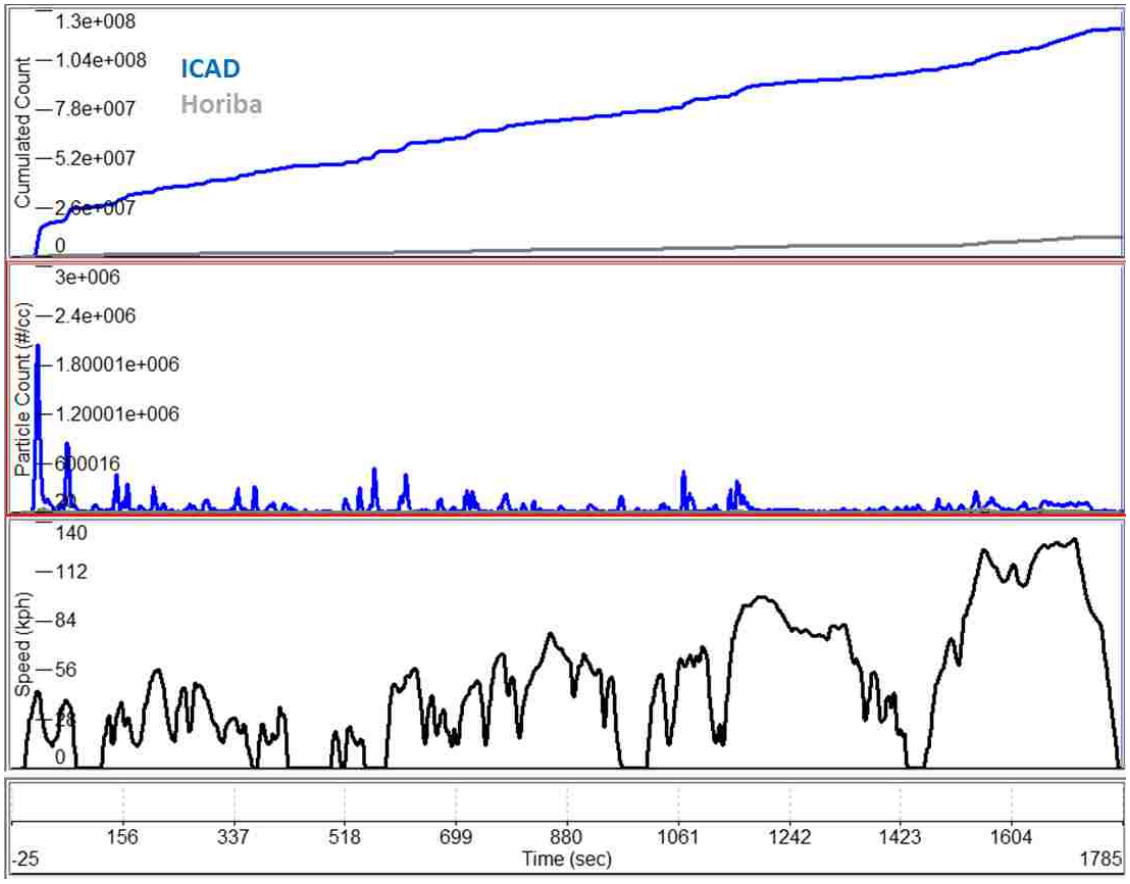

Figure 62: Setup 2- Hot Tests Results

The count illustrated by the blue trace in the figure above is a dominated by the count of the last two hot tests, while the first hot test conducted showed a significant smaller count (exemplified in Figure 63 on the following page). For this experiment, the ICAD measured a total of 6.53E+7 Particles while the Horiba counted 4.64E+6 Particles. Although these tests do not include a cold start condition, the ICAD seems to still be sensitive to those first few transients, while the Horiba (in this test) measures an insignificant amount. It is important to note that the EM signal for this entire set of tests was within the acceptable values.

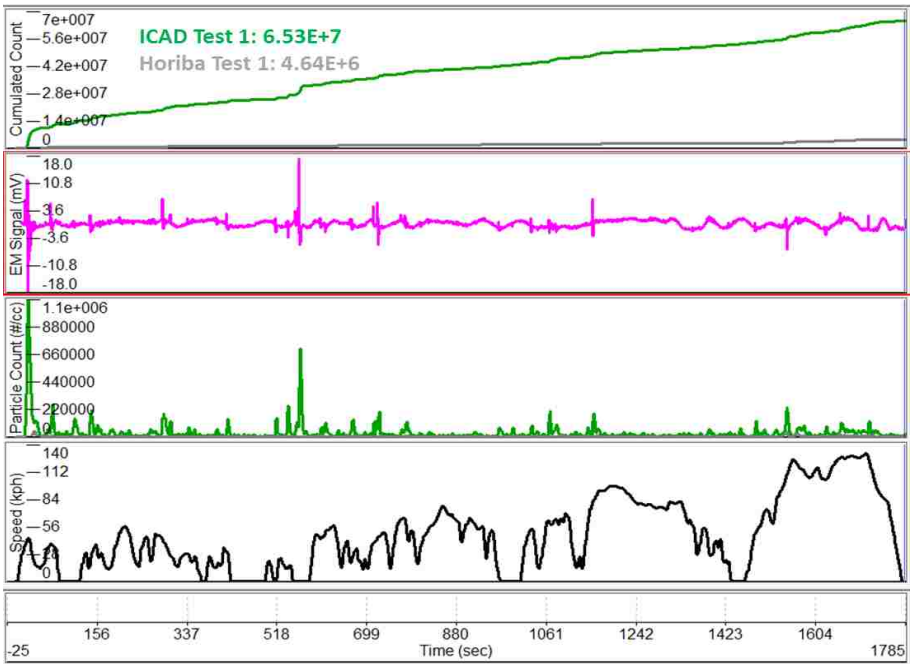

Figure 63: Setup2 Hot Test 1 Results

Hot tests 2 & 3 are combined into Figure 64 .This was done as, unlike the previous tests that have been analyzed, the last two for setup 2 were performed consecutively on the same day, and it appears there is some correlation due to the ICAD results.

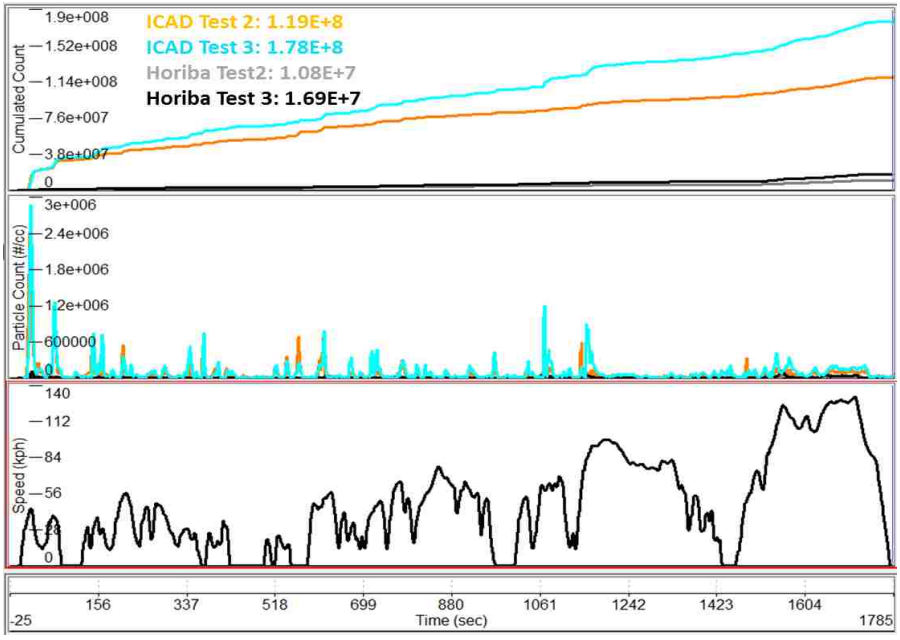

Figure 64: Setup 2 Hot Test 2&3 Results

For hot tests 2 & 3, the ICAD measured 1.19E+8 and 1.78E+8 particles respectively. These results yield a difference in instrument reading of 40%, the lowest the ICAD had experienced to this point (within the same setup). The Horiba was able to measure 1.08E+7 Particles for Test 2 and 1.69E+7 for Test 3, resulting in a difference of 44% (difference appears smaller on the graph due to the scaling required to fit the ICAD data).

5.1.3 GDI Dyno Bench Tests – Setup 3

For setup 3 observed in Figure 65, the plan was to have an alternate solution in the event that not enough particles were detected in setup 1. These tests would also help validate whether the ICAD could operate in a complete raw exhaust configuration. This would be desirable if this instrument was to be used as a PEMS instrument, since it would potentially mean less apparatus' needed in the vehicle. There were 5 total tests conducted in this configuration, 3 Cold and 2 hot. Since the ICAD operated in a raw configuration, no dilution factor correction was needed for these results.

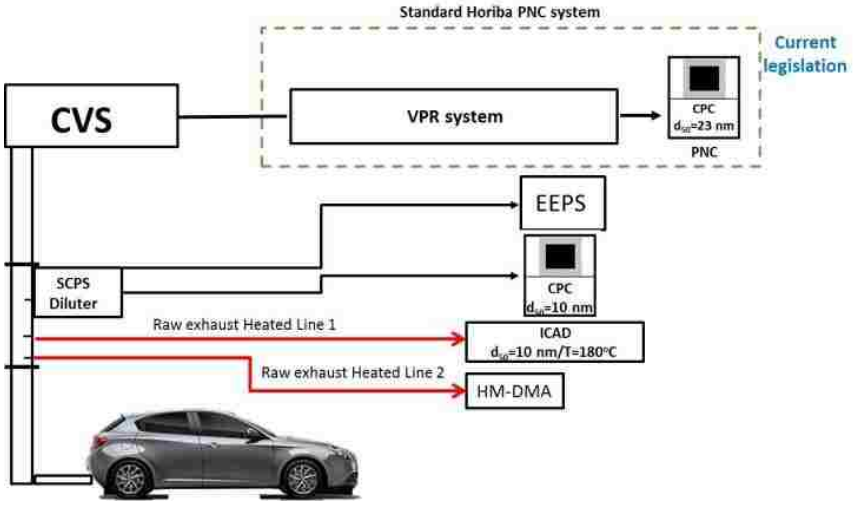

Figure 65: Setup3

Figure 66 depicts the average results found for the cold tests performed in setup 3.

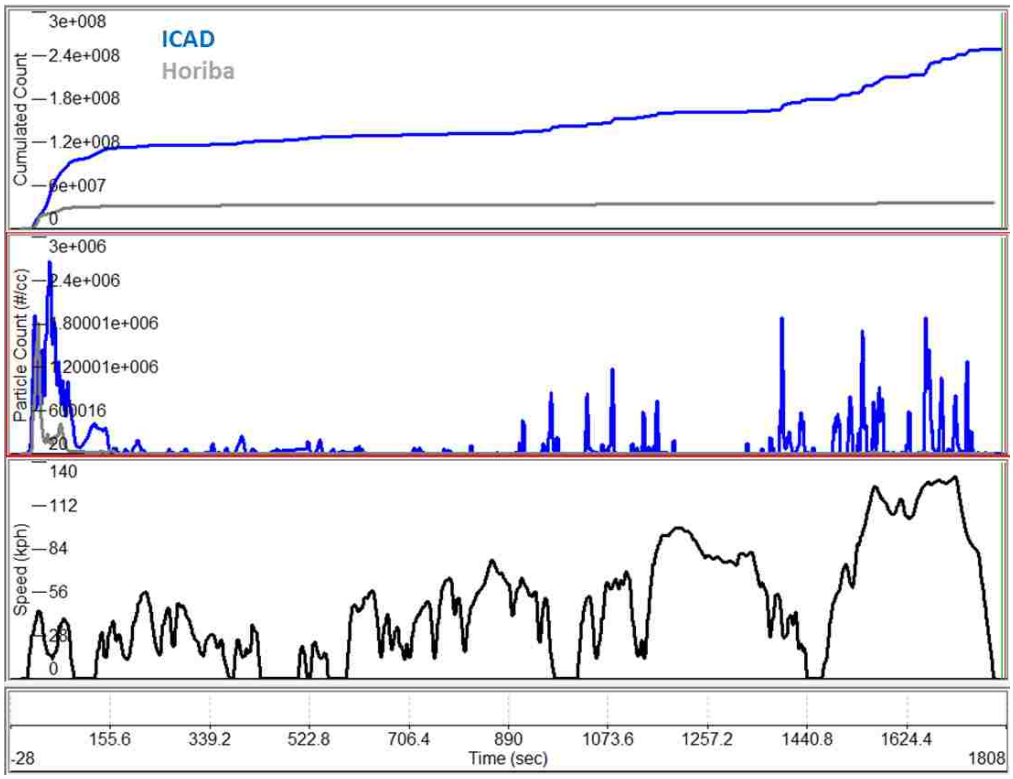

Figure 66: Setup 3 Cold Results

With its raw exhaust configuration and the lower particle diameter cutoff, the ICAD was expected to count several more particles than the Horiba instrument. The results above demonstrate the ICAD counted 2.48E+8 particles compared to that of 3.69E+7 from the Horiba. When comparing the ICAD count to previous setups, a higher count was expected due to the fact that no dilution procedure or VPR were present in this configuration. When the average in the figure above was deconstructed into the respected tests, it can be observed on Figure 67 that test 2 caused the average count to be lower. While test 1 and 3 measured a particle count of 4.43E+8 and 2.78E+8 respectively (a difference of 45.8%), test 2 measured a magnitude lower, with 2.36E+7. It is important to note that when the EM signals (middle graph) are analyzed, both test 1 and 3 show multiple instances where the instrument appears to be saturated (values of ±2000mV) while test's 2 signal is within the appropriate range. This could signify that even though test 2 had an unusual low count, the instrument could benefit from some type of dilution or VPR to avoid the over saturation observed in these tests.

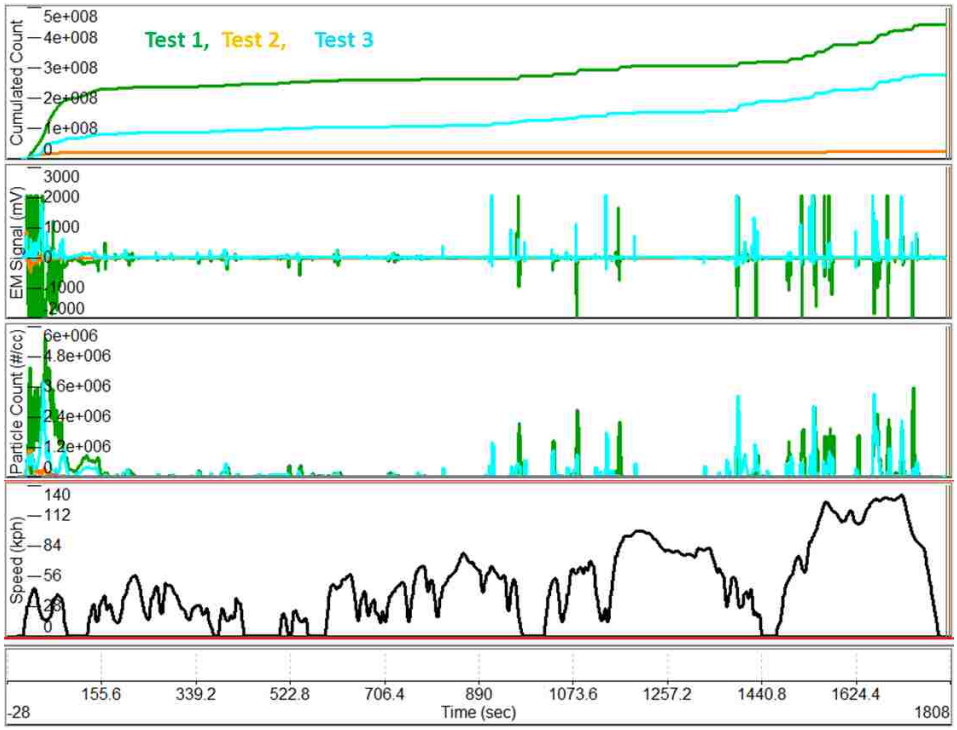

Figure 67: Setup 3 Cold Tests 1, 2 and 3

The average of the Hot tests presented in Figure 68 was a result of two consecutive test performed on the same day (like two of the previous hot tests in setup2).

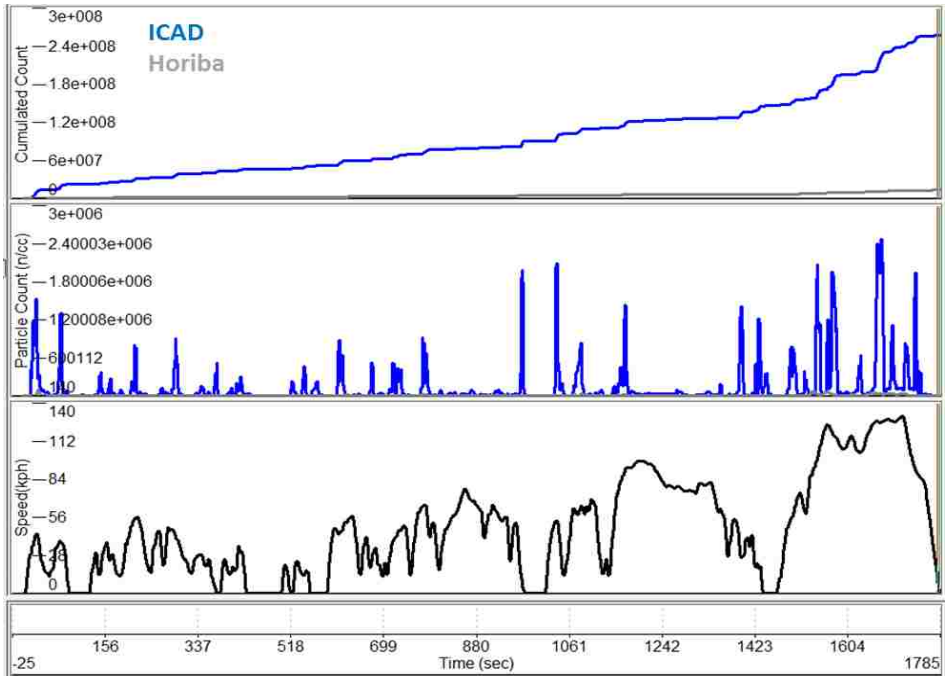

Figure 68: Setup 3 Hot Test Results

For this portion of the testing campaign, the ICAD measured a total of 2.57E+8 Particles while the Horiba measured 1.33E+7. An interesting result is that once again, during these consecutive tests, the ICAD's difference in count was below 50%, with test 1 counting 2.03E+8 particles and test 2 with 3.11E+8 (42%diff). The Horiba also demonstrated a similar trend with regards to an increase in count from test 1 to 2, measuring 1.08 E+7 and 1.62E+7 respectively (40%diff). Figure 69 represents these results, with the top figure having an adjusted second axis with a magnitude smaller (black) to display the Horiba results alongside the ICAD. The second graph from the top (EM Signal) once again displays values reaching the ±2000mV threshold for both tests, which correlate with the highest PN spikes.

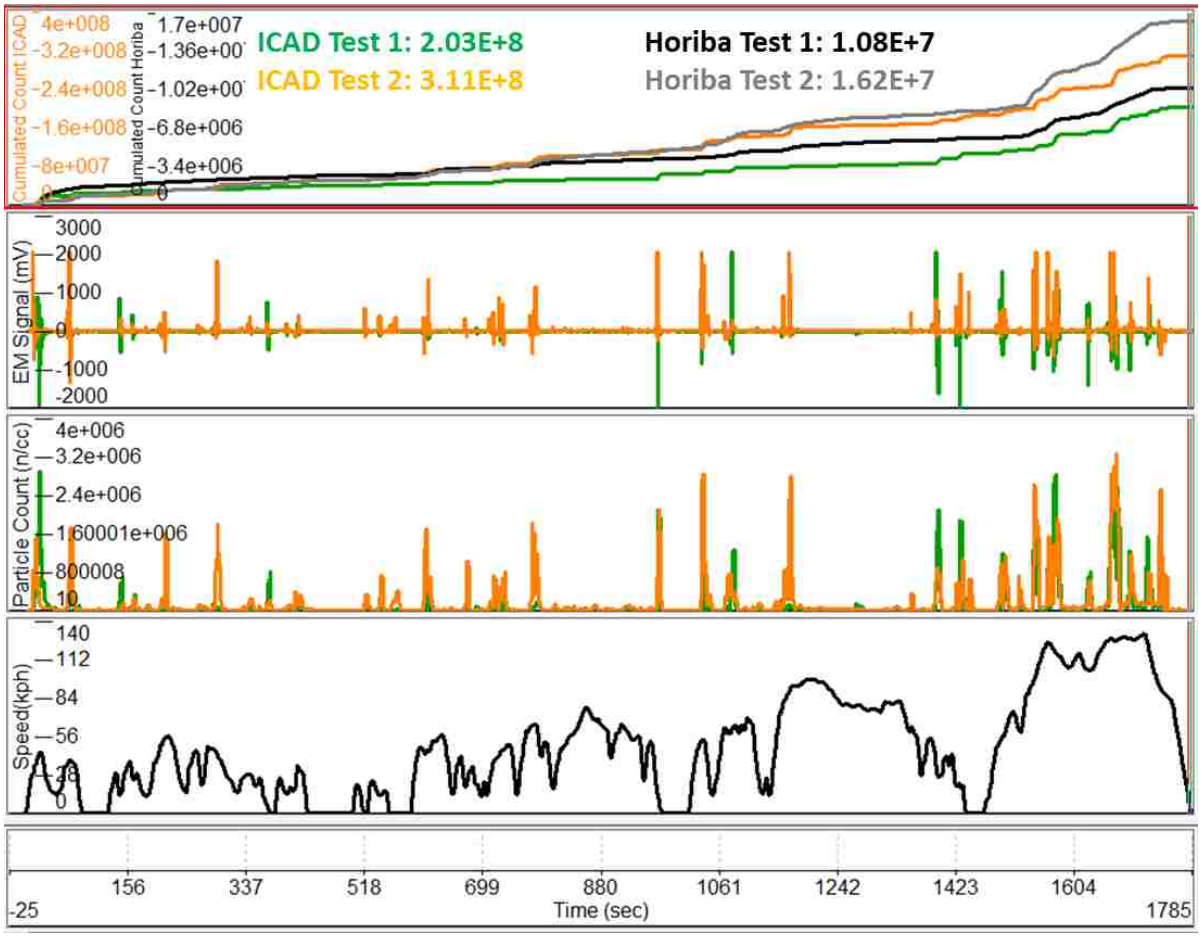

Figure 69: Setup 3 Hot Test 1&2 Results

5.2 Dyno Test Results Summary

For this part of the testing campaign, multiple instruments were examined in order to acquire a better understanding of the impact of sub 23nm particles as well as the performance of new prototypes being developed for future portable emission testing. The following is a summary of the results found between the Induced Current Aerosol Detection (ICAD) System and the current homologation system, the Horiba MEXA-2000SPCS.

Table 14 outlines the number of WLTP tests performed for each of the setups described in the previous section while Table 15 highlights the difference in particle number found for the different instrument setups, displaying only the average results for each test and instrument.

1.8L GDI+GPF WLTP Cycles Performed		
Configuration	Number of Cold Tests	Number of Hot Tests
Setup 1	2	2
Setup 2	2	3
Setup 3	3	2

Table 14: Number of WLTP Tests Performed

	Cold Tests		Hot Tests	
Configuration	ICAD	Horiba	ICAD	Horiba
Setup 1	3.24E+8	1.68E+7	1.16E+8	7.28E+6
Setup 2	2.27E+8	1.60E+7	6.53E+7	4.64E+6
Setup 3	2.48E+8	3.69E+7	2.57E+8	1.33E+7

Table 15: Summary of Results

For each of the setups and tests, the ICAD constantly measured a magnitude above that of the Horiba. Although a 30 % higher count was expected (due to the lower cutoff of the ICAD), the experiments showed differences that were magnitudes higher. This could be due to multiple factors within the ICAD, as a lot of the higher counts correlated with EM signal values that indicate oversaturation of the instrument.

One possible explanation for these results could be what some of the developers of the ICAD found in an experiment (Fierz et.al [31]). They established that a pulse to pulse variability in the chargers ion directly translated to instrument noise. Moreover, due to this pulsing, the time resolution is given by one pulse per period, and this cannot be changed easily since the faraday cage size, flow rate within the instrument and pulse period are interconnected. The researchers concluded that these factors make the ICAD less sensitive than other diffusion charging instruments, since an AC amplitude is evaluated and a non-zero baseline appears even when there is particle-free exhaust [31].

When the instrument was paired with the SCPS (setup2), it can be observed from Table 15 how the ICAD count was reduced for both cold and hot tests. This is a clear indication the CS is having an impact on the particle count, whether removing volatiles that are being detected as particles in setup 1 and 3 or negatively impacting results by eliminating particles <100nm through diffusion and thermophoresis. Unfortunately without having a method to examine particle composition, it is difficult to determine the exact impact of the CS on final particle count. Setup 2 was also the only set of tests where no EM signal values were abnormal, leading to the conclusion that the ICAD benefits from having some type of dilution, especially during cold starts and aggressive cycle transients.

Lastly, a standard error analysis (illustrated in Figure 70) for each instrument was performed to examine how the cold and hot engine conditions affected the instruments readings.

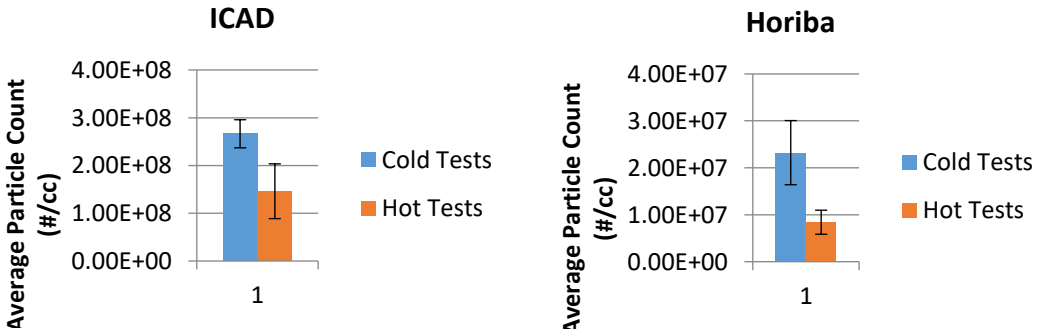

Figure 70: Standard Error Analysis for Both Instruments

Although discrepancies were expected for the ICAD since the configurations were changed, it is interesting to note that most of the variations in the results came from the hot tests, where there is less of a divergence in count through the cycle in comparison to when cold start conditions are present. This seems to be a result of test 1, in setup 2, where the instrument counted a magnitude less compared to the other two tests. The Horiba instrument on the other hand was expected to have little variation within the respected tests. However, from Figure 70 Table 15 it can be observed the instrument counted a significant amount more particles than in the previous two setups, something not expected since the configuration did not change. Perhaps the errors that occurred for the measurement of the exhaust flow (which prevented this data from being represented in particles/sec) are linked to this discrepancy, but at the time of this work, the reasons are still inconclusive.

5.3 PEMS Instrument Comparison

As it was mentioned in section 3.3, the ICAD (in a setup 1 configuration) was also examined against the Horiba PEMS instrument (OBS one), currently used for calibration procedures and research. The 2 tests conducted were both WLPT cold cycles and also the last experiments conducted in preparation for the RDE tests. Unlike the previous experiments, the Horiba PEMS is equipped with an exhaust flow meter. This allowed the data to be processed in terms of particles per second for both instruments, resulting in a more accurate representation of particle emission. To do this, Equation 7 was used;

$$\left(\frac{\#}{sec}\right) = \left(\frac{\#}{cc}\right) * ExhFlow\left(\frac{kg}{sec}\right) * \left(\frac{m^3}{1.29kg}\right) * \left(\frac{1*10^6 cc}{m^3}\right) * DR_{ICAD} \quad [7]$$

The results illustrated in Figure 71, display similar results (with regards to particle count discrepancy) as those measured in the previous tests. With the ICAD having an overall count of 1.38E+13 compared to that 1.39E+12 of the Horiba. Like in previous tests, there is also a large discrepancy between test 1 and 2, as demonstrated in Figure 72 and Figure 73.

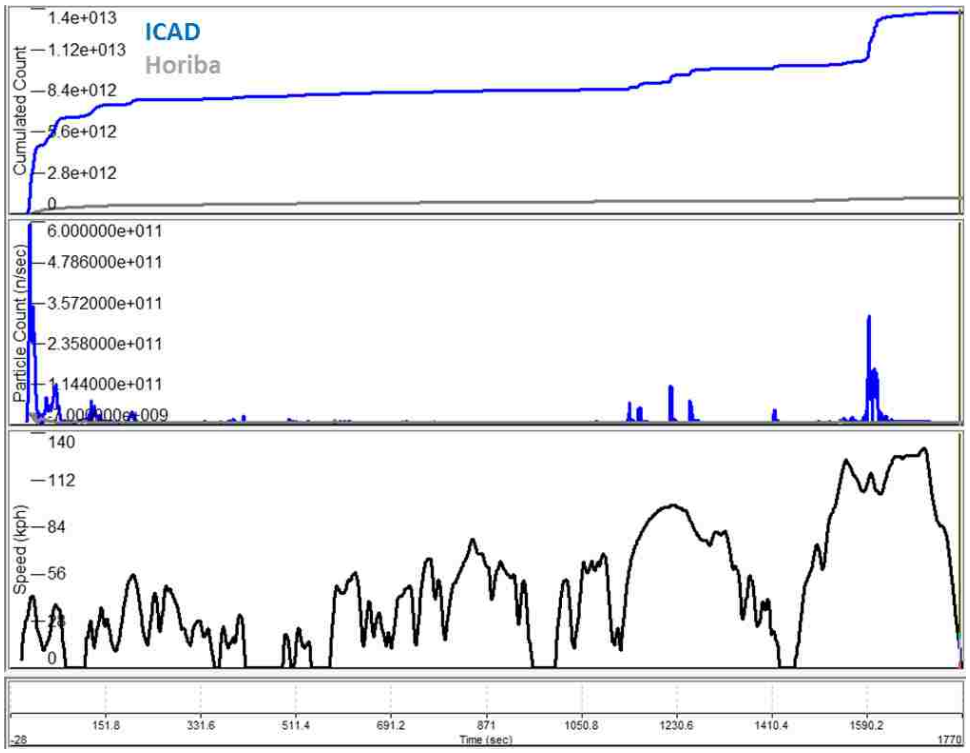

Figure 71: PEMS Results

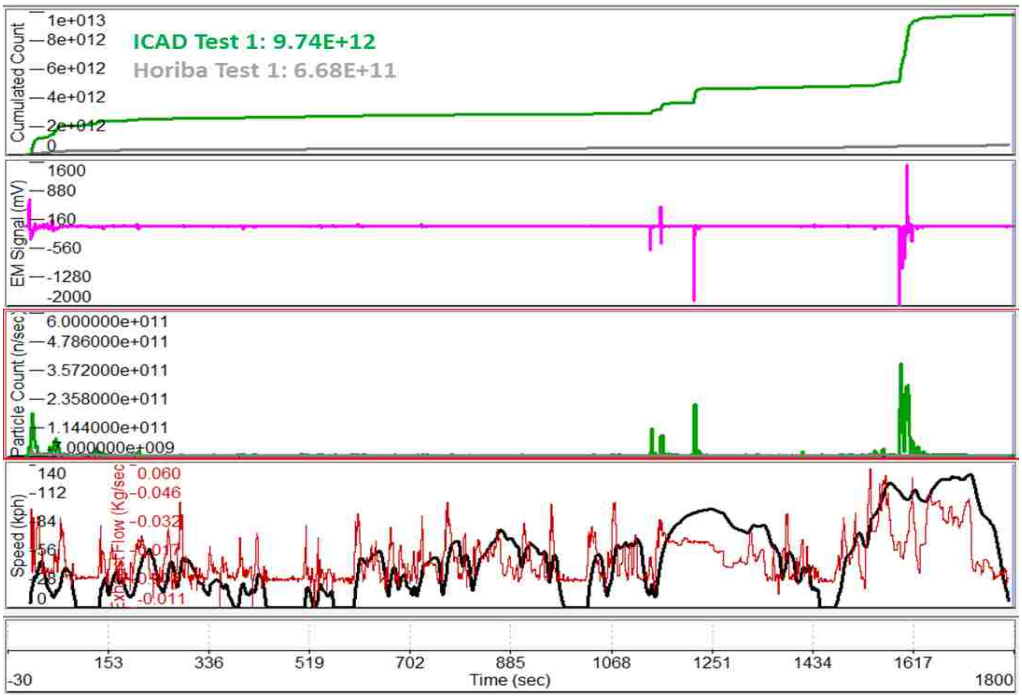

Figure 72: PEMS Test 1 Result

For this test, the ICAD completed the cycle with a cumulated count of 9.74E+12 while the Horiba counted a total of 6.68E+11. Table 16 depicts a breakdown of the mean particle count throughout different phases of the cycle.

Phase of Cycle	0-500sec	500-1020sec	1020-1470sec	1470-1800sec
Horiba	3.28E+11	4.38E+11	5.06E+11	6.08E+11
ICAD	2.28E+12	2.78E+12	3.98E+12	7.62E+12

Table 16: PEMS Test 1 Cycle Breakdown

Although the difference is large between the two instruments in the first two phases (low and medium), as the cycle progresses, the ICAD' count dramatically increases for the last two sections, resulting in a count much greater than that of the Horiba. These PN spikes observed in the third graph correlate to the EM Signal value spikes, which reach and surpass the threshold of ±2000mV which once again mean the instrument is saturated. Moreover, the last phase shows PN numbers much larger than those of the cold start, something that in theory is very unlikely to happen, leading to the conclusion that the PN number observed during these phases is most likely incorrect.

Figure 73 illustrates the second test, where the ICAD has an opposite effect in the measurement of particles. The ICAD counted 1.78E+13 particles while the Horiba had a total of 2.21E+12.

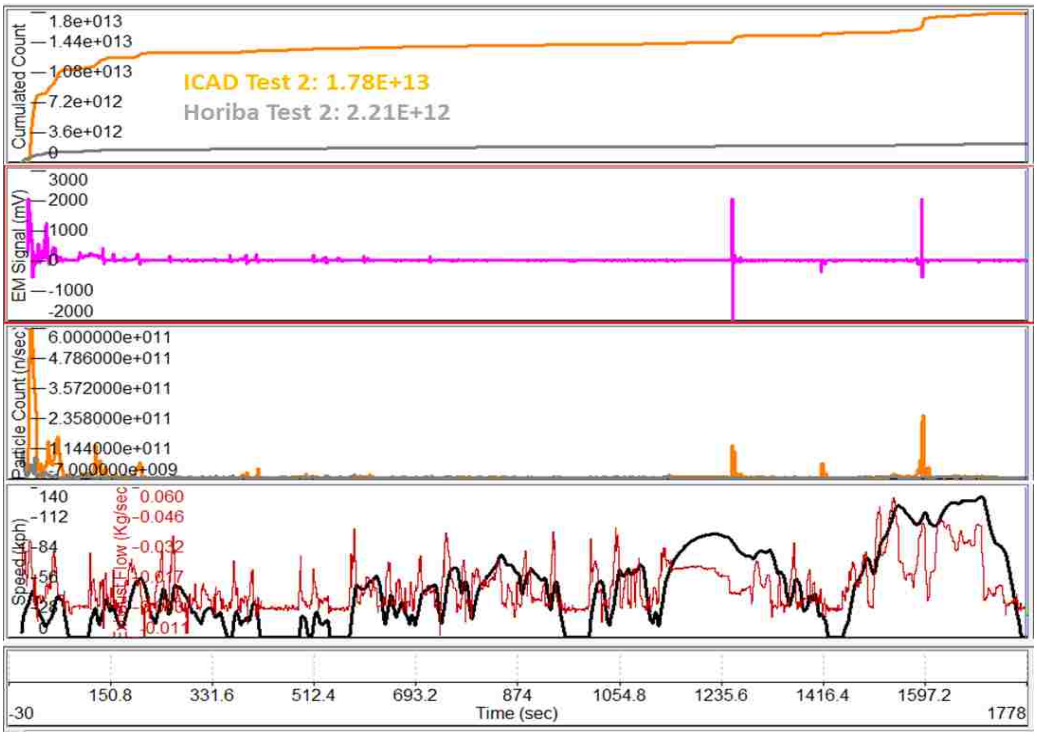

Figure 73: PEMS Results Test 2

Table 17 illustrates the distribution of count for both instruments throughout the cycle. In this occasion the ICAD detected a magnitude higher number of particles during the cold start phase than the previous test. This large PN spike was also accompanied with an EM signal exceeding the thresholds of the ICAD. The results of these tests also illustrate how PN spikes happen even in time ranges (1256 sec and 1400) where there is an exhaust flow decrease, as illustrated by the red, bottom trace.

Phase of Cycle	0-500sec	500-1020sec	1020-1470sec	1470-1800sec
Horiba	1.42E+12	1.77E+12	1.91E+12	2.09E+12
ICAD	1.22E+13	1.39E+13	1.47E+13	1.68E+13

Table 17: PEMS Test 2 Cycle Breakdown

Figure 74 below is an enlarged version of tests 2 showing the PN spike at the 1256 seconds, when the exhaust flow is decreasing and the vehicle is undergoing a coast phase. Although it appears small in this graph, this peak represents a measurement of 1.28E+11 particles compared to that of the Horiba (not visible in the graph due to the scale) of 5.68E+7. The EM Signal has also been plotted on the top graph to illustrate the effects of possible saturation.

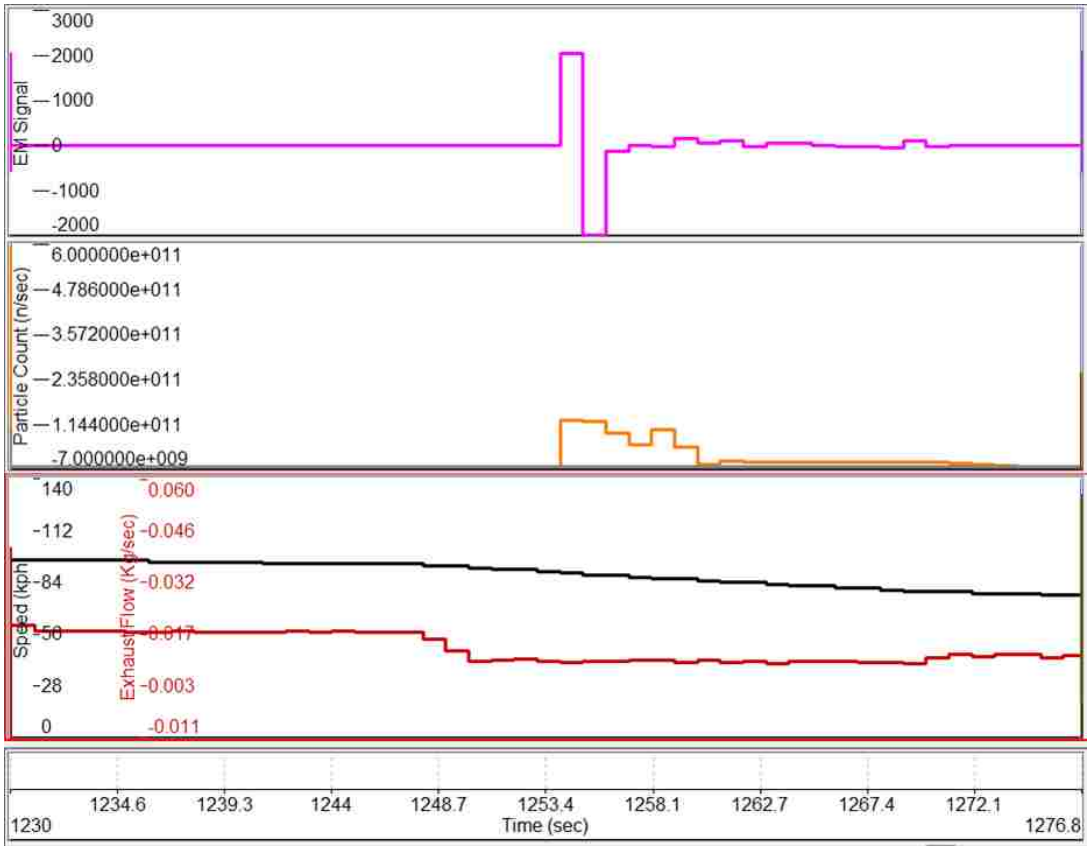

Figure 74: Zoomed in Test 2 PN Spike

5.4 RDE Test Results.

For this last phase of the Sureal23 campaign, the ICAD was compared to one of the PEMS currently used in the industry, the Horiba OBS one. An RDE cycle which consisting of urban, rural and motorway driving was performed under cold start conditions, and repeated three times over a one week period. For details on this cycle, refer back to section 3.3.1. Figure 75 illustrates the results found for these tests represented as averages for each parameter.

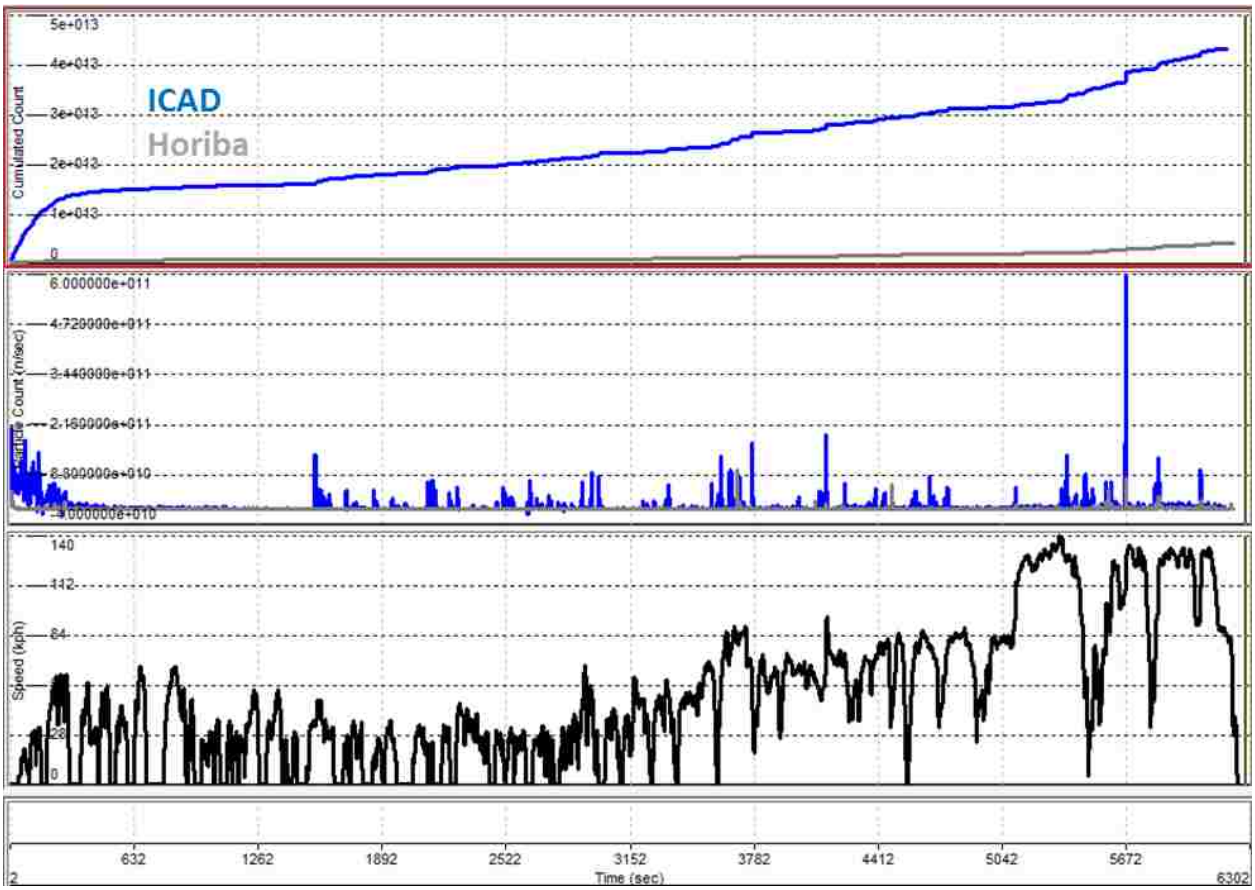

Figure 75: RDE Test Results

The combination of the three tests performed resulted in an average ICAD count of 4.32E+13 and 4.19E+12 for the Horiba. Because these tests were performed in real world driving conditions over a period of three days which consisted of different traffic levels, slight changes in weather, etc. the following section will describe the tests individually, as different observations can be made for each test.

5.4.1 RDE Test 1

Figure 76 represents the trace data for Test 1 while Table 18 outlines the summary of the trip. All three tests were performed with the same instrument payload of 100kg.

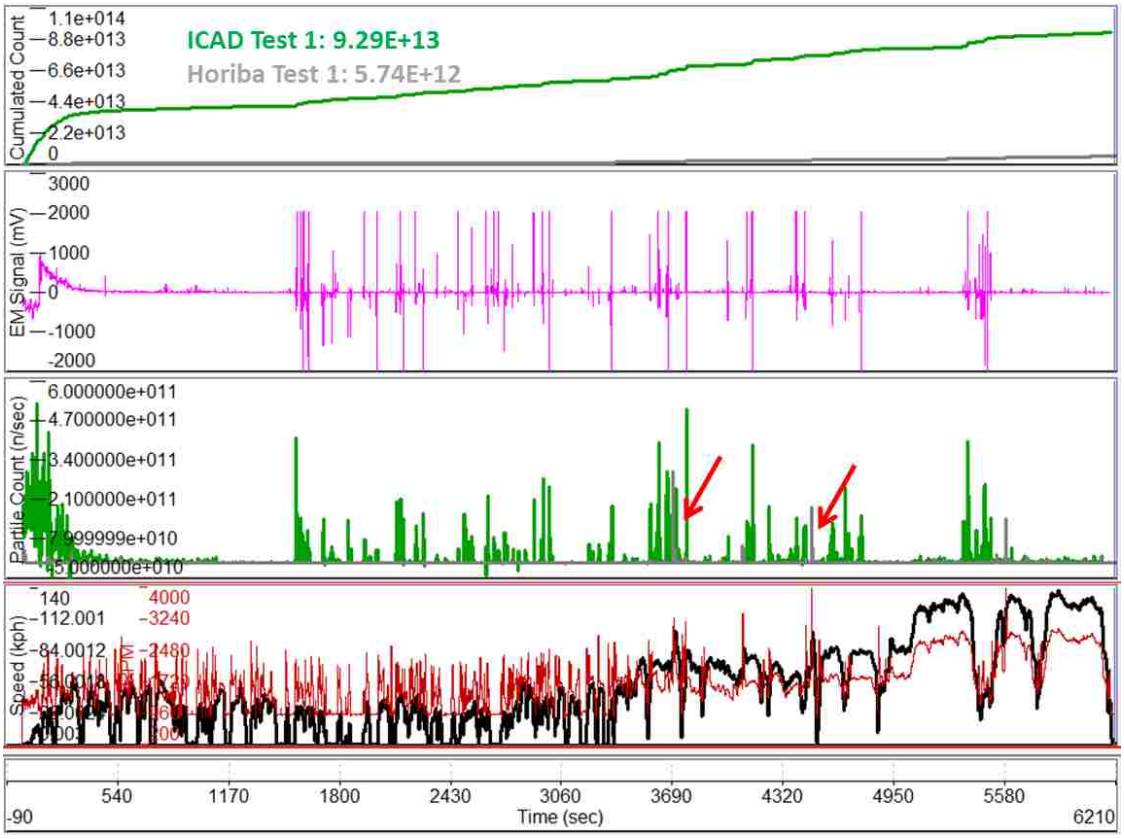

Figure 76: RDE Test 1 Results

Total Trip Distance (km)	86.53
Total Trip Duration (hh:min:sec)	1:46:48
Trip Average Speed (kph)	48.6
Total Stop Duration (sec)	785
Max/Min Temp (°C)	34.6 / 28

Table 18: RDE Test 1 Summary

The total count for the ICAD for Test 1 was 9.29E+13 particles while the Horiba measured 5.74E+12. This was the highest count the ICAD recorded through this testing campaign. It can be noted from the EM signal graph in Figure 76 how often the value reach the saturation levels of ±2000mV. Once again this seems to correlate with PN spikes measured by the ICAD. Moreover, although it is less noticeable, the Horiba instrument also displayed unexpected values indicated by the red arrows, in the second

graph from the bottom. These peaks had values a magnitude higher than those of the cold start (10^{11} vs10^{10}), something unexpected from this instrument.

5.4.2 RDE Test 2

Figure 77 depicts the results obtained for Test 2. Although the cycle is the same, and the test summary (Table 19) is very similar to the previous, a big reduction in count was observed for both instruments. The ICAD measured a total of 8.28E+12 particles (a magnitude smaller than the previous) while the Horiba counted around half as much as the first test, with 2.11E+12 as the final count. It can be observed once again that larger peaks are measured in the last part of the cycle, where the highway section of the test takes place. For this test however, the signal of the electrometer (pink graph) varied between -200 and 300mV, indicating the instrument was not saturated.

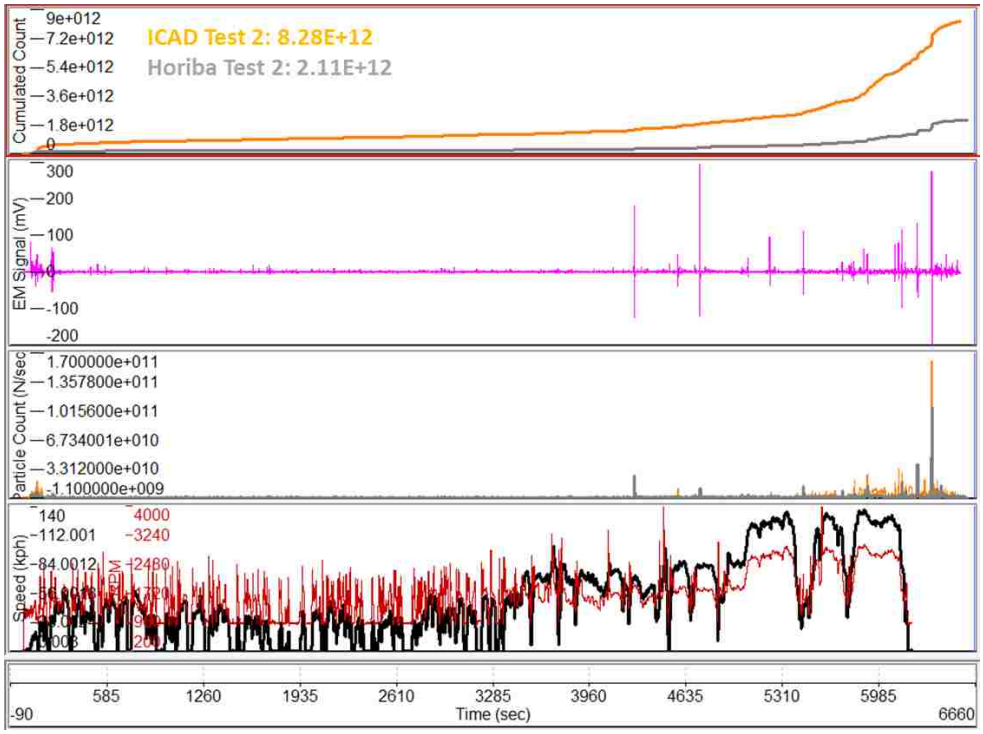

Figure 77: RDE Test 2 Results

Total Trip Distance (km)	86.53
Total Trip Duration (hh:min:sec)	1:50:14
Trip Average Speed (kph)	47.1
Total Stop Duration (sec)	919
Max/Min Temp (°C)	30.6 / 25.9

Table 19: Test 2 Summary

Initially these low results were thought to be a result of an incorrect exhaust flow measurement, as this is the only variable in Equation 6, and a lower number for test 2 would then yield a lower count. However, after examining the exhaust flows for all three tests, all three averaged a value of about 0.014kg/sec.

5.4.3 RDE Test 3

Test 3 depicted in the figure below demonstrates results similar to those of Test 1 with the ICAD measuring a total particle count of 3.11E+13 while the Horiba counted 5.39E+12. Once again, saturation occurrences (pink graph) can be noted in the cold start of the cycle with values exceeding 2000mV.

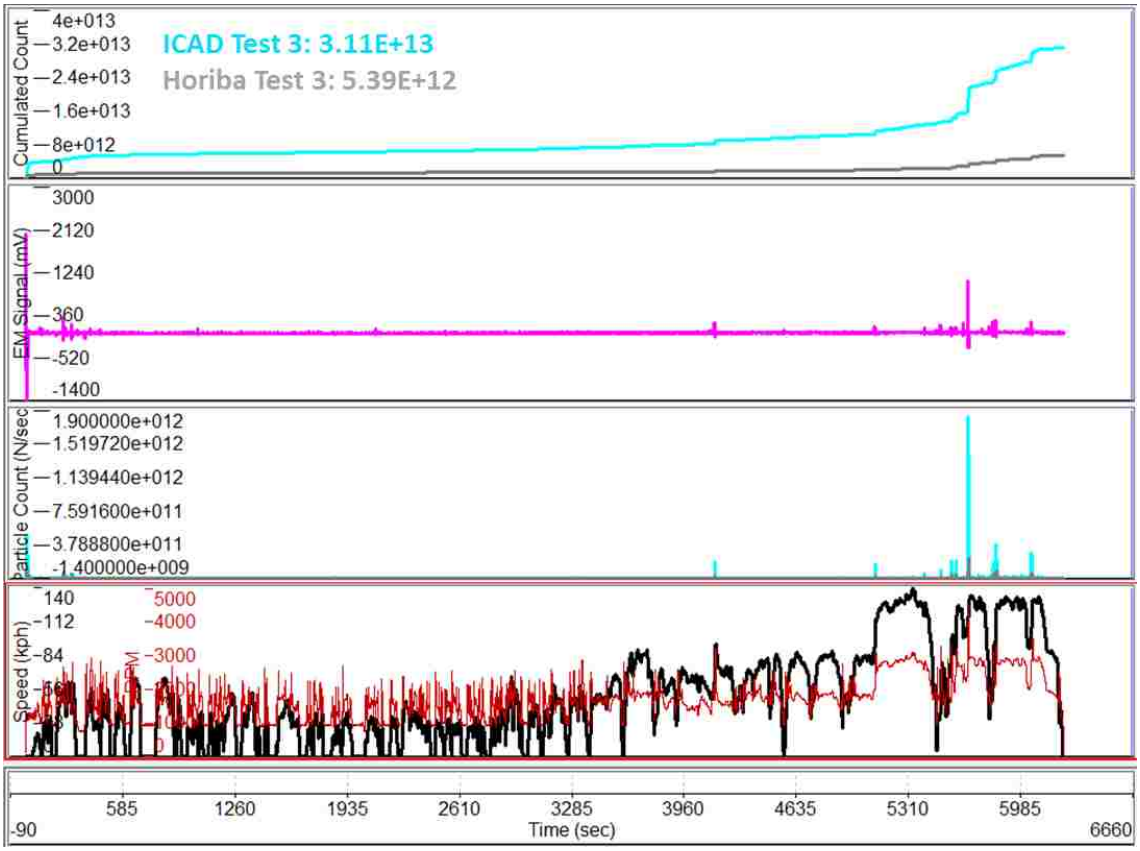

Figure 78: RDE Test 3 Results

Total Trip Distance (km)	86.516
Total Trip Duration (hh:min:sec)	1:46:04
Trip Average Speed (kph)	48.9
Total Stop Duration (sec)	825
Max/Min Temp (°C)	29.7/ 25.8

Table 20: Test 3 Summary

5.4 RDE Test Summary

Since these are real world driving tests, accuracy for both the cycles and instrument readings is hard to achieve due to unforeseen tests conditions like weather, traffic, etc. although the tests conducted were similar in these conditions (as outlined by the summary tables). Figure 79 demonstrates how the three cycles used for the aforementioned results vary in vehicle speed (therefore load) even though the route was the same for all three days.

Figure 79: Trace of each test conducted according to vehicle speed

The tests performed will help in the near future with the validation and further developing of the ICAD. From the figure below which illustrates the standard error of each machine for the aforementioned tests, It can be concluded that at this moment in time, there is too much variation from the measurements of the ICAD to consider it accurate. It is also difficult to determine how sub23nm particles affect this count, since it variates by sometimes magnitudes during the same type of cycle. Therefore, multiple more tests are recommended in order to get a baseline of where the ICAD is operating correctly.

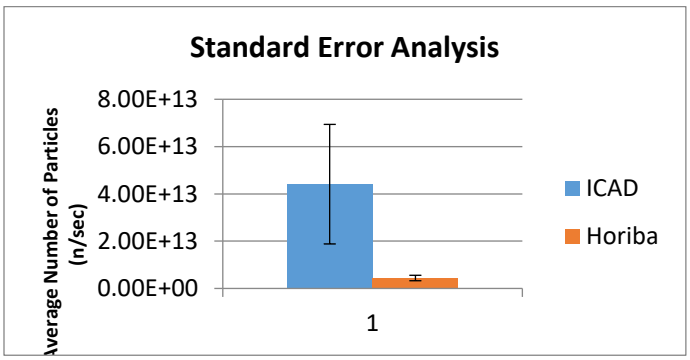

Figure 80: Standard Error Analysis for ICAD and Horiba Instruments

Chapter 6: Conclusions and Future Work

This chapter contains a summary of the outcomes found during this project. Moreover, it also outlines some suggestions for future work and improvement of the results.

6.1 Conclusions:

This study has contributed in the further understanding of sub 23nm particles emissions in gasoline engines as well as the performance of current and future PN measuring instruments. 2.0 and 1.8L GDI powered vehicles were tested both in North America and Europe throughout different cycles and with different instruments. A 2.4L PFI engine was also examined in the North America region in order to determine oil consumption and PN correlation.

The GDI vehicle in North America was tested in both WLTP and RDE cycles. The vehicle was paired with a fast particulate spectrometer (DMS500 by Cambustion) and an industry standard CPC system (AVL APC489). The capability of the DMS to distribute particles into different size ranges allowed for an in-depth analysis of the emissions throughout the cycles as well as a comparison against the current state of the art instrument.

The PFI engine was paired with the DMS as well as a Lubrisense system which examines oil consumption. It was tested throughout two different cycles (FTP75 and PT7BRK) to observe whether an increase in oil consumption correlated with increase in sub23nm particle emissions.

Lastly, in Europe, this project was part of the Sureal23 campaign. A continent wide project devoted to the understating of sub23nm particles as well as the development of new particle measuring technology for RDE testing. This project analyzed current lab and PEMS technology from Horiba and compared it to a new prototype in development which uses induced currents. Lab tests included consisted of various WLTP cycles, while RDE testing was done in a newly developed cycle by the Fiat Research Center (CRF) in Turin, Italy.

The outcomes obtained are outlined below, separated into general conclusions as well as those obtained from the methodology and equipment.

- Conclusions General:
    - Fuel derived particles are the primary source of emission spikes during aggressive transients in the cycle, with 78% of the total count being 23nm and above.
    - Hot Operation (part of the cycle after the first 90 sec of engine startup) particle size distribution matches that of the previous literature with regards to the amount of particles not being counted by current regulations (30% of particles between 10-23nm are being unaccounted for).
    - Oil consumption spikes during the cycles correlate with an increase in particles larger than 23nm as the oil becomes less viscous.

- Conclusions: Methodology and Equipment
    - Throughout the WLTP, the percentage difference in the readings between DMS (above 23nm) and AVL489 remains constant at 37.6%. This is likely due to the low signal strength observed by the DMS during the more demanding areas of the cycle.
    - A signal strength lower than 2.4 is considered insufficient for accurate readings, which often occur during deceleration or fuel shut off, both factors that are more prominent in the less demanding WLTP cycle.
    - During the spike in emissions throughout the RDE cycle, AVL's APC counted more particles than the DMS. This reduction in particle count by the DMS was found to be due to the catalytic stripper used in these experiments, which during hot operation could lead to loss of particles <100nm due to diffusion, and particle thermophoresis.
    - Although some of the oil consumption spikes throughout the cycle demonstrated a large quantity of sub 23nm particles (46% of the count in some cases), it was found that the largest oil consumption spikes produced particles larger than 23nm.

- The high Electrometer signals noticed with the ICAD indicates the instrument was experiencing saturation for setup 1 and setup3, meaning the instrument requires a better dilution system.
- The ICAD showed better accuracy in its particle count when consecutive tests were performed, demonstrating differences as low as 40% in consecutive test compared to differences such as 120% when tests were performed on different days.

6.2 Future Work and Recommendations:

Although this work provided better insight into sub 23nm PN and the instruments used in the industry, future work for this type of project could benefit from soot material analysis. TEM (Transmission electron microscopy) techniques would add immense value to this type of research for its ability to break down the soot composition, leading to more definite conclusions of particle pathways. Moreover, a comparison against a 10nm cutoff CPC would be useful, as the DMS and ICAD counts could then be put in direct comparison. With regards to the oil consumption tests, this work would benefit from analyzing the oil consumption vs PN results found in a GDI engine and compared them to those from the PFI.

The Sureal23 campaign involved multiple standard PN instruments and another prototype. Once all of the results are compared, this work will be useful to the other partners in this project when presenting the results to the European Union. Due to the length and nature of the RDE tests in this campaign, more tests with the Horiba and ICAD are necessary. Unexpected variables such as weather, traffic, etc. make the results vary by large margins during this type of testing. Therefore, increasing the number of tests would yield more accurate and concrete results. The results found in the study also concluded that the ICAD needs to be accompanied by a VPR or dilution type of system to prevent the instrument to become saturated, mostly on cold engine starts and aggressive transients.

Since the near future will most likely involve GDI engines equipped with GPF's, this work could benefit from repeating the experiments with a controlled (regeneration wise) GPF rather than a passive one. This would allow better representation of the behavior of soot particles if the load on the GPF is known and controlled. Moreover, it is recommended that the ICAD is calibrated alongside the Horiba (or the comparison instrument) before the any tests are conducted. This calibration should also be done by the user rather than the manufacturer for future integration of the prototype into the day to day operations performed by the company.

Lastly, with the completion of this project, it is recommended that manufacturers implement a type of cycle more aggressive than that of current homologation tests into their vehicle development programs. This would ensure that the vehicles meet the regulations required. In order to complete the calibration of engines prior to homologation tests, manufacturers would benefit from the use of a fast particulate spectrometer like that of the DMS500. This instrument has proven to be an effective measurement instrument especially due to its capabilities to sample from raw exhaust, its fast response time and its compact characteristics.

References

[1] J. Mcnally, "July 26, 1943: L.A. Gets First Big Smog," 26 July 2010. [Online]. Available: https://www.wired.com/2010/07/0726la-first-big-smog/.

[2] J. Weidman, "Green News: Soot Pollution," 10 Agust 2010. [Online]. Available: https://www.americanprogress.org/issues/green/news/2012/08/10/12007/soot-pollution-101/.

[3] D. B. kittelson, "Engines and Nanoparticles: A Review," *Elsevier Science,* 1997.

[4] "BG Nebraska," 2015. [Online]. Available: file:///C:/Users/Alfredo/Zotero/storage/5TUVEHZC/bg-gdi-solution.html.

[5] J. May, C. Favre and D. Bosteels, "Emission from Euro 3 to Euro 6 light-duty vehicles equipped with a range of emissions control technologies," *Association for Emissions Control ,* 2015.

[6] G. Archer, "Particle Emissions from Petrol Cars," 2013.

[7] A. Mamakos, "Feasibility of Introducing Particulate Filters on GAsoline Direct Injeaction Vehicles," JRC Scientific and Policy Reports, 2011.

[8] G. Fiengo and A. di Gaeta, "Common Rail System for GDI Engines; Modeling, Identification and Control," *Springer,* 2013.

[9] F. Zhao, M.-C. LAi and H. D.L, Progress in Energy and Combustion Science, 1999.

[10] S. Chincholkar and J. Suryawanshi, "Gasoline Direct Injection: An Efficient Technology," *Science Direct,* 2015.

[11] F. Millo, "Politecnico di Torino," 2018. [Online]. [Accessed 2018].

[12] D. Siano, "Gasoline Direct Injection," *Fuel Injection InTech,* 2010.

[13] A. Isenstadt and J. German, "Downsized, boosted gasoline engines," *The International Council On Clean Transportation ,* 2016.

[14] A. YAn-zhao, L. Xiang and T. Sheng-ping, "Development of a soot particle model with PAHs as precursors through simulations and experiments," *Science Direct,* 2016.

[15] . L. L. . P. Sanghwan Cho, "Synthesis of Primary-Particle-Size-Tuned Soot Particles by Controlled Pyrolyisi of Hydrocarbon Fuels, Energy Fuels 30," 2016.

[16] J. Fenske, Director, *Catalytic Converters-Explained.* [Film]. 2013.

[17] B. Morey, "Articles; Cooled EGR Shows Benefit for Gasoline Engines," 17 September 2014. [Online]. Available: http://articles.sae.org/13530/.

[18] W. Majewski, "Diesel Technology Guide: DPF," March 2011. [Online]. Available: https://www.dieselnet.com/tech/dpf.php.

[19] C. Lambert, T. Chanko, D. Dobson, X. Liu and J. Pakko, "Gasoline Particle Filter Development," *Emission Control Science Technology,* 2017.

[20] A. Reyers, "How can the GPF cut emissions of ultrafine particles form gasoline engines?," *Association for Emission Control by Catatalyst,* 2017.

[21] A. Maier, K. Ulrike, A. Dreizler and H. Rottengruber, "Fuel-Independent particulate Emissions in an SIDI Engine," *SAE Intenational ,* 2015.

[22] A. Mayer, A. Ulrich, J. Czerwinski and J. Mooney, "Metal-Oxide Particles in Combustion Exhaust," *SAE International,* 2010.

[23] N. Hannoschoxk, "Piston Ring Lubrication and Abrasion," Zurich, 1984.

[24] G. M., "Issues in Measurement of Particle Size Distribution from In-Use Heavy-Duty Vehicles.," in *ETH Conference on Nanoparticle Measurement* , 2002.

[25] C. De Petris, V. Giglio and G. Police, "Some Insights on mehcanisms of oil

Consumption," *SAE Tech,* 1991.

[26] E. Yilmaz, T. Tian, V. W. Wong and J. B. Heywood, "The Contribution of different Oil Consumtion Sources to Total Oil Consumption in a Spark Igntion Engine," *SAE,* 2004.

[27] E. Yilmaz, T. Tian, V. Wong and J. Heywood, "The Contribution of Different Oil Consumption Sources to Total Oil Consumption in a Spark Ignition Engine," *SAE International ,* 2004.

[28] A. L. Miller, C. B. Stipe, M. C. Habjan and G. G. Ahlstrand, "Role of Lubrication Oil in Particulare Emissions from a Hydrogen-Powered Internal Combustion Engine," *Environmental Science Technology,* 2007.

[29] B. Giechaskiel, "Calibration and accurcy of a particle number measurement system," *Measurement Science and Technology ,* 2010 .

[30] N. Cavina, L. Poggio, F. Bedogni, V. Rossi and L. Stronati, "Benchmark Comparison of Comercially Available Systems for Particle Number Measurement.," *SAE International,* 2013.

[31] M. Fierz, D. Meier, P. Steigmeier and H. Burtscher, "Aerosol Measurement by Induced Currents," *Aerosol Science and Technology,* 2014.

[32] W. e. a. Xiaoliang, "ImprovementofEngineExhaustParticleSizer(EEPS)size," *Journal of Aerosol Science,* 2016.

[33] D. 5. U. Manual.

[34] B. Gierchaskiel, T. Lahde and Y. Drossinos, "Regulating partile number mesurements from tailpipe of light duty vehciles: The next step?," *Elsevier,* 2017.

[35] A. A. Yusuf and F. L. Inambao, "Effect of cold start emmissionds from gasolne fueled engines of light duty vehicles at low and high ambient remperatures:Recent Trends," *Elsevier,* 2019.

[36] D. Net, "Conference report: 22nd ETH Conference on Combustion Generated Nanoparticles," Zurich, 2018.

[37] J. Pavlovic, "Influence and Efficiency of a Catalytic Stripper in Organic Carbon Removal from Laboratory Generated Soot Aerosols," Minneapolis, 2012.

[38] "Conference report: 22nd ETH Conference on Combustion Generated Nanoparticles," Diesel Net, Zurich, 2018.

[39] J. Koczak, A. Boehman and M. Brustarr, "Particulate Emissions in GDI Vehicle Transients: An Examination of FTP, HWFET, and US06 Measurements," *SAE Technical Paper,* 2016.

[40] Z. L. X. Z. S. S. L. Chen, "Characterizing Particulate matter emissions from GDI and PFI vehicles under transient and cold start conditions," *Fuel,* 2017.

[41] M. C. Andreas, U. Andrea, C. Jan and J. J. Mooney, "SAE International," *Metal-Oxide Particles in Combustion Engine Exhaust,* 2010.

[42] S. Brandenberger, M. Mohr, G. Koni and H. Neukom Peter, "Contribution of unburned lubricating oil and diesel fuel to particulate emission from passenger cars," *Athmospheric Environment ,* 2005.

[43] J. Gidney, T. Martyn and K. David, "Effect of Organometallic Fuel Additives on Nanoparticle Emissions from a Gasoline Passenger Car," in *Cambridge Patricle Meeting*, Cmbridge , 2009.

[44] A. Miller, G. Ahlstrand, K. David and M. Zachariah, "The fate of metal (Fe) during diesel combustion: Morphology, chemistry, and formation pathways of nanoparticles," *Combustion and Flame,* 2007.

[45] Bonatesta, Chiappetta and L. Rocca, "Part-load particulate matter from a GDI engine and the connection with combustion Characteristics," *Applied Energy,* 2014.

[46] Czerwinski, Petermann, Ulirch, Mueller and Wichser, "Particel Emissions of a TDI-

Engine with Different Lubricating Oils," *SAE International,* 2005.

[47] [Online]. Available: https://cateraninc.com/catalytic-converter/.

[48] Gidney, Twigg and Kitteleson, "Effect of Organometallic Fuel Additives on Nanoparticle Emissions from a Gasoline Passenger CAr," 2010.

[49] R. King, "MICKSGARAGE SHOP," 26 September 2015. [Online]. Available: https://www.micksgarage.com/blog/whats-all-this-in-the-news-about-car-emissions/.

[50] I. khalek, "Particle Emissions from Direct Injection Gasoline Engines," *Technology Today,* 2011.

[51] Cedinox, "Activities: Detail Highlighted," 30 January 2017. [Online]. Available: https://www.cedinox.es/en/actividades/highlighted/detail-highlighted/EGR-Systems/.

[52] H. Burtscher and W. Majewski, "Exhaust Gas Sampling and Conditioning," *Ecopoint,* 2016.

[53] M. Saffaripour, T. W. Chan, L. Fengshan, K. A. Thomson, G. J. Smallwood, J. Kubsh and R. Brezny, "Effect of Drive Cycle and Gasoline Particulate Filter on the Size Morphology of Soot Particles Emitted from a Gasoline-Direct-Injection Vehicle," *Envirmental Science & Technology ,* 2015.

Vita Auctoris

Name: Alfredo Tellez

Place of Birth: Medellin, Colombia

Year of Birth: 1993

Education: Carleton North High School, Florenceville Canada 2011

University of New Brunswick, Fredericton, Canada 2017

University of Windsor, M.Sc., Windsor, ON, 2019

Politecnico di Torino, Torino, Italy, 2019